THESIS FOR THE DEGREE OF DOCTOR OF PHILOSOPHY

Uncertainty and sensitivity analysis applied to LWR neutronic and thermal-hydraulic calculations

AUGUSTO HERNÁNDEZ-SOLÍS

Division of Nuclear Chemistry
Department of Chemical and Biological Engineering
CHALMERS UNIVERSITY OF TECHNOLOGY
SE-412 96 Göteborg, Sweden 2012

Uncertainty and sensitivity analysis applied to LWR neutronic and thermal-hydraulic calculations
AUGUSTO HERNÁNDEZ-SOLÍS
ISBN 978-91-7385-734-5

Doktorsavhandlingar vid Chalmers Tekniska Högskola
Ny serie nr 3415
ISSN 0346-718X

Nuclear Chemistry
Department of Chemical and Biological Engineering
Chalmers University of Technology
SE-412 96 Göteborg
Sweden
Telephone +46 (0) 31-772 1000

Cover: Illustration of the uncertainty analysis performed on nodal core calculations of LWRs

Chalmers Reproservice
Göteborg, Sweden 2012

Uncertainty and sensitivity analysis applied to LWR neutronic and thermal-hydraulic calculations

AUGUSTO HERNÁNDEZ-SOLÍS
Division of Nuclear Chemistry
Department of Chemical and Biological Engineering
Chalmers University of Technology

ABSTRACT

Nowadays, with an increased number of light water reactors (LWRs) around the world, there is a large interest in improving deterministic safety analysis as an essential tool for demonstrating the safety of nuclear power plants. Best estimate (BE) computer codes were developed to model the complex and strong coupling that exists between the neutron and thermal-hydraulic fields that are present in the core of nuclear reactors. At present, these are employed (among other applications) in the prediction of the safety margins of nuclear power plants during normal and off-normal operating conditions. Nevertheless, even if the best available science is applied in the modeling of nuclear reactors, uncertainties are always present in the calculations. In recent years, it has been recognized by the nuclear community that if useful conclusions are to be obtained from BE codes, these should be supplemented by a quantitative uncertainty analysis. In this thesis, uncertainty and sensitivity analysis is performed on neutronic and thermal-hydraulic calculations of LWRs. A statistical approach is employed, where the non-deterministic treatment of a physical model that induces a stochastic nature on the code outputs is based on a sampling methodology. The preferred sampling strategy for the current study corresponds to the quasi-random Latin Hypercube Sampling (LHS). This technique allows a much better coverage of the input uncertainties than simple random sampling (SRS) because it densely stratifies across the range of each input probability distribution. This is one of the first works that employs LHS to sample the input uncertain space, and then relies on the concept of non-parametric tolerance intervals for the code output uncertainty assessment for both neutronic and thermal-hydraulic calculations. It is shown at the different stages in the modeling of LWRs that LHS offers the possibility to assess more realistic non-parametric tolerance limits than SRS, because code non-linearities are much better handled when the input space is covered in an efficient way.

The deterministic modeling of LWRs begins with the computation of energy-collapsed and homogenized macroscopic cross-sections by means of a lattice code. Once these parameters are functionalized as a function of the reactor state variables and discretized in space, they are used as input variables by core simulators in order to calculate the spatial distribution of the neutron flux and thus, the spatial distribution of the power. Once the power is determined, the thermal-hydraulic variables are updated, and the process repeated until convergence. This thesis is divided in three different parts related to the possible neutronic and thermal-hydraulic modeling strategies. In the first part, microscopic cross-section uncertainties based on two modern nuclear data libraries such as JENDL-4 and ENDF/B-VII.1 were derived in multi-group format. These were propagated through lattice calculations in order to perform uncertainty analysis on the infinite neutron multiplication factor (k_∞), and on two-group homogenized macroscopic cross-sections corresponding to a PWR fuel segment. The aim is to compare the uncertainty assessment on k_∞ and on the macroscopic cross-sections when the different nuclear libraries are employed. It was found that the computed uncertainties based on JENDL-4 are much higher than the computed uncertainties based on ENDF/B-VII.1. A sensitivity analysis showed that the multi-group variances of the Uranium-235 fission reaction based on JENDL-4 are very high, being this the main reason of the observed large discrepancies in the different uncertainty assessments.

In the second part of the thesis, two types of uncertainty analyses were performed on core simulations. The first one corresponds to the forward approach of input uncertainty propagation, where the input uncertain space formed by the nodal two-group macroscopic cross sections and diffusion coefficients is sampled both with SRS and LHS. The possible ranges of variation of such an input space are based on data from a depletion calculation corresponding to the cycle 26 of the Swedish Ringhals-1 BWR. The aim of this study is to compare the efficiency of the uncertainty assessment performed on the nodal thermal flux when SRS and LHS are employed. On the other hand, in the second type of uncertainty analysis presented in this chapter, discrepancies between spatial measured and calculated fluxes in Ringhals-1 are used to perform an inverse

uncertainty analysis on the spatial dependence of the different core parameters. This analysis is carried out using Bayesian statistics, where, for a certain cycle, the frequency distributions of macroscopic cross-sections and diffusion coefficients at every assembly node are updated based on the error distribution of the spatial thermal flux. Emphasis was made on performing uncertainty analysis as well on the coefficients of a nodal cross-section model. Although a very simple model was derived, the aim is to propose an uncertainty assessment based on replicated sampling techniques such as the general bootstrap method.

Finally, in the third part of the thesis, uncertainty and sensitivity analyses were applied to thermal-hydraulic calculations. The objective is to show that when experimental data are available, uncertainty analysis can be used in the validation process of a BE code. Quantitative limits based on a statistical theory were computed to validate code thermal-hydraulic features in predicting pressure drop, void fraction and critical heat flux based on the macroscopic exercises of the OECD/NRC BWR Full-Size Fine-Mesh Bundle Test (BFBT) benchmark.

The present study performs a realistic analysis of nuclear reactors, particularly in the uncertainty prediction of important neutronic and thermal-hydraulic parameters of light water reactors.

Keywords*: Nuclear best estimate codes, uncertainty analysis, sensitivity analysis, Latin Hypercube Sampling, simple random sampling.*

Puedes llamarme Cuauhtecuhtli, el Señor de las Águilas. He venido a llevarte a tu lugar en el centro de las Cuatro Sendas; por tu valentía y honor has ganado la entrada en los Cuacuahtzin, los Caballeros Águila…

LIST OF PUBLICATIONS

This thesis is based on the work contained in the following papers:

PAPER I

Hernández-Solís A., Demazière C., Ekberg C. *"Uncertainty and sensitivity analyses applied to the DRAGONv4.05 code lattice calculations and based on JENDL-4 data"*
Submitted to Annals of Nuclear Energy

PAPER II

Hernández-Solís A., Demazière C., Ekberg C. *"Uncertainty analyses applied to the UAM/TMI-I lattice calculations using the DRAGONv4.05 code and based on JENDL-4 and ENDF/B-VII.1 covariance data"*
Submitted to Science and Technology of Nuclear Installations

PAPER III

Hernández-Solís A., Demazière C., Ekberg C. *"Bayesian uncertainty analysis of BWR core parameters based on flux measurements"*
ANS Winter Meeting Transactions, Vol. 105, 2011.

PAPER IV

Hernández-Solís A., Ekberg C., Demazière C. *"Uncertainty analysis of a nodal cross-section model based on Ringhals 1 data by means of a non-parametric bootstrap method"*
Submitted to Progress in Nuclear Energy

PAPER V

Hernández-Solís A., Ekberg C., Ödegård-Jensen A., Demazière C., Bredolt U. *"Statistical uncertainty analyses of void fraction predictions using two different sampling strategies: Latin Hypercube and random sampling"*
18th International Conference on Nuclear Engineering (ICONE), 30096, 2011.

PAPER VI

Hernández-Solís A., Ekberg C., Demazière C., Ödegard-Jensen A., Bredolt U. *"Uncertainty and sensitivity analyses as a validation tool for BWR bundle thermal-hydraulic predictions"*
Nuclear Engineering and Design, Vol. 241 (9), 2011.

LIST OF PUBLICATIONS NOT INCLUDED IN THIS THESIS

Pazsit I., Demazière C., Sunde C., Bernitt P., Hernandez-Solis A. *"Final Report on the Research project Ringhals Diagnostics and Monitoring Stage 12".* CTH-NT-220/RR-14, August 2008.

Hernández-Solís A., Vinai P., Bredolt U. *"An assessment study of the POLCA-T code bases on NUPEC data"*. ANS Annual Meeting Transactions, Vol. 100, 2009.

Hernández-Solís A. *"Uncertainty and sensitivity analysis applied to the validation of BWR bundle thermal-hydraulic calculations".* Licentiate thesis, CTH-NT-231, Chalmers University of Technology, 2010.

Hernández-Solís A., Carlsson F. *"Diagnosis of submersible centrifugal pumps: A motor current and power signature approach"*. European Power Electronics and Drives Journal, Vol. 20 (1), 2010.

Pazsit I., Montalvo C., Hernández-Solís A., Bernittt-Cartemo P., Nylen H. *"Diagnostics of core barrel and fuel assembly vibrations in the Swedish Ringhals PWRs".* 7th International Topical Meeting on Nuclear Plant Instrumentation, Control, and Human-Machine Interface Technologies 2010, NPIC and HMIT 2010, Las Vegas, NV, USA.

Hernández-Solís A., Demazière C., Ekberg C., Ödegaard–Jensen A. *"Statistical uncertainty analysis applied to the DRAGONv4 code lattice calculations and based on JENDL-4 covariance data".* On the proceedings of PHYSOR 2012-Advances in Reactor Physics, Knoxville TN, USA.

Hernández-Solís A., Demazière C., Ekberg C. *"Statistical uncertainty analysis applied to the neutron flux predictions of a BWR core using two different sampling strategies: Latin Hypercube and random sampling"*. Manuscript.

CONTENTS

CHAPTER 1

INTRODUCTION

"A nuclear power plant is infinitely safer than eating, because 300 people choke to death on food every year"

James Allen

1.1 Background

At the end of the year 2011, nuclear energy provided about 15% of the world's electricity as a continuous and reliable based-load power. Nowadays, nuclear energy is experiencing a renaissance because it represents a very good option to fulfill the growing demand for electricity around the globe. Concerns over climate change and dependence on unsecure supplies of fossil fuels are the main reasons for such a renaissance. According to a 2012 joint study between the OECD Nuclear Energy Agency (NEA) and the International Atomic Energy Agency (IAEA) [1], although the Fukushima Daiichi nuclear accident has affected nuclear power policies and projects in some countries, nuclear power remains a key part of the global energy mix. Several governments have plans for constructing new nuclear plants, with the strongest expansion expected in China, India, Republic of Korea and the Russian Federation. Therefore, with an increased number of light water reactors (LWRs) in the world, there is a huge interest in improving deterministic safety analysis as an essential tool for demonstrating the safety of nuclear power plants. The main objective of safety analysis is to demonstrate in a robust way that all safety requirements are met; that is, that sufficient margins exist between the real values of important parameters (e.g. peak cladding temperature) and the threshold values at which the barriers against release of radioactivity would fail [2].

The strong coupling between the neutron kinetics and thermal-hydraulics is a unique feature of LWRs, which makes the calculation of their behavior a very challenging task. The so-called nuclear best estimate (BE) codes are complex tools developed to predict how the neutron density field (i.e. the spatial and temporal distribution of the neutron density throughout the core) interacts with the density field of the coolant and the temperature field of the fuel (i.e. the spatial and temporal distribution of the enthalpy of the coolant/temperature of the fuel throughout the core). The common modeling strategies all rely on separate modeling tools for resolving the different fields and possibly the different scales. The interdependence between the different fields/scales is usually accounted for by software coupling. Nuclear codes are used nowadays not only to estimate the transient behavior of light water nuclear power plants during off-normal conditions, but also for the evaluation of safety margins. The training of operators, the optimization of the plant design and related emergency operating procedures are some of the applications of such codes. Nevertheless, even though modern nuclear codes are based on the best available science, uncertainties are always present in the calculations. They originate from different sources like for instance, a lack of knowledge in the physical interpretation and representation of the code models, as well as plant and fuel parameters that are input data for the code. Therefore, it has been recognized by the nuclear community that if useful conclusions are to be obtained from BE calculations, these should be supplemented by a quantitative uncertainty analysis. On the other hand, the study of how output uncertainty can be apportioned to the different input sources, known as sensitivity analysis, is an important complement to uncertainty quantification since it identifies the parameters where a

reduction of the uncertainty will have the greatest benefit for the reduction of the total simulation uncertainty.

Prior to having the capability to calculate the uncertainty of key values that define a nuclear power plant operational limits, conservative calculations of the safety margins were performed during the 1970s. For example, in the United States, prior to the existence of Appendix K to Title 10 Part 50 of the Code of Federal Regulations (10 CFR 50) [3], regulatory bodies required that all calculations of the limiting parameters should be performed using specified conservative procedures. In 1988, the 10 CFR 50.46 amendment allowed the use of BE codes for performing safety analysis, stipulating that uncertainties must be identified and quantified. At present, in the existing International Atomic Energy Agency (IAEA) safety standards [4], the use of BE codes with realistic input data plus uncertainty analysis is recognized as an acceptable option for demonstrating that safety is ensured with an adequate margin. This constitutes the backbone of state-of-the art international licensing regulations. The modern concept of safety margin is presented in figure 1.1.

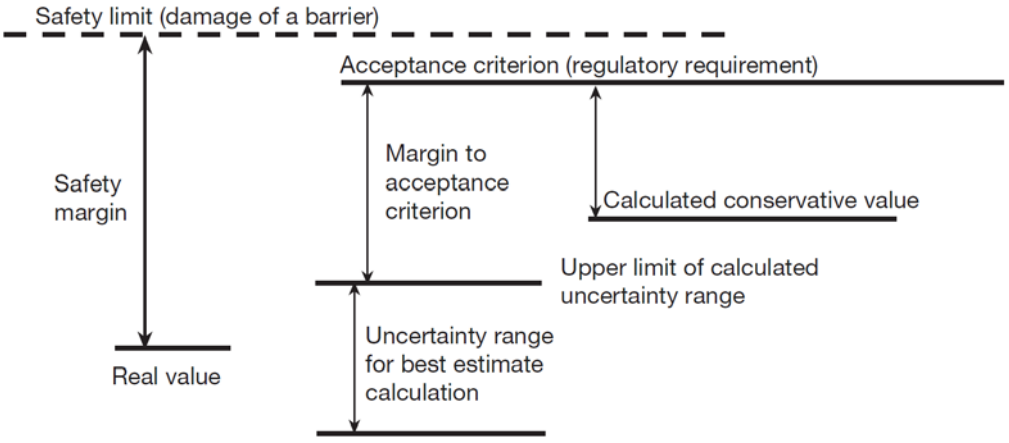

Fig. 1.1. Concept of safety margin given by the IAEA [3]

1.2 Objectives

In this thesis, uncertainty analysis is performed at different neutronic and thermal-hydraulic LWR modeling stages using a Monte Carlo-based approach, where the non-deterministic treatment of a physical model that induces a stochastic nature on the code outputs is based on a sampling methodology. In this approach, the code input space defined by input parameters, boundary and initial conditions, sub-models, etc. are treated as random variables. Thereafter, values of these inputs are selected according to a random or quasi-random sampling strategy and then propagated through the code in order to assess the output uncertainty in the corresponding calculations. This framework has been highly accepted by many scientific disciplines not only because of its solid statistical foundations, but also because it is affordable in practice and relatively easy to implement thanks to the tremendous advances in computing capabilities.

The preferred sampling strategy for the current study corresponds to the quasi-random Latin Hypercube Sampling (LHS). This technique allows a much better coverage of the input uncertainties than simple random sampling (SRS) because it densely stratifies across the range of each input probability distribution. In fact, LHS was born in the field of safety analysis of nuclear reactors [5], and one of the goals of this work is to prove the benefits and efficiency of using LHS over SRS in both LWRs neutronic and thermal-hydraulic predictions. Once a sample of the code output has been taken, a statistical inference of the output population parameters is performed. During recent years, it has been common in the field of nuclear reactor safety to use the theory of non-parametric

tolerance limits for the assessment of code output uncertainty. This approach is based on the minimum sample size required to infer a certain coverage of a population, with a certain confidence. Thus, the different code output uncertainty assessments performed in this work along the neutronic and thermal-hydraulic calculations are based on the concept of non-parametric tolerance limits. In this thesis, emphasis is made in the computation of multivariate tolerance limits when the code output space is comprised by several parameters that are correlated, because the statistical coverage of the output space depends on the number of correlated parameters. The fact that this statistical theory is solely based on the ranking of the output space sample, makes it possible to use it even if the input space has been sampled with LHS or any kind of stratification, and not only with SRS. This is explained in much more detail in the next chapter.

All in all, the main objective of the thesis was to perform an uncertainty analysis at all possible stages in the deterministic neutronic and thermal-hydraulic modeling of LWRs, in order to have a quantitative measurement of the uncertainties that are associated to the different parameters that are used to study the physical behavior of light water reactors.

1.3. Outline of the thesis

This thesis begins with a review of the statistical approach to perform uncertainty analysis, where LHS and SRS are explain in detail. The following chapters are related to the three main stages that are currently employed in the modeling of the neutronic and thermal-hydraulic fields of the core of LWRs. In chapter 3, microscopic cross-section covariance data in multi-group form was derived from modern nuclear data libraries. The different covariance matrices were propagated through the DRAGONv4.05 lattice code, in order to assess a degree of uncertainty to the energy-collapsed and homogeneized macroscopic cross-sections and diffusion coefficients. Thus, a comparison between the computed uncertainties based on JENDL-4 and ENDF/B-VII.1 data was performed on a 15x15 PWR fuel segment test case corresponding to the Exercise I-2 of the OECD/NEA UAM benchmark. Also, a brute sensitivity analysis is made on a 17x17 PWR case based on JENDL-4 data, in order to know which microscopic cross-section has the biggest influence on the infinite neutron multiplication factor.

Chapter 4 deals with a forward and inverse uncertainty analysis performed by core calculations. The forward analysis aims to prove that LHS is much more computational efficient than SRS in the computation of the maximum achievable uncertainty of the nodal thermal flux. On the other hand, the inverse study aims to obtain posterior PDFs of nodal macroscopic cross-sections and diffusion coefficients using a Bayesian uncertainty analysis. This is based on the discrepancies between spatial measured and calculated fluxes that were used in the fuel loading strategy of the Ringahls 1 BWR during cycle 26. Therefore, the goal is to obtain uncertainty ranges of the nodal core parameters that rely on experimental data.

In chapter 5, uncertainty and sensitivity analyses were performed to steady-state and transient void fraction predictions. One of the main objectives is to enhance the validation process of the thermal-hydraulic features of the Westinghouse code POLCA-T. This is achieved by computing a quantitative validation limit based on statistical uncertainty analysis. Finally, some general conclusions about this work are given in chapter 6, as well as some reflections about what can be done in the future in the field of uncertainty analysis applied to nuclear reactors simulations.

CHAPTER 2

PROPAGATION OF UNCERTAINTY IN THE ANALYSIS OF NUCLEAR SYSTEMS

"Statistics are like bikinis. What they reveal is suggestive, but what they conceal is vital"

Aaron Levenstein

One of the main parts of the uncertainty analysis consists in the identification and characterization of the relevant sources of uncertainty, which define the so called "input uncertainty space". Some authors have classified the different sources under five general categories [6,7]. A few neutronic and thermal-hydraulic examples of each category are given in table 2.1.

Table 2.1. Different sources of uncertainty that are commonly present in LWR calculations

	Neutronic	*Thermal-hydraulic*
Code or model uncertainty	Approximations on the angle dependence of the neutron flux (i.e. only taking into consideration up to the P1 component), or the use of diffusion theory in the prediction of the nodal neutron flux in the reactor core.	Including only some terms in the field equations (e.g. the viscous stress terms are sometimes not included), uncertainties in constitutive correlations, assuming that fully developed flow exists in the system are only a few examples included in this group.
Representation uncertainties	The chosen numerical method to discretize the neutron flux spatial dependence.	The chosen nodalization of the system that define the control volumes where the field equations are going to be solved.
Scaling uncertainties		Using data recorded in scaled experiments and the reliance on scaling laws if applicable, constitute a source of uncertainty.
Plant uncertainty	Neutron cross-sections were obtained mainly from experiments. Nowadays, the trend is to simulate the possible probabilities of neutron interactions with matter.	Boundary and initial conditions of the nuclear power plant into consideration are uncertain because in many cases they come from measurements. Other system components parameters such as the time when a pump or valve is tripped, controller parameters, etc., are also considered here.
User effect	It has been recognized that the degree of user expertise and experience in handling complex BE codes, can add uncertainty to the desired results. It should be acknowledged at the beginning of any input deck design that this type of uncertainty exists, so the user can take the necessary actions to reduce this effect.	

Generally speaking, sources of uncertainty can arise from two different broad categories. First, there is the uncertainty that arises because the system under study can behave in many different ways. This type of uncertainty is often referred to as stochastic or aleatory uncertainty, and is a property of the system under consideration due to random or inherent variation [8]. This uncertainty is irreducible and includes the basic statistical concepts of variability and the definition of probability as describing the uncertainty associated with the outcome of an experiment or event. An example of this type of uncertainty is, for instance, the time when a pump is tripped during a power plant transient. Second, there is the uncertainty that arises from an inability to specify the exact value of a

quantity that is assumed to have a constant value within a particular analysis. This type of uncertainty is often referred to as subjective or epistemic uncertainty [8]. By contrast to the aleatory uncertainty, epistemic uncertainty is reducible and stems from a lack of knowledge. The other main part of the uncertainty analysis characterizes the methodology to quantify the global influence of the combination of the input uncertainties on selected output parameters, which now define the so called "output uncertainty space". It can be said that the two main items of uncertainty analysis may be treated differently by different methodologies.

Within the most important methodologies applied in the reactor safety analysis field, uncertainties are evaluated using two approaches: a) Propagation of input uncertainties or b) Extrapolation of output uncertainties. In the first approach, uncertain input parameters are characterized by specific ranges and/or probability density functions (PDFs), and calculations are performed varying such parameters. Deterministic and statistical methodologies follow this approach. However, in the extrapolation of output uncertainty approach, the output uncertainty is based on comparisons between calculation results and significant experimental data. These two approaches are illustrated in figure 2.1.

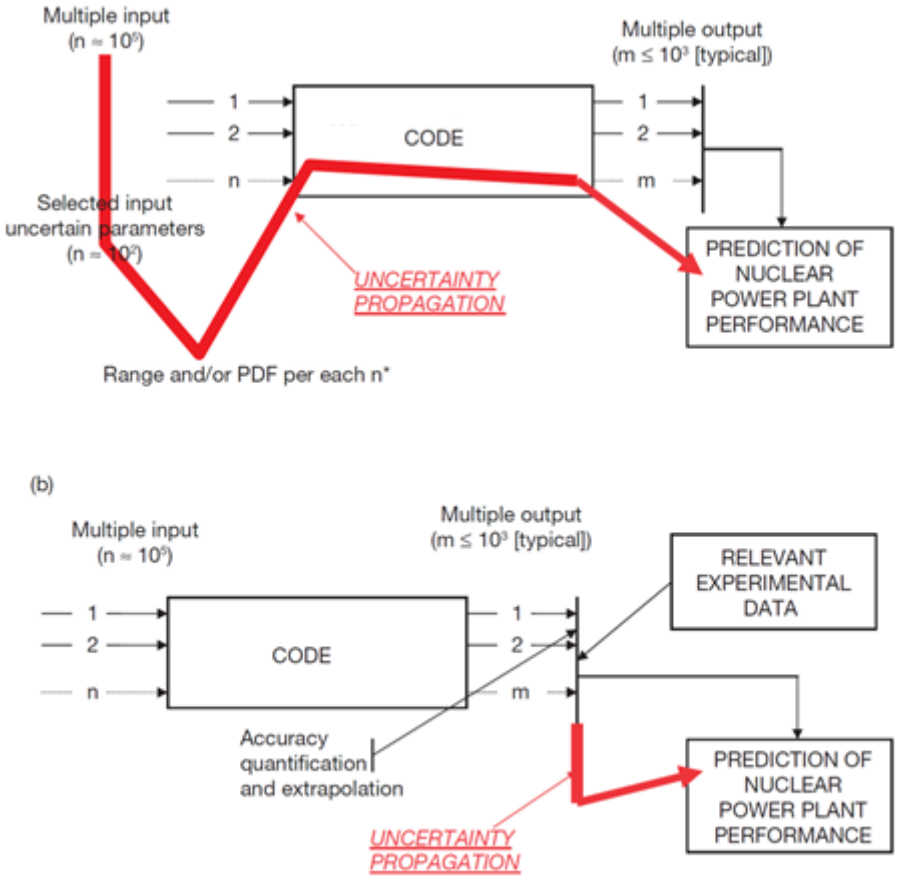

Fig. 2.1. Uncertainty classification. a) Propagation of input uncertainty; b) Propagation of output uncertainties [3]

In this chapter, sampling-based methods that are employed for performing uncertainty and sensitivity analysis are presented, since the work of this thesis is based on this approach. A literature review of other uncertainty methodologies that are used in the safety analysis of nuclear reactors

such as the deterministic adjoint sensitivity analysis procedure (ASAP), or the one belonging to the propagation of output uncertainties approach, such as the uncertainty methodology based on accuracy extrapolation (UMAE), was made at the beginning of the present PhD project and can be found in the corresponding Licentiate thesis [9].

2.1 Overview of the statistical methodology

The non deterministic treatment of a physical model that induces a stochastic nature on the result can be studied with statistical methods. The first step of this framework is to identify the most important uncertain parameters defined as $\bar{X} = (x_1, x_2, \dots, x_k)$. They should be characterized by a sequence of probability density functions (PDFs) $D_1, D_2, \dots, D_k$, defining the uncertain input space. Then, a sampling strategy is used to generate a sample of size *N* from such input space which is propagated through the code in order to treat the output calculations $y_1, y_2, \dots, y_N$ as random variables. This scheme is shown in figure 2.2.

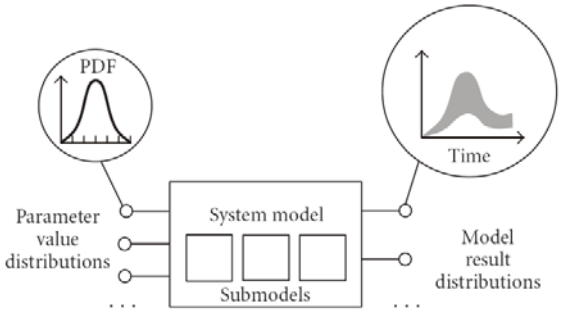

Fig. 2.2. Scheme of statistical uncertainty analysis [10]

The definition of the PDFs is one of the most important parts of the statistical methodology because these distributions determine both the size and the distribution of the uncertainty in the model results. Nevertheless, their characterizations have been widely based on formal expert review processes. In this case, the investigator decides the plausible range of variation for each input. A small range usually maintains numerical stability of the code meanwhile a large range will lead to more useful information about the code behavior. However, the choice is made by intuition or guesses and might have to be revised after some model runs [11,12]. The next step is to assign probability distributions to characterize a degree of belief with respect to where the appropriate value of each $\bar{X}$ element is located. Unfortunately, contrary to the aleatory uncertainty where observational and/or experimental results might help to find out a probability distribution, data will often not be available to characterize epistemic uncertainty, thus making the distribution assignment somewhat arbitrary. Common choices for distributions are the uniform, normal and lognormal for continuous variables. For discrete variables probability functions like the binomial or Poisson distributions can be used.

The care and effort used in the definition of the distributions are dependent on both the purpose of an analysis and the amount of time and resources available for its implementation. It is expected that experts could offer assistance in understanding and estimating uncertainties in the modeling process without contributing to additional uncertainty. However, an analyst's decision can contribute to the overall uncertainties in the modeling process from the cognitive biases that affect subjective judgment. Some authors [13] have expressed their concern about how the so-called expert opinion underestimates uncertainty quantification. Other human facts that may affect uncertainty assessment are:

- Availability. How analysts account for certain events depends upon whether they have experienced them or not.

- Misimpression. Poor, incorrect or bad translation of information.

- Anchoring. Some analysts tend to anchor to preconceptions even in light of new data or information.

During the last years, the effort to generate relevant experimental data designed to study important phenomena such as separate effect tests, have raised the question whether expert opinion should be replaced by a quantitative uncertainty assessment based on the difference between code and experimental agreements. For instance, the Canadian regulatory body agrees on the BE plus uncertainty approach for licensing purposes if input uncertainties are assessed against relevant experiments [2]. Signal processing techniques based on Bayesian statistics in order to quantify a posteriori distributions based on experiments, is a good example of such a type of assessment [14].

2.1.1 Sampling strategies

The statistical methodology relies on a sampling strategy in order to propagate input uncertainties through the code. The simplest sampling procedure for developing a mapping from analysis inputs to analysis results is random sampling. In this procedure, each sample element is generated independently of all other sample elements; however, there is no assurance that a sample element will be generated from any particular subset of the input space. In particular, important subsets with low probability but high consequences are likely to be missed if the sample is not large enough. Furthermore, if sampled values fall closely together, the sampling is quite inefficient. In order to overcome this issue, the stratified-based Latin hypercube sampling was derived.

A brief but good historical review of the Latin Hypercube development is made by Helton et al. in [5]. LHS has its origins in the reactor safety community during the mid 1970's, when the treatment of uncertainty in analyses related to the safety of NPP started being a big concern, leading to an active interest from the US Nuclear Regulatory Commission (NRC) and its contractors in the propagation of uncertainty through models of complex systems. LHS is done according to the following scheme to generate a sample of size N from the $\bar{X}$ input space in consistency with their PDFs. The range of each variable (i.e. the x_j) is exhaustively divided into N disjoint intervals of equal probability and one value is selected at random from each interval. The N values thus obtained for x_1 are paired at random without replacement with the N values obtained for x_2. These N pairs are combined in a random manner without replacement with the N values of x_3 to form N triples. This process is continued until a set of N $K-tuples$ is formed. In this way, a good coverage of all the subsets defining the uncertain input space can be achieved. Therefore, LHS can be viewed as a compromise, since it is a procedure that incorporates many of the desirable features of random and stratified sampling. The LHS procedure is exemplified in figure 2.3 for two different possible input distributions, one corresponding to a uniform distribution and the second to a normal distribution, respectively.

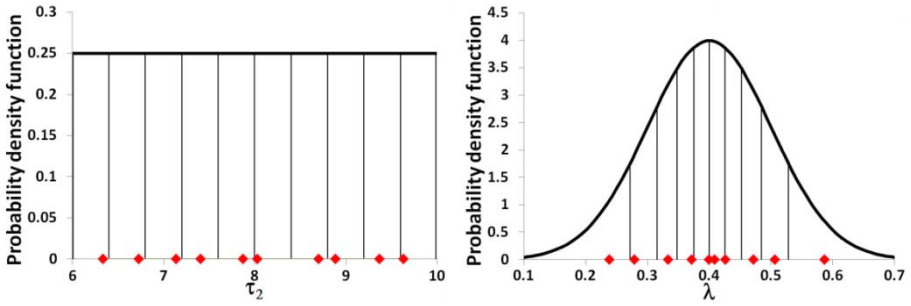

Fig. 2.3. Coverage of a probability space formed by a uniform and normal distributions using LHS and for a sample size of 10 elements

If the coverage performed with LHS is to be compared to the SRS case, it is straightforward to see that LHS will perform better or at least equivalently in covering the joint range of the PDFs depending on the type, number of distributions forming the space and desired number of samples. For instance, in figure 2.4, the samples of 10 elements obtained from the previous two distributions are paired using both LHS and SRS, so a comparison of the coverage computed by the two sampling techniques can be made.

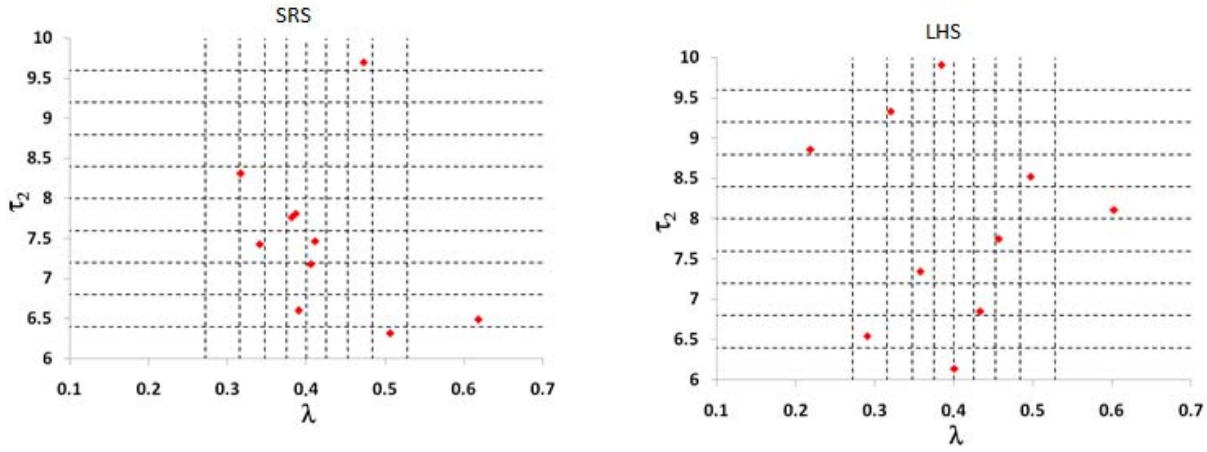

Fig. 2.4. Performance of LHS vs. SRS in covering with 10 samples the space formed by a uniform and normal PDFs

It can be seen from the pairing of the different samples that for the SRS case, parts of the space where not even covered, while in the LHS case for every row and column there is at least one point being sampled. Thus, for the same sample size, LHS covered much better the input space than SRS.

It is of interest to study the properties of the different sampling techniques used for estimating the mean, variance and confidence depending on the range of variation of a particular output variable from code predictions defined as $y_i = f(\bar{X}),\ \ i = 1, \dots, N$. McKay et al. [15] established that if y_i is monotonic in each of the x_j, then the variance of the estimated output mean using LHS would be less than or equal to the variance of the estimated output mean using SRS, i.e.:

$$Var\left(\hat{E}(y)_{LHS}\right) \leq Var\left(\hat{E}(y)_{SRS}\right) \tag{2.1}$$

Where:

$$\hat{E}(y) = \bar{y} = (1/N)\sum_{i=1}^{N} y_i \tag{2.2}$$

For each sampling method, the form for the estimator of the output variance is given by:

$$S^2 = (1/(N-1))\sum_{i=1}^{N} (y_i - \bar{y})^2 \tag{2.3}$$

When using the SRS procedure, it is well known that Eq. (2.3) is an unbiased estimator of the output variance, i.e. $E(S^2_{SRS}) = S^2$. However, if LHS is employed, $S^2_{LHS} = S^2$ is an asymptotically biased estimator. McKay et al. [15] also proved that, if y_i is monotonic in each of the x_j, the expected value of the LHS variance estimator varies between:

$$\left[\frac{N}{(N-1)}\right] Var(y) \leq E(S^2_{LHS}) \leq Var(y) \tag{2.4}$$

Even if S^2_{LHS} was found to have a little bias, it was also found to have less sampling variability than S^2_{SRS}. This result, together with Eq. (2.1), suggests that the $(1-\alpha)$ confidence interval of the predicted output mean is smaller for the LHS strategy than for the SRS one, considering that both have the same sample size N. Such confidence interval can be computed as:

$$\bar{y} \pm t_{1-\frac{\alpha}{2}} \frac{S}{\sqrt{N}} \tag{2.5}$$

Where $t_{1-\frac{\alpha}{2}}$ corresponds to the $1-\alpha/2$ quantile of the t-distribution with $N-1$ degrees of freedom.

Thus, the uncertainty analysis is more efficient with LHS not only for presenting less sampling variability on the estimation of the output parameters, but also due to the fact that it can much better handle the code non-linearities. The reason lies with a much better coverage of important regions of the input space than SRS, if the sample size is the same.

The LHS methodology previously described assumes that the different variables are independent. Nevertheless, Iman and Conover [16] developed a Latin hypercube procedure developed for sampling correlated variables. Such procedure is based not directly on the covariance matrix but instead, on the correlation matrix (which should be positive definite).

The procedure begins by taking an LHS sample based on the individual variances, and assuming that the input parameters are independent, e.g.:

$$\bar{X} = \begin{bmatrix} x_{11} & x_{12} & \cdots & x_{1n} \\ x_{21} & x_{22} & \cdots & x_{2n} \\ \vdots & \vdots & \vdots & \vdots \\ x_{m1} & x_{m2} & \cdots & x_{mn} \end{bmatrix} \tag{2.6}$$

Where *m* is the total number of inputs, and *n* the number of samples. The aim of this procedure is to rearrange the values in the individual columns of $\bar{X}$, so that a desired rank correlation structure results among the individual variables. This can be achieved by somehow relating the correlation coefficients of the $\bar{X}$ matrix, to the total correlation matrix $\bar{C}_{new}$.

If the correlation matrix of $\bar{X}$ is called $\bar{T}$, the method applies a Cholesky decomposition to both $\bar{T}$ and $\bar{C}_{new}$ in order to obtain, respectively, the $\bar{Q}$ and $\bar{P}$ lower triangular matrices that satisfy the following relationships:

$$\bar{C}_{new} = \bar{P}\,\bar{P}'$$

$$\bar{T} = \bar{Q}\,\bar{Q}' \tag{2.7}$$

Then, the target or desired matrix $\bar{X}^*$ can be computed such as:

$$\bar{X}^* = \bar{X}\bar{S}' \tag{2.8}$$

Where the $\bar{S}$ matrix relates $\bar{T}$ and $\bar{C}_{new}$ as follows:

$$\bar{C}_{new} = \bar{S}\bar{T}\bar{S}' \tag{2.9}$$

In the end, $\bar{X}^*$ has a correlation matrix equal to $\bar{C}_{new}$, and the values of each variable in $\bar{X}$ must be rearrange so that they have the same rank (order) as the target matrix $\bar{X}^*$. That is why this method is known as the rank-induced method.

2.2 Uncertainty assessment using non-parametric tolerance limits

Once a sample of the code output has been taken, a statistical inference of the output population parameters is performed. During recent years, it has been common in the field of nuclear reactor safety to use the theory of non-parametric tolerance limits for the assessment of code output uncertainty. This approach, proposed by Gesellschaft für Anlagen- und Reaktorsicherheit (GRS) [17], is based on the work done by Wilks [18,19] to obtain the minimum sample size in order to infer a certain coverage of a population, with a certain confidence. One first assumes that the uncertainty assessment is only performed in one output parameter. For the one-sided tolerance limit case, where $\beta \times 100$ (%) represents the confidence level that the maximum code result will not be exceeded with an $\alpha \times 100$ (%) probability, the required sample size *n* is given by [20]:

$$1 - \alpha^n \geq \beta \tag{2.10}$$

This means that once the output sample is ranked, the maximum value of the sample infers the $\alpha \times 100$ percentile of the output population with a $\beta \times 100$ (%) of confidence. For example, for an estimation of the 95th percentile with a 95% of confidence a sample of 59 elements is required.

For the two-sided case, where the coverage of the output population is expected to be inferred from the $(100 - (\alpha \times 100))$ percentile to the $(\alpha \times 100)$ percentile with a $\beta \times 100$ (%) of confidence, the minimum sample size is given by the following implicit equation [20]:

$$1 - \alpha^n - n(1-\alpha)\alpha^{n-1} \geq \beta \tag{2.11}$$

For example, if the 5th and 95th percentiles of the population are to be inferred with a 95% of confidence, a sample size of 93 elements is required. It should be noticed that this analysis is solely based on the number of samples and applies to any kind of PDF the output may follow. Also, since the input space is only used as an indirect way to sample the output space, the use of non-parametric tolerance limits is independent from the number of uncertain input parameters. When

the code output is comprised by several variables that depend on each other, the uncertainty assessment should be based on the theory of multivariate tolerance limits. Wald [21,22] was the first to analyze the statistical coverage of a joint distribution-free PDF. In Guba et. al. [23], the concern about assessing separate tolerance limits to statistically dependent outputs was raised within the nuclear reactor safety community. In this work, it was shown that the general equation developed by Noether [24] for simultaneous upper and lower tolerance limits can be used to determine the minimum sample size required to cover, in a distribution-free manner, a joint PDF depending on the number of output variables. Such equation reads as follows:

$$\sum_{i=0}^{r+m-1} \binom{n}{i} (1-\alpha)^i \alpha^{n-i} \leq 1-\beta \tag{2.12}$$

Where *r* is related to the number of upper tolerance limits and *m* is related to the number of lower tolerance limits to be assessed. For instance, in the case of two-sided tolerance limits for a single variable, $r = m = 1$ and Eq. (2.12) turns out to be the same as Eq. (2.11). On the other hand, for the case of one-sided tolerance limit (i.e. upper limit) of a single variable, $r = 1$ and $m = 0$ and Eq. (2.12) will be the same as Eq. (2.10). Therefore, if a two-sided uncertainty assessment is going to be performed to 2 statistically dependent output variables then $r = m = 2$, and so on. It should be noticed that the sample size in the multivariate case depends on the correlation among the different parameters. Guba et. al. [23] exemplified this fact for a bivariate normal distribution. It was then shown that if the variables were highly correlated, the required sample size to cover the joint PDF is smaller than for the poorly correlated case. Nevertheless, if nothing is known about the output space PDF, Eq. (2.12) would give the required sample size for the desired multivariate coverage with a desired confidence independently of the correlation (or covariance) among the output parameters. This is a very powerful statistically significant way to assess uncertainty in the design of computational experiments since in general, nothing is known about the PDF from which the calculations are coming from.

Other authors have done some work deriving the minimum sample size for multivariate non-parametric tolerance limits, such as the equation presented by Scheffé et. al. [25]:

$$n = (r+m)\frac{\left(\frac{\chi^2_{\alpha,2(r+m)}}{2(r+m)} - 1\right)\sqrt{\beta} + 1}{1-\beta} \tag{2.13}$$

Where $\chi^2_{\alpha,2(r+m)}$ is the value of the χ^2-distribution with $2(r+m)$ degrees of freedom. Ackermann et. al. [26] tabulated Eq. (2.13) as a function of the desired coverage and confidence, respectively, for a large number of tolerance limits the space in study may be comprised with. These tables are in agreement with for instance, table No. 4 shown in [23] with respect to the solution of Eq. (2.12) for the two-sided case and up to 3 variables in question.

2.3 LHS and the uncertainty assessment based on non-parametric tolerance limits

Michael McKay, one of the creators of LHS, stated in reference [27] that there are no exact methods for constructing tolerance intervals for an output using LHS. It is claimed there that the output values from an LHS do not constitute a random sample from its distribution. Nevertheless, other authors [5,28] have suggested that the use of LHS applied to the inference of code output tolerance limits in a non-parametric way is valid. In this thesis, these are the following reasons why it is believed that LHS can be used to estimate tolerance limits in the field of computational experiments:

1) LHS does not restrict the stratification to any particular region of the input space. Moreover, the intention of LHS is to cover in a more efficient way the dimensions of the different input parameters than with SRS, when the sample size is the same.
2) The individual parameters are the ones that are stratified along their possible ranges of variation, but the different permutations are taken randomly. Therefore, it can be assumed that the output sample is a random sample of the output population. Even if LHS is employed, the different code outputs are independent samples of the same distribution (e.g. i.i.d samples).
3) The concept of tolerance limits applied to the code uncertainty assessment does not assume any kind of parametric distribution of the code output space, and is only founded in the ranking of a statistically significant number of samples. If LHS is used to cover much better the input space and ergo, much better to handle the code non-linearities, the intention is to try to infer more realistic output percentiles that the ones SRS might infer for the same sample size, and for the same level of confidence.

It should be recalled that LHS was created as a variance reduction technique, where the main objective was to reduce the number of code runs of complex and time consuming physical models. However, just as stated by Matala in [28], there is no reason to think that for the same sample size, LHS would not have as much coverage as SRS with the same statistical confidence.

CHAPTER 3

UNCERTAINTY AND SENSITIVITY ANALYSIS APPLIED TO LATTICE CALCULATIONS

"We turned the switch, saw the flashes, watched for ten minutes, then switched everything off and went home. That night I knew the world was headed for sorrow."

Leo Szilard, reflecting on the first nuclear chain reaction

In the current procedure for light water reactor analysis, during the first stage of the neutronic calculations, the so-called lattice code is used to calculate the neutron flux distribution over a specified region of the reactor lattice by solving deterministically the transport equation. This region may be a fuel pin or a fuel assembly, modeled in one or two dimensions, respectively. The calculated neutron flux may be used to get sets of macroscopic cross-sections homogenized and condensed over chosen sub regions and in a chosen broad energy group structure. These are used as input material data for other codes solving the neutron transport or diffusion equation, over the whole reactor or any fraction of it.

Lattice calculations use nuclear libraries as input basis data, describing the properties of nuclei and the fundamental physical relationships governing their interactions (e.g. cross-sections, half-lives, decay modes and decay radiation properties, γ rays from radio nuclides, etc.). Experimental measurements on accelerators and/or estimated values from nuclear physics models are the source of information of these libraries. Once evaluated, the nuclear data are added in a specific format to so-called evaluated nuclear data files, such as ENDF-6 (Evaluated Nuclear Data File-6). The information of the evaluation files can differ because they are produced by different working groups all around the world (e.g. ENDF/B for the USA, JEFF for Europe, JENDL for Japan, BROND for Russia, etc.). The data can be of different types, containing an arbitrary number of nuclear data sets for each isotope, or only one recommended evaluation made of all the nuclear reactions for each isotope. Finally, these data are fed to a cross section processing code such as NJOY [29], which produces the isotopic cross section library used by the lattice code. This process can create a multi-group library specifically formatted for the lattice code in use. For instance, Hébert [30] developed a nuclear data library production system that recovers and formats nuclear data required by the advanced lattice code DRAGON version 4. For these purposes, a new post-processing module known as DRAGR was included in NJOY99, which is capable of creating the so called DRAGLIB nuclear data library for the DRAGONv4.05 code.

In the major nuclear data libraries (NDLs) created around the world, the evaluation of nuclear data uncertainty is included as data covariance matrices. The covariance data files provide the estimated variance for the individual data as well as any correlation that may exists. The uncertainty evaluations are developed utilizing information from experimental cross-section data, integral data (critical assemblies), and nuclear models and theory. The covariance is given with respect to point-wise cross-section data and/or with respect to resonance parameters. Thus, if such uncertainties are intended to be propagated through deterministic lattice calculations, a processing method/code must be used to convert the energy-dependent covariance information into a multi-group format. For example, the ERRORJ module of NJOY99 or the PUFF-IV code are able to process the covariance for cross-sections including resonance parameters, and generate any desired multi-group correlation matrix.

In this chapter, microscopic cross-section uncertainties in multi-group format that were computed with ERRORJ are presented for important LWRs nuclides. Such multi-group uncertainties are based on two modern NDLs: JENDL-4 and the recently released ENDF/B-VII.1. The intention is to compare the size of the variances computed with different libraries for many nuclides and reactions. These variances define the uncertain input space dimensions, and the microscopic cross-sections of certain isotopes of various elements belonging to the 172 groups DRAGLIB library format are considered as normal random variables. Multi-group nuclide uncertainty is propagated through the DRAGONv4.05 code in order to assess the output uncertainty on k_∞ and on the different 2-group homogenized macroscopic cross-sections. This is performed on two different PWR lattice exercises, as shown hereafter.

3.1 Multigroup uncertainty based on JENDL-4 and ENDF/B-VII.1

The uncertainty information in the major NDLs is included in the so called "covariance files" within the ENDF-6 formalism. The following covariance files are defined:

- Data covariances for number of neutrons per fission (MF31)
- Data covariances for resonance parameters (MF32)
- Data covariances for reaction cross-sections (MF33)
- Data covariances for angular distributions (MF34)
- Data covariances for energy distributions (MF35)

To propagate nuclear data uncertainties in reactor lattice calculations, it is necessary to begin by converting energy-dependent covariance information in ENDF format into multi-group form. This task can be performed conveniently within the latest updates of NJOY99 by means of the ERRORJ module. In particular, ERRORJ is able to process the covariance data of the Reich-Moore resolved resonance parameters, the unresolved resonance parameters, the *P1* component of the elastic scattering cross-section and the secondary neutron energy distributions of the fission reactions [31]. ERRORJ was originally developed by Kosako [32] as an improvement of the original ERRORR module in order to calculate self-shielded multi-group cross-sections, as well as the associated correlation coefficients. These data are obtained by combining absolute or relative covariances from ENDF files with an already existing cross-section library, which contains multi-group data from the GROUPR module.

In the presence of narrow resonances, GROUPR handles self-shielding through the use of the Bondarenko model [29]. To obtain the part of the flux that provides self-shielding for the isotope *i,* it is assumed that all other isotopes are represented with a constant background cross-section σ_0. Therefore, at resonances the flux takes the following form:

$$\phi^i(E) = \frac{C(E)}{\sigma^i(E) + \sigma_0} \tag{3.1}$$

The most important input parameters to ERRORJ are the smooth weighting function *C(E)* and the background cross-section σ_0. It should be noticed that these are assumed to be free of uncertainty.

In this section, results of the ERRORJ module are shown from figures 3.1 to 3.3, respectively, for important reactions of 3 important nuclides: ^1H, ^{235}U and ^{238}U. Results for ^1H are based on JENDL-3.3 data since JENDL-4 does not contain uncertainty information for this isotope. The value of the microscopic cross-sections and their relative variances in percentage were computed for an energy-

grid of 172 groups by using a weighting flux that corresponds to the $1/E + fission\ spectrum + thermal\ maxwellian$ shape. For all cases, an infinite dilution condition was assumed (i.e. $\sigma_0 = 1 \times 10^{10}$ barns) and the temperature was considered to be 293 K. For each figure, the plot on the top corresponds to the multi-group relative variances, while the plot on the right shows the actual nominal value of the cross-section. The correlation matrix appears in the center. All the important reactions of these and more nuclides can be found in paper No. 2.

a) JENDL-3.3 *b) ENDF/B-VII.1*

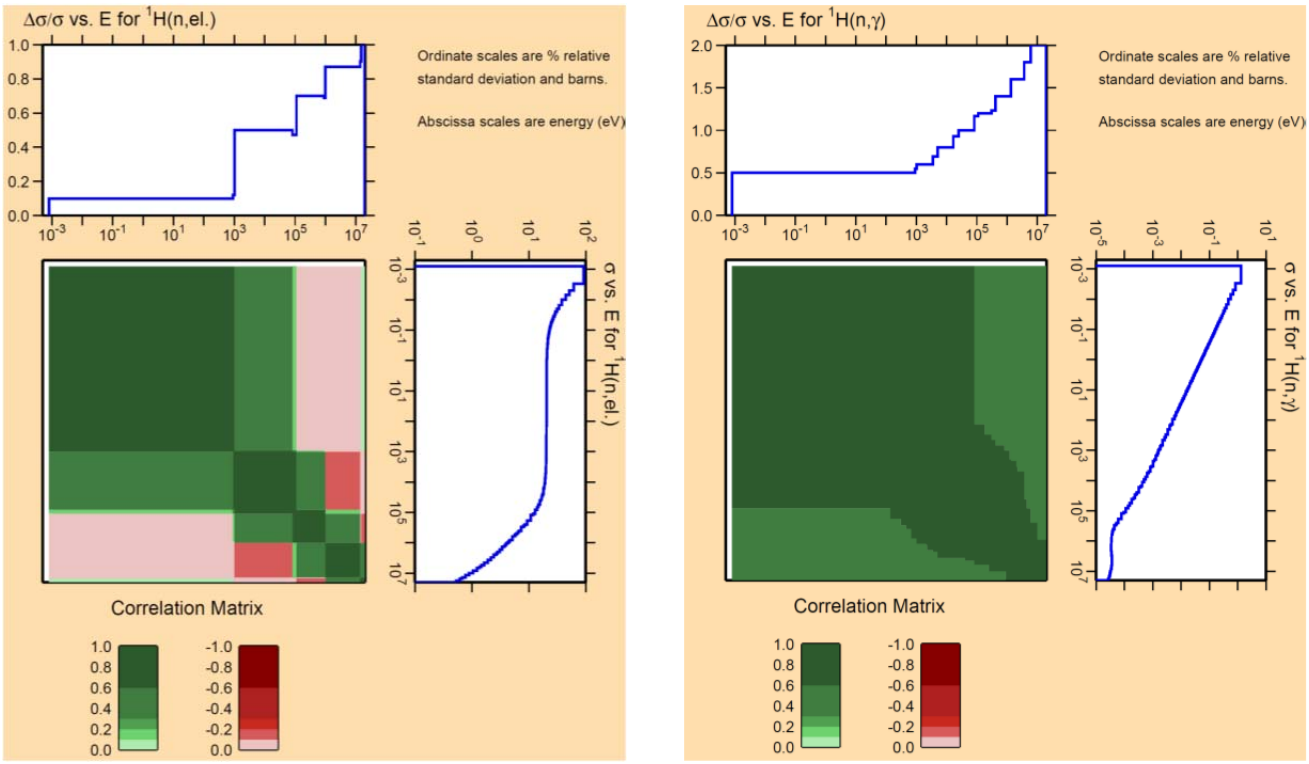

Fig. 3.1. Covariance plot for $^1H(n, el.)$ based on a) JENDL-3.3 and b) ENDF/B-VII.1

a) JENDL-4 *b) ENDF/B-VII.1*

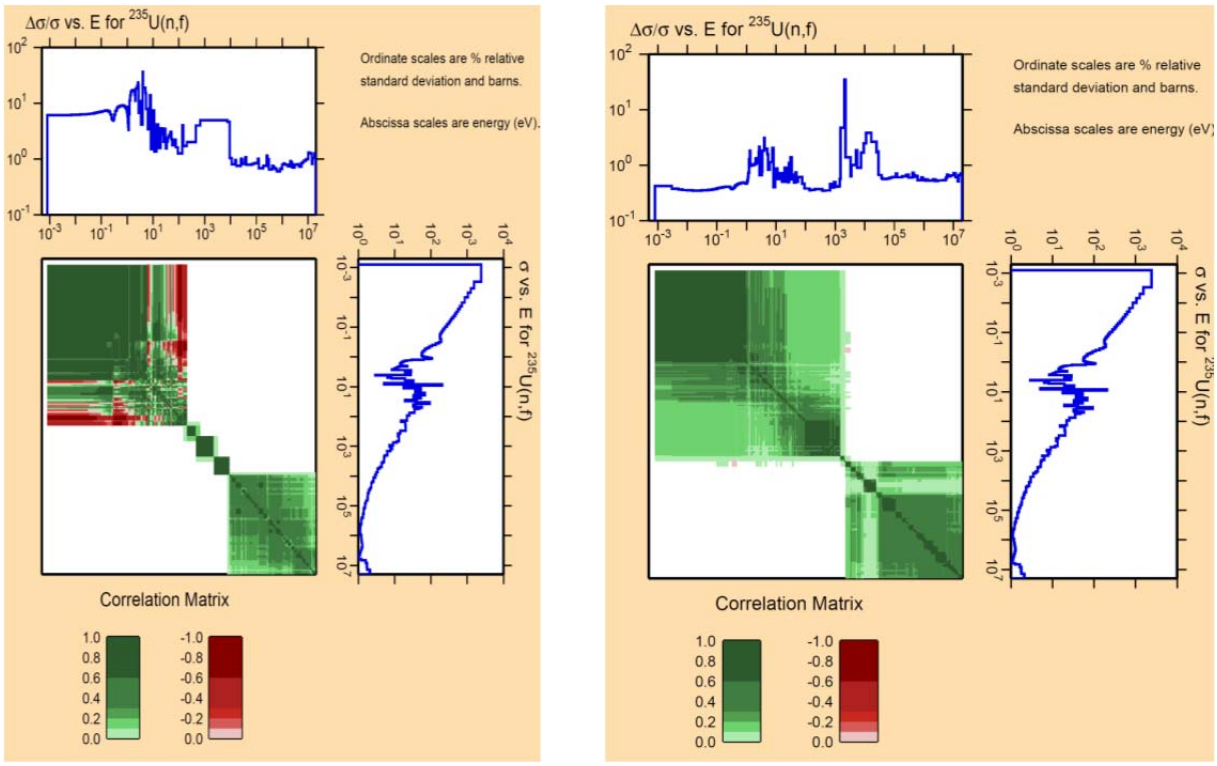

Fig. 3.2. Covariance plot for $^{235}U(n, fission)$ based on a) JENDL-4 and b) ENDF/B-VII.1

a) JENDL-4 *b) ENDF/B-VII.1*

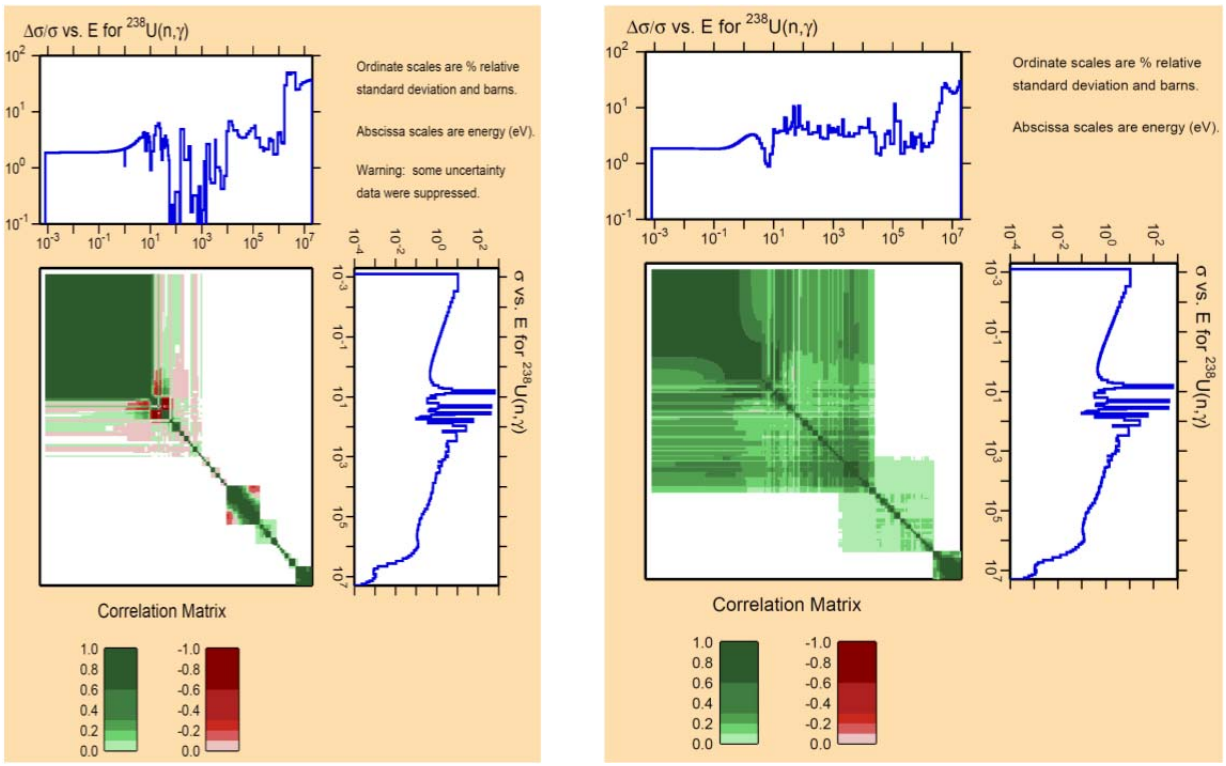

Fig. 3.3. Covariance plot for $^{238}U(n, \gamma)$ based on a) JENDL-4 and b) ENDF/B-VII.1

As seen in the previous figures, for each cross-section of a given nuclide, the variability of the probability of interaction at a certain energy group is related to the probability of interactions at other energy groups since the same measuring equipment was used when determining such probabilities. Such correlation can be studied through the self-reaction covariance matrix. In the same way, the variability of the probability of interaction at a certain energy group of a certain type of reaction, is also related to the probability of interaction of a second type of reaction at the same energy group due to the same reason as above. Such correlation can be studied through the multi-reaction covariance matrix.

An important issue that was noticed while computing the different reaction covariances was the fact that resonance uncertainties in JENDL-4 are absolute. This means that self-shielded relative variances (or relative standard deviations) will change as a function of temperature and dilution at the resonant groups. This is illustrated in papers No. 1 and No.2, where relative standard deviations at the resonant groups for different background cross-sections were computed for the $^{235}U(n,f)$ and $^{238}U(n,\gamma)$ reactions. This fact is supported by the results obtained by Chiba et. al. [33], where a dependency between relative multi-group covariances and background cross-sections at the resonances was observed when JENDL-3.2 data were employed. This is very important to take into account when sampling the different isotopic reactions, because just as the nominal cross-sections are self-shielded, their respective variances should be self-shielded as well. However, JENDL-4 data does not exhibit a temperature-dilution dependence of the variances at the resonances of important actinides. Nevertheless, in this thesis, absolute variances at the resonances were self-shielded, assuming that the relative variances do not change as a function of temperature nor dilution.

Regarding the ENDF/B-VII.1 resonant uncertainties, only an absolute dependency was observed, leaving the relative terms intact for any temperature and/or dilution conditions. This is an important issue, because as will be seen in the next sections, it is very easy to implement the perturbation methodology based on relative uncertainties.

3.2 Determination of the sample size according to two-group diffusion theory

Since uncertainty analysis in this work is performed on both k_∞ and homogeneized two-group macroscopic cross-sections, the minimum sample size to assess multivariate uncertainty based in non-parametric tolerance limits is dependent on the number of macroscopic cross-sections that are required to calculate k_∞. For example, by following the solution of the two-group diffusion equation in a homogenous system and applying vacuum boundary conditions [34], the well-known four factor formula can be derived:

$$k_\infty = \varepsilon p f \eta = \frac{\upsilon\Sigma_{f,2} + \upsilon\Sigma_{f,1} \cdot \left(\frac{\Sigma_{a,2}}{\Sigma_r}\right)}{\Sigma_{a,2}} \times \frac{\Sigma_r}{\Sigma_r + \Sigma_{a,1}} \tag{3.2}$$

It is common that thermal up-scattering is not present and thus, $\Sigma_r = \Sigma_{s0,1\to2}$. Therefore, when assessing the covariances between k_∞ and the two-group macroscopic cross-sections, a minimum of 6 output parameters are in question (i.e. $\upsilon\Sigma_{f,1}$, $\upsilon\Sigma_{f,2}$, $\Sigma_{a,1}$, $\Sigma_{a,2}$, $\Sigma_{s0,1\to2}$ and k_∞). According to table 1b present in [26], for a two-sided 95% coverage of 6 variables with a 95% of confidence, a minimum of 361 samples are required. Nevertheless, if the uncertainty assessment is extended to other parameters such as diffusion coefficients, a sample size of 410 elements is needed, because diffusion coefficients are related to k_∞ through the transport cross-section. Therefore, since one of the main goals of performing lattice calculations is to prepare a set of homogenized and energy collapsed parameters for any further core analysis, the output sample for the multivariate uncertainty analysis should contain at least 410 elements.

3.3 Main features of the DRAGON code and the DRAGLIB library

The DRAGON code is the result of an effort made at *École Polytechnique de Montréal* to rationalize and unify the different models and algorithms used to solve the neutron transport equation into a single code.

The management of a cross-section library requires capabilities to add, remove or replace an isotope, and the capability to reconfigure the burnup data without re-computing the complete library. For these purposes, DRAGR was developed by Hébert [30], and is an interface module to perform all these functions while maintaining full compatibility with NJOY99 and its further improvements. DRAGR produces DRAGLIB, a direct access cross section library in a self-described format that is compatible with DRAGON or with any lattice code supporting that format. The DRAGR Fortran module was written as a clean and direct utility that makes use of the NJOY modules PENDF and GENDF. For each nuclide within DRAGLIB, the cross-sections for the following neutron-interaction reactions are described: *(n,total), (n,elastic), (n,2n), (n,3n), (n,4n), (n, fission), (n,gamma)*. Also, Nu-Sigma-Fission, the released neutron energy spectrum *(CHI)*, and the *P0* and *P1* scattering matrices are included. Since the uncertainty study reported hereafter is either based on JENDL-4 data or JENDL-4 and ENDF/B-VII.1 data, DRAGLIB libraries of 172 groups were needed to be produced using JENDL-4 and ENDF/B-VII.1 information for different temperatures and background cross-sections. The first 79 groups correspond to the thermal region; the next 46 groups correspond to the resonant region and the last 47 groups correspond to the fast region. An example of microscopic cross-sections for different reactions included in DRAGLIB can be found in figures 3.1, 3.2 and 3.3 for ^{1}H, ^{235}U and ^{238}U, respectively. These cross-sections were calculated at 293 K and considering an infinite dilution.

The DRAGON code solves the multi-group transport equation at the pin cell level using the collision probability theory, and at the fuel assembly level by means of the method of characteristics. In its integro-differential form, the zero-level transport corrected multi-group equation is given by:

$$\overline{\Omega}\cdot\nabla\phi_g(\boldsymbol{r},\overline{\Omega})+\Sigma^0_{T,g}\phi_g(\boldsymbol{r},\overline{\Omega})=\frac{1}{4\pi}\sum_{g'=1}^{G}\Sigma^0_{s,g'\to g}\phi_{g'}(\boldsymbol{r})+\frac{\chi_g}{4\pi k}\sum_{g'=1}^{G}\bar{\nu}_{g'}\Sigma_{f,g'}\phi_{g'}(\boldsymbol{r}),$$

$$g=1,\dots,G \tag{3.3}$$

The left hand side of Eq. (3.3) is related to how neutrons disappear in space by leakage and any absorption or scattering reaction at the group *g*, while the right hand side is related to how neutrons are being produced at the *g* energy level through the sum of the scattering and fission contributions coming from the different neutron energy groups. Then, the input uncertain space is composed by the different microscopic cross-sections, χ_g and $\overline{\upsilon_g}$. If any statistical perturbation on a type of reaction is going to be made in one side of the transport equation, it should be somehow propagated to the other side as well in order to preserve the neutron balance. However, some uncertainty information (depending on the type of reaction and nuclide in question) cannot be directly computed directly from the NDLs. For example, straightforward covariances cannot be obtained for the scattering matrices, and so on. Therefore, in this thesis, different methodologies were derived for a proper propagation of microscopic cross-section uncertainty, which are detailed in the next sub-sections.

3.3.1 Uncertainty analysis of the scattering cross-section

The scattering source can be expanded as:

$$S^g = \frac{1}{4\pi}\sum_{g'=1}^{G}\Sigma^0_{s,g'\to g}\phi_{g'}(\boldsymbol{r}) = \frac{1}{4\pi}\sum_{x=1}^{2}\sum_{j}N_j\sum_{g'=1}^{G}\sigma^0_{x,j,g'\to g}\phi_{g'}(\boldsymbol{r}) \tag{3.4}$$

Where the *x*-index indicates if the reaction is elastic or inelastic, and *j* refers to the nuclide index. In general, the *P0* and *P1* scattering matrices in multi-group format computed by NJOY are based, within the ENDF-6 formalism, on the MF=6 file which accounts for energy-angle distributions of different reactions. For example, the MT=2 reaction is considered for elastic scattering, while all the reactions that are present in the file between MT=51 and MT=91 should be taken into account for inelastic scattering.

One can start by analyzing the *P0* matrix. For the nominal case, the following relationship between energy-integrated cross-sections and the scattering matrix can be derived:

$$\sigma_{x0,j,g\to g'} = p_{x0,j,g\to g'}\sigma_{x0,j,g} \quad \Rightarrow$$

$$p_{x0,j,g\to g'} = \frac{\sigma_{x0,j,g\to g'}}{\sigma_{x0,j,g}} \tag{3.5}$$

Since uncertainties are only given to the isotropic scattering reaction $\sigma_{x0,j,g}$, an approximation was derived to propagate any sampling of the form $\sigma^{(*)}_{x0,j,g}$ through the scattering matrix. By assuming that the nominal transfer matrix $p_{x0,j,g\to g'}$ remains constant, such uncertainty propagation takes the following form:

$$\sigma^{(*)}_{x0,j,g\to g'} = p_{x0,j,g\to g'}\sigma^{(*)}_{x0,j,g} \tag{3.6}$$

In the nominal case of the transport corrected version, a degree of linear anisotropy can be taken into account by modifying the diagonal of the scattering matrix as follows:

$$\sigma^0_{x,j,g\to g} = \sigma_{x0,j,g\to g} - \sigma_{x1,j,g} \Rightarrow$$

$$\sigma^0_{x,j,g\to g} = \sigma_{x0,j,g\to g} - \overline{\mu_g}\sigma_{x0,j,g} \tag{3.7}$$

As explained in papers 1 and 2, uncertainties for the average of the cosine of the scattering angle *mu-bar* are defined in JENDL-4 only for some actinides, while the ENDF/B-VII.1 library does not include any uncertainty information of this parameter. If perturbations are to be considered for *mu-bar*, a direct statistical perturbation of the anisotropic term $\bar{\mu}^{(*)}_g$ can be performed through the use of the *mu-bar* covariance matrix. Therefore, once the terms $\sigma^{(*)}_{x0,j,g\to g}$ are computed with Eq. (3.6), perturbations can now be as well propagated to the transport corrected terms:

$$\sigma^{0\,(*)}_{x,j,g\to g} = \sigma^{(*)}_{x0,j,g\to g} - \bar{\mu}^{(*)}_g\sigma^{(*)}_{x0,j,g} \tag{3.8}$$

Finally, any perturbation should be balanced in the transport equation since the total microscopic cross-section is given by the sum of the absorption and the corrected scattering cross-sections. This means that:

$$\sigma_{j,T,g}^{0\,(*)} = \sigma_{j,a,g}^{(*)} + \sigma_{j,s,g}^{0\,(*)} = \sigma_{j,a,g}^{(*)} + \sum_{x=1}^{2}\sum_{g'=1}^{G} \sigma_{x,j,g\to g'}^{0\,(*)} \tag{3.9}$$

Where the capture and fission perturbations expressed as:

$$\sigma_{j,a,g}^{(*)} = \sigma_{j,c,g}^{(*)} + \sigma_{j,f,g}^{(*)} \tag{3.10}$$

can be directly sampled from the covariance matrices computed with ERRORJ.

3.3.2 Uncertainty analysis of the fission spectrum

Eq. (3.3) is expressed in such a way that the fission spectrum should always satisfy the following normalization condition:

$$\sum_{g=1}^{G} \chi_g = 1 \tag{3.11}$$

If a sample is to be drawn for the different groups, the perturbed spectrum should be carefully re-normalized to unity. In the statistical uncertainty approach, this can be achieved by dividing each of the perturbed group-terms of the spectrum by the sum of all of the perturbed group-terms. For example, for a certain sample, this can be illustrated as follows:

$$\chi_g^{(*,n)} = \frac{\chi_g^{(*)}}{\sum_{g=1}^{G} \chi_g^{(*)}} \tag{3.12}$$

Where the new perturbed fission spectrum will satisfy the normalization condition, i.e.:

$$\sum_{g=1}^{G} \chi_g^{(*,n)} = 1 \tag{3.13}$$

3.4 Sampling the DRAGLIB library

For our study, the multi-group microscopic cross-sections of certain isotopes are treated as random variables following a normal PDF. Therefore, for each cross-section of a given nuclide, the nominal cross-section value at each energy group corresponds to the mean value. The Latin hypercube procedure developed by Iman and Conover that was explained in chapter 2 for sampling correlated variables was followed. This procedure is based not directly on the covariance matrix but instead, on the correlation matrix. Nevertheless, it can be applied in a very straightforward manner because the ERRORJ output can be processed by the NJOYCOVX [35] program in order to obtain directly, for each reaction, the variance of each group and the associated correlation matrices.

Since ERRORJ only can evaluate one dilution at a time, a methodology was developed in this work to shield the cross-sections covariances at all dilutions and temperatures. Due to the fact that ERRORJ gives both the relative and absolute covariance matrices, only one evaluation is necessary at one temperature and one dilution (i.e. infinite dilution and 273 K). Afterwards, it is only required to multiply the cross-sections value at each energy group by the relative multi-group covariance matrix. The flow diagram of this scheme can be found in figure 9 of paper No. 1. In the case of a DRAGLIB based on JENDL-4 data where resonant variances are absolute values, the relative variance at infinite

dilution and at 293 K was considered as a constant value from which, once multiplied by the cross-section at any temperature and dilution, a self-shielded value of the variance will be obtained.

For moderators and some other materials, only (n,γ) and the *P0* matrix are to be perturbed already in the DRALGIB format. It is important to modify the total cross-section according to the different (n,γ) and *P0* perturbations, since the total cross-section is used by the code and the neutron balance must be preserved. For important actinides present in LWRs, the *(n,fission)*, Nu-Sigma-Fission and fission spectrum should be as well modified in DRAGLIB. The total cross-section for these cases should be modified and transport corrected according to Eqs. (3.9) and (3.10). In principle, according to the code developers [36], the transport correction is made at the code level and thus, the total cross-section included in DRAGLIB should only be based on isotropic terms. However, in this implemented statistical methodology, DRAGLIB is modified to include the transport corrected version at each sample and therefore, while performing lattice calculations, a flag must be raised at the input deck level in order to inform the code to not perform the transport correction.

3.5 Uncertainty and sensitivity analysis applied to a 17x17 PWR fuel lattice without poison

This test case, to which the uncertainty analysis as previously explained was applied, corresponds to a 17x17 PWR fuel assembly segment without poison at full power conditions (i.e. pellet temperature at 933 *K)*. This is the test case that is solved in paper No. 1. The input deck of this case corresponds to an example included with the DRAGONv4.05 code package that illustrates how to use the code. Important geometrical rod parameters can be found in table I from paper No. 1.; more information like isotopic composition, etc., can be found in [36]. For the uncertainty analysis presented hereafter, it should be noted that only the following nuclides were statistically perturbed: ^{1}H, ^{16}O, ^{56}Fe, ^{235}U and ^{238}U. The perturbed DRAGLIB of this case is based only on JENDL-4 data; therefore, perturbations were performed to all the reactions, including *mu-bar* for actinides.

One of the goals of this work is to demonstrate in a neutronic application that LHS, indeed, covers much more efficiently the uncertain input space than SRS. Some authors have already proven this by studying the variability of the mean in replicated samples [5], [37]. 10 different k_∞ samples were taken both with LHS and SRS in order to do the aforementioned analysis. The histograms of each sample can be found and are compared in paper No. 1. If the relative uncertainty for k_∞ is defined such as:

$$\frac{\%\Delta k}{k} = \frac{\sigma_{STD}}{\overline{k_\infty}} \times 100 \tag{3.14}$$

The statistical properties and uncertainties of the different samples are presented here in table 3.1, while the standard deviations of the replicated means for both sampling techniques are shown in table 3.2.

Table 3.1. Statistical properties of the different LHS and SRS computed samples

LHS						*SRS*				
Sample	*Min.*	*Max.*	*Mean*	σ_{STD}	$\frac{\%\Delta k}{k}$	*Min.*	*Max.*	*Mean*	σ_{STD}	$\frac{\%\Delta k}{k}$
1	1.23169	1.36461	1.25832	0.02746	2.182	1.23040	1.32691	1.25760	0.01884	1.498
2	1.23161	1.32478	1.25833	0.01578	1.254	1.24525	1.28559	1.25635	0.00865	0.689
3	1.20876	1.29655	1.25795	0.01713	1.362	1.24430	1.31954	1.25813	0.01196	0.952
4	1.23612	1.30328	1.25852	0.01029	0.817	1.23174	1.30801	1.25861	0.01505	1.196
5	1.23445	1.31279	1.25818	0.01299	1.032	1.24690	1.28616	1.25987	0.00737	0.585
6	1.24991	1.30314	1.25845	0.00892	0.708	1.22969	1.33913	1.26092	0.02126	1.686
7	1.23852	1.31699	1.25839	0.01440	1.144	1.24035	1.33274	1.25960	0.01766	1.402
8	1.24588	1.31644	1.25852	0.01266	1.006	1.24969	1.28537	1.26039	0.00688	0.546
9	1.24656	1.30785	1.25850	0.00977	0.776	1.23899	1.33148	1.25743	0.01767	1.405
10	1.24338	1.31244	1.25856	0.01161	0.923	1.23615	1.29056	1.25872	0.01015	0.806

Table 3.2. Statistical properties of the replicated mean

Sampling technique	Replicated mean	σ_{STD} of the replicated mean
LHS	1.25837	0.00018
SRS	1.25876	0.00143

It can be seen that the standard deviation of the replicated mean is almost ten times higher for the SRS case than for the LHS one (i.e. 18 pcm vs. 143 pcm). This is a clear indication that the uncertain input space is much better covered with LHS than with SRS, and that the variability of the computed k_∞ mean is much lower for the LHS case.

The uncertainty analysis is performed by collecting all the samples into a sample of 1,000 elements. Both final samples are shown in figure 3.5, where it can be seen that the highest and lowest values were obtained with LHS. For this particular study, even though it can be said that both samples cover the same space with the same confidence since they have the same number of elements, a more conservative estimation of the population percentiles is achieved with LHS because the computed uncertainties with this technique are simply larger.

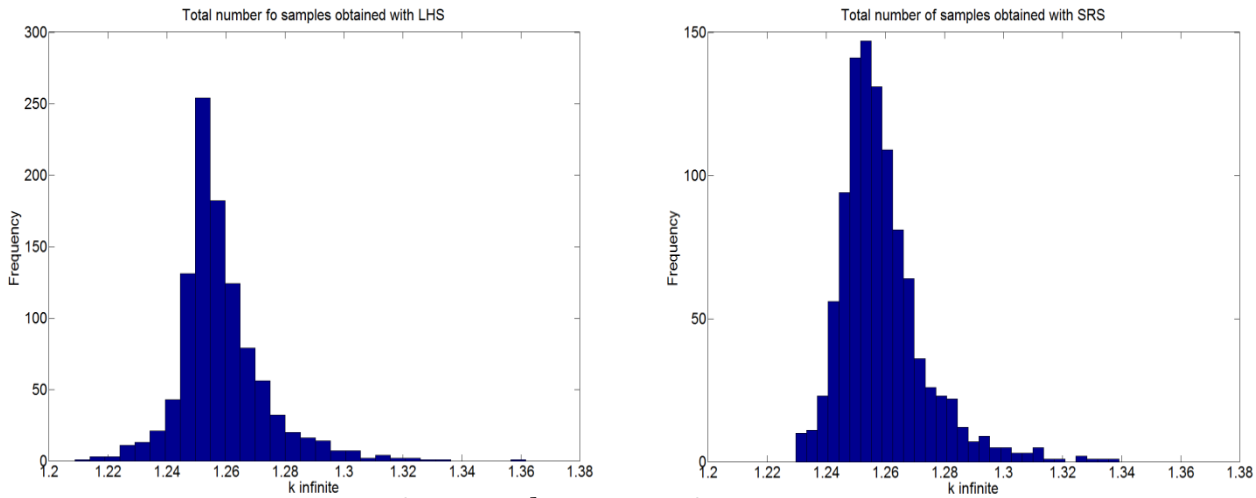

Fig. 3.5. Comparison of the total k_∞ number of samples obtained with LHS and SRS

3.5.1 Uncertainty analysis of k_∞ and two-group macroscopic cross-sections

Because of the advantages of using LHS in lattice calculations, uncertainty results are only presented for this methodology. The final sample of 1,000 elements is significant to cover more than 95% of the output space formed by the different homogenized macroscopic cross-sections and k_∞ with a 95% of confidence, since all one needs is a sample size of 361 as previously explained. In table 3.3, k_∞ results are presented, while for two-group macroscopic cross-sections and diffusion coefficients, uncertainty results are shown in tables 3.4, 3.5 and 3.6, respectively.

Table 3.3. Uncertainty analysis of k_∞

Max. value	*Min. value*	*Mean*	σ_{STD}	$\frac{\%\Delta k}{k}$
1.36461	1.20876	1.25837	0.01493	1.186

Table 3.4. Uncertainty analysis of homogenized macroscopic cross-sections (fast group)

Parameter	*Min. value (1/cm)*	*Max. value (1/cm)*	*Mean (1/cm)*	σ_{STD} *(1/cm)*
Total	0.49235	0.49866	0.49541	90.340e-5
NUSIGF	0.00575	0.00617	0.00593	4.385e-5
Absorption	0.00897	0.00921	0.00908	2.952e-5
Scattering (in- group)	0.46542	0.47172	0.46846	89.250e-5
Scattering (out-group)	0.01762	0.01798	0.01786	4.026e-5

Table 3.5. Uncertainty analysis of homogenized macroscopic cross-sections (thermal group)

Parameter	*Min. value (1/cm)*	*Max. value (1/cm)*	*Mean (1/cm)*	σ_{STD} *(1/cm)*
Total	1.20202	1.21082	1.20601	69.351e-5
NUSIGF	0.09666	0.12090	0.10934	219.901e-5
Absorption	0.06450	0.07406	0.06945	63.296e-5
Scattering (in- group)	1.12795	1.14632	1.13656	130.076e-5
Scattering (out-group)	0	0	0	0

Table 3.6. Uncertainty analysis of fast and thermal diffusion coefficients

	Min. Value (cm)	*Max. Value (cm)*	*Mean (cm)*	σ_{STD} *(cm)*
Fast diffusion coefficient	1.02091	1.10189	1.05758	0.00863
Thermal diffusion coefficient	0.30292	0.30573	0.30448	0.00023

3.5.2 Sensitivity analysis

Due to the fact that the computed uncertainties for k_∞ are high, it will be very useful to know which input parameter has the highest absolute influence on the computation of the tolerance limits. This can be achieved with a "brute" sensitivity analysis, where the output variable is only changing due to a perturbation from a specific parameter. Each important microscopic cross-section for

^{1}H, ^{16}O, ^{56}Fe, ^{235}U and ^{238}U was sampled 100 times. The respective changes on k_∞ are presented in figures 3.6, 3.7 and 3.8 as boxplots. The region represented by the box accounts for 50% of the predicted output sample, whereas the limits of the dashed lines correspond to the 2nd and 98th sample percentiles. Therefore, with 100 calculations, these limits represent 95% of the k_∞ population with at least a 95% confidence.

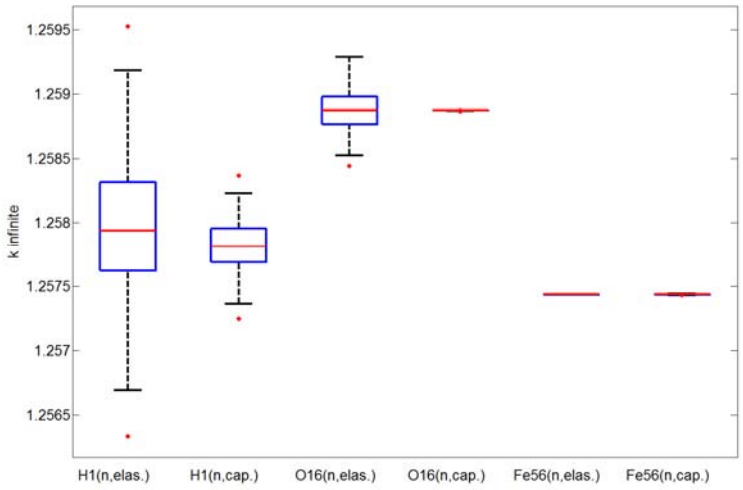

Fig. 3.6. Sensitivity analysis on k_∞ for ^{1}H, ^{16}O and ^{56}Fe microscopic cross-sections

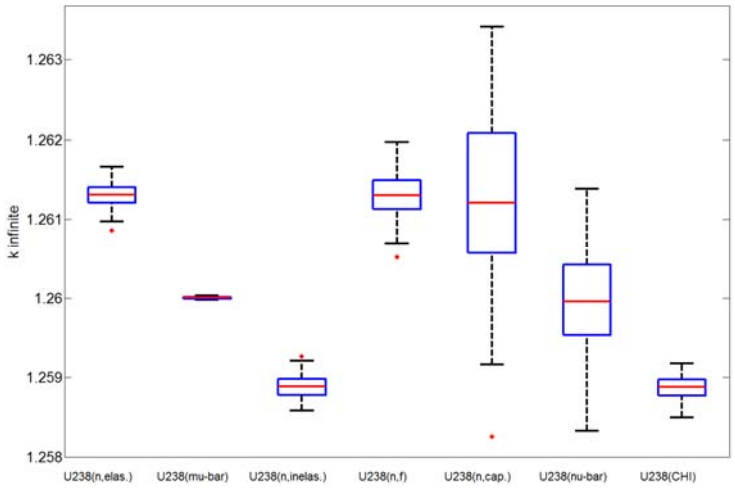

Fig. 3.7. Sensitivity analysis on k_∞ for ^{238}U microscopic cross-sections

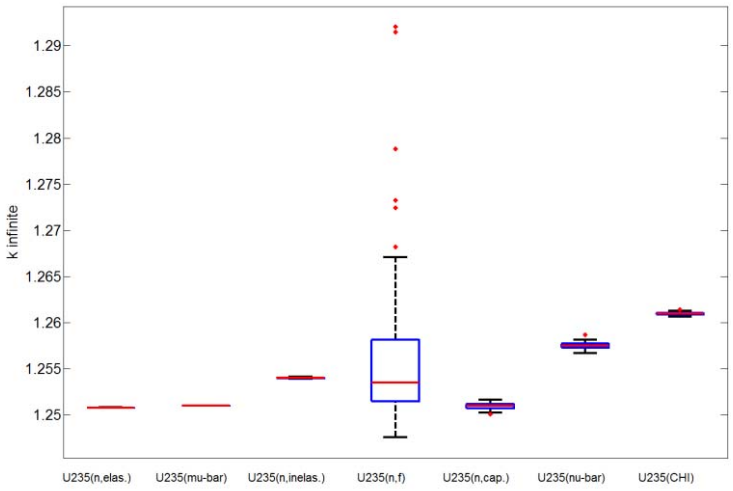

Fig. 3.8. Sensitivity analysis on k_∞ for ^{235}U microscopic cross-sections

By far, the microscopic cross-section with the highest impact on k_∞ corresponds to $^{235}U(n, fission)$. This is highlighted by the outliers (red dots) in figure 3.8. This result supports the fact that the thermal Nu-Sigma-Fission macroscopic cross-section has the highest standard deviation of all homogenized cross-sections. From figure 12, it can be seen that the $^{238}U(n,\gamma)$ reaction has a great impact on k_∞. Some authors have found that this is the most significant reaction in lattice calculations while using the extrapolated SCALE covariance matrices [38], [39]. In fact, it is natural to think that perturbations in the capture microscopic cross-sections should have a considerable impact on k_∞, because these are the only reactions that affect one side of the transport equation. Therefore, the obtained results suggest that the covariance matrix of the $^{235}U(n, fission)$ reaction based on JENDL-4 is very large.

3.6 Uncertainty analysis applied to a 15x15 PWR fuel lattice with poison based on both JENDL-4 and ENDF/B-VII.1 covariance data

This test case corresponds to the Three Mile Island-1 (TMI-1) Exercise I-2 that is included in the neutronics phase (Phase I) of the "Benchmark for Uncertainty Analysis in Modeling (UAM) for design, operation and safety analysis of LWRs", organized and led by the OECD/NEA UAM scientific board [39]. The lattice is a 15x15 PWR fuel assembly segment with poison at full power conditions (i.e. pellet temperature at 900 *K)*. Four fuel pins are doped with gadolinium as a burnable poison. The actual $UO_2 - Gd_2O_3$ fuel has a density of 10.144 g/cm^3, the fuel enrichment is 4.12 w/o and the Gd_2O_3 concentration is 2 wt%. Important geometrical rod parameters, isotopic composition, etc., can be found in [40].

The aim is to propagate the multi-group nuclide uncertainty through the DRAGONv4.05 code, in order to assess and compare the different code outputs uncertainties while using both JENDL-4 and ENDF/B-VII.1 data. These are the main results of paper No. 2. A sample of 450 elements is significant to cover 95% of the output space formed by the different homogenized macroscopic cross-sections, k_∞ and diffusion coefficients with a 95% of confidence, since all one needs is a sample size of 410 as previously explained. Then, uncertainty results for k_∞ are presented in table 3.7. For the two-group macroscopic cross-sections and diffusion coefficients, uncertainty results based on JENDL-4 are shown from tables 3.8 to 3.10, while other results based on ENDF/B-VII.1 are shown from tables 3.11 to 3.13.

Table 3.7. Uncertainty analysis of k_∞

	Max. value	*Min. value*	*Mean*	σ_{STD}	$\frac{\%\Delta k}{k}$
JENDL-4	1.47408	1.36896	1.40101	0.00250	0.178
ENDF/B-VII.1	1.41076	1.38967	1.40236	0.01532	1.094

Table 3.8. Uncertainty analysis of homogenized macroscopic cross-sections (fast group, JENDL-4)

Parameter	*Min. value (1/cm)*	*Max. value (1/cm)*	*Mean (1/cm)*	σ_{STD} *(1/cm)*
NUSIGF	0.00679	0.00719	0.00697	7.341e-05
Absorption	0.00861	0.00895	0.00878	4.124e-05
Scattering (in- group)	0.46812	0.47424	0.47120	81.742e-05
Scattering (out-group)	0.01826	0.01864	0.01851	5.630e-05

Table 3.9. Uncertainty analysis of homogenized macroscopic cross-sections (thermal group, JENDL-4)

Parameter	*Min. value (1/cm)*	*Max. value (1/cm)*	*Mean (1/cm)*	σ_{STD} *(1/cm)*
NUSIGF	0.13188	0.14736	0.13744	219.328e-05
Absorption	0.07938	0.08202	0.08074	29.239e-05
Scattering (in- group)	0.99676	0.99820	0.99734	23.322e-05
Scattering (out-group)	0	0	0	0

Table 3.10. Uncertainty analysis of fast and thermal diffusion coefficients (JENDL-4)

	Min. Value (cm)	*Max. Value (cm)*	*Mean (cm)*	σ_{STD} *(cm)*
Fast diffusion coefficient	1.42150	1.49531	1.45501	0.01118
Thermal diffusion coefficient	0.58332	0.58582	0.58472	0.00042

Table 3.11. Uncertainty analysis of homogenized macroscopic cross-sections (fast group, ENDF/B-VII.1)

Parameter	*Min. value (1/cm)*	*Max. value (1/cm)*	*Mean (1/cm)*	σ_{STD} *(1/cm)*
NUSIGF	0.00689	0.00716	0.006974	2.831e-05
Absorption	0.00868	0.00888	0.00879	2.786e-05
Scattering (in- group)	0.46901	0.47385	0.47127	87.040e-05
Scattering (out-group)	0.01847	0.01859	0.01852	1.794e-05

Table 3.12. Uncertainty analysis of homogenized macroscopic cross-sections (thermal group, ENDF/B-VII.1)

Parameter	*Min. value (1/cm)*	*Max. value (1/cm)*	*Mean (1/cm)*	σ_{STD} *(1/cm)*
NUSIGF	0.136721	0.13750	0.13710	6.904e-05
Absorption	0.08014	0.08103	0.08077	2.904e-05
Scattering (in- group)	0.99708	0.99742	0.99732	2.938e-05
Scattering (out-group)	0	0	0	0

Table 3.13. Uncertainty analysis of fast and thermal diffusion coefficients (ENDF/B-VII.1)

	Min. Value (cm)	*Max. Value (cm)*	*Mean (cm)*	σ_{STD} *(cm)*
Fast diffusion coefficient	1.42330	1.48890	1.45488	0.01123
Thermal diffusion coefficient	0.58439	0.58470	0.58474	0.00005

3.7 Analysis of the results

As can be appreciated from the previous study, computed uncertainties in the output parameters are much higher for the JENDL-4 case, than for the ENDF/B-VII.1 case. For example, the standard deviation of the JENDL-4 Nu-Sigma-Fission cross-section for JENDL-4 is 78 times larger than its ENDF/B-VII.1 counterpart. In the sensitivity study applied to a 17x17 PWR fuel segment and based specifically on JENDL-4, it was found that the most dominant input parameter corresponded to the $^{235}U(n, fission)$ reaction. If one compares the computed ERRORJ variances from both NDLs for such a reaction (see figure 3.2), uncertainties based on JENDL-4 data are much larger than the uncertainties based on ENDF/B-VII.1 up to the energy region of 1000 eV. The effect on the sampling of such microscopic cross-section using both libraries variances can be seen in figure 3.9, where LHS samples of 100 elements were drawn for each case.

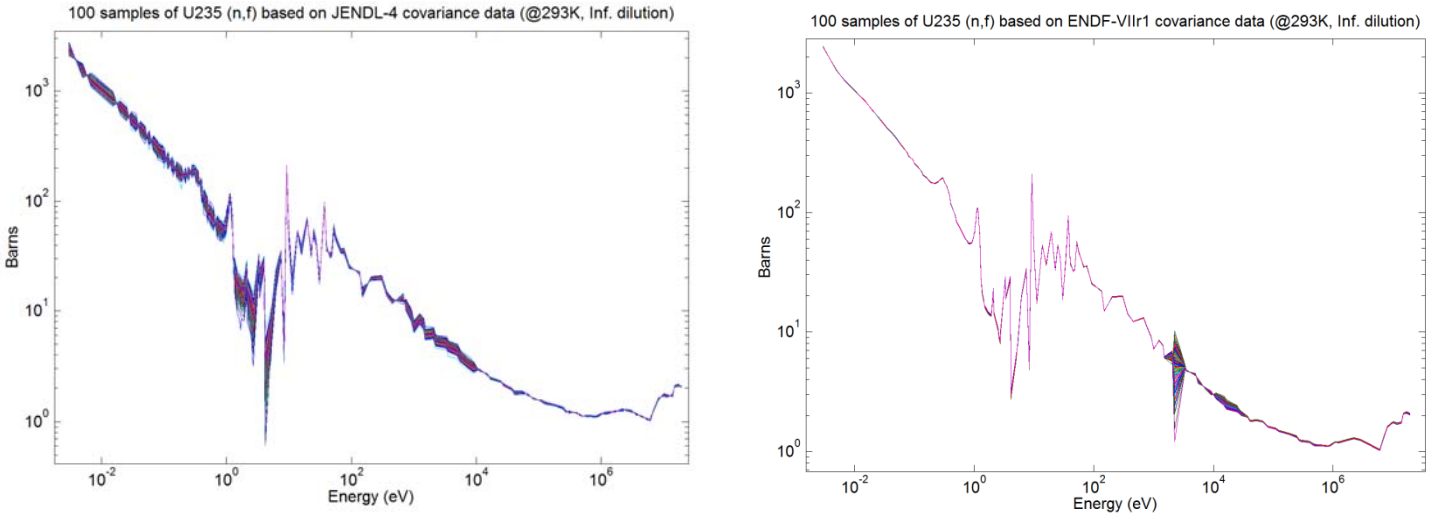

Fig. 3.9. 100 LHS samples taken from the $^{235}U(n, fission)$ cross-section and based on the different JENDL-4 and ENDF/B-VII.1 covariance matrices

A large difference is observed in the spread of the samples for thermal energies and almost up to the last resonant energies. The fact of having large relative variances in JENDL-4 for the thermal groups (~ 7%) compared to small relative variances in ENDF/B-VII.1 (~0.5%), and also large variance differences (up to 10 times) at the resonances, is the cause of such a huge sampling variability between both libraries.

Since uncertainties included in JENDL-4 for $^{235}U(n, fission)$ are very high compared with for instance, the ones included in the ENDF/B-VII.1 library, such a reaction becomes the most dominant. As mentioned before, it is natural to think that capture cross-sections has a big impact on lattice calculations, since it is the only reaction that imbalance only one side of the neutron transport equation (i.e. disappearance at a certain energy group). Nevertheless, unfair uncertainties among different input reactions make the uncertainty computations to be very biased.

CHAPTER 4

FORWARD AND INVERSE UNCERTAINTY ANALYSIS APPLIED TO NEUTRONIC CORE SIMULATORS

"Inside every nonBayesian there is a Bayesian struggling to get out"

Dennis V. Lindley

During recent years, fuel loading strategies of many nuclear power plants have been based on best estimate (BE) calculations, allowing an optimization of the fuel depletion efficiency along the different cycles of the plant life. At the beginning of the pattern design of any plant cycle, a set of macroscopic cross-sections are computed for the different fuel segment types that comprise each of the core fuel assemblies. As seen in chapter 3, such homogenized and energy-collapsed macroscopic cross-sections and diffusion coefficients can be obtained by means of a lattice code. Once these parameters are functionalized and discretized as a function of reactor state-variables such as moderator temperature and density, fuel temperature, burnup, history variables, etc., they are used as inputs to the BE core simulators. In general, core simulators aim to solve the nodal two-group diffusion equation in order to predict the spatial dependence of the scalar neutron flux at every burnup point within a cycle. This calculation is not only fundamental to achieve the desired energetic efficiency but also to ensure that the safety limiting parameters are never exceeded along the cycle, since the thermal flux is proportional to the produced thermal power.

Ringhals 1 (R1) is an ASEA-Atom Boling Water Reactor (BWR) located at the Ringhals power plant complex in western Sweden. It employs the Westinghouse POLCA7 core simulator for the design of the reactor fuel cycle, and utilizes the so-called Core Master 2 (CM2) graphical interface to store and analyze the data of past and future cycles. CM2 is a practical tool where a view of the nodalized core is available, and nodal, assembly or core thermal-hydraulic parameters, thermal margins, power and critical power ratio (CPR) (among others) are easily displayed. CM2 is part of the Westinghouse software for reactor analysis [41] that interacts and calls POLCA7 in order to calculate desired parameters at any burnup point within a cycle. 36 traversing incore prove (TIP) detectors are permanently positioned within the R1 core, and during each cycle a few TIP measurements at different burnup conditions are performed in order to estimate the actual spatial core neutron flux and thus, the core power and thermal margins. Therefore, the accuracy of core simulator calculations along the cycle can be assessed by computing the difference between predicted and measured quantities. Such procedure builds confidence in using the simulator for the long term fuel loading plans.

In this chapter, two types of uncertainty analyses are performed on core simulations. The first one corresponds to the forward approach of input uncertainty propagation, where the input uncertain space formed by the nodal two-group macroscopic cross sections and diffusion coefficients is sampled both with SRS and LHS. The possible ranges of variation of such input space are based on data from the depletion calculation corresponding to the cycle 26 of R1. The aim of this study is to compare the efficiency of the uncertainty assessment performed on the nodal thermal flux when SRS and LHS are employed. On the other hand, in the second type of uncertainty analysis presented in this chapter, discrepancies between spatial measured and calculated fluxes in R1 are used to perform an inverse uncertainty analysis on the spatial dependence of the different core parameters. This analysis is carried out using Bayesian statistics, where, for a certain cycle, the frequency distributions

of macroscopic cross-sections and diffusion coefficients at every assembly node are updated based on the error distribution of the spatial thermal flux. Finally, the bootstrap method is employed to estimate a multivariate linear regression model of the space formed between nodal macroscopic cross-sections and core reactor state variables. Nodal cross-sections are sampled from posterior probability density functions (PDFs) that were obtained from the BWR core Bayesian uncertainty analysis.

4.1 Uncertainty analysis applied to the thermal neutron flux predictions using SRS and LHS

4.1.1 Creation of the input uncertain space

The input uncertain space is formed by the thermal and fast absorption and fission cross-sections, removal cross-section, energy released by fission (κ), average number of neutrons per fission (ν) and diffusion coefficients per node. The dimensions of such a space are based on the R1-cycle 26 depletion calculation. 62 different Equivalent Full Power Hour (EFPH) points compose the core burnup distribution of such a cycle, and at each of these points nodal information of the different core parameters can be extracted by the POLUT model of POLCA7. Therefore, the mean and standard deviation of the nodal core parameters, which are now considered as normal random variables, are obtained from the samples formed by the different 62 EFPH points at each node. The aim is to perform an uncertainty study based on information from the whole cycle. For example, the tree format of cycle 26 in CM2 is shown in figure 4.1, where different EFPH points are illustrated.

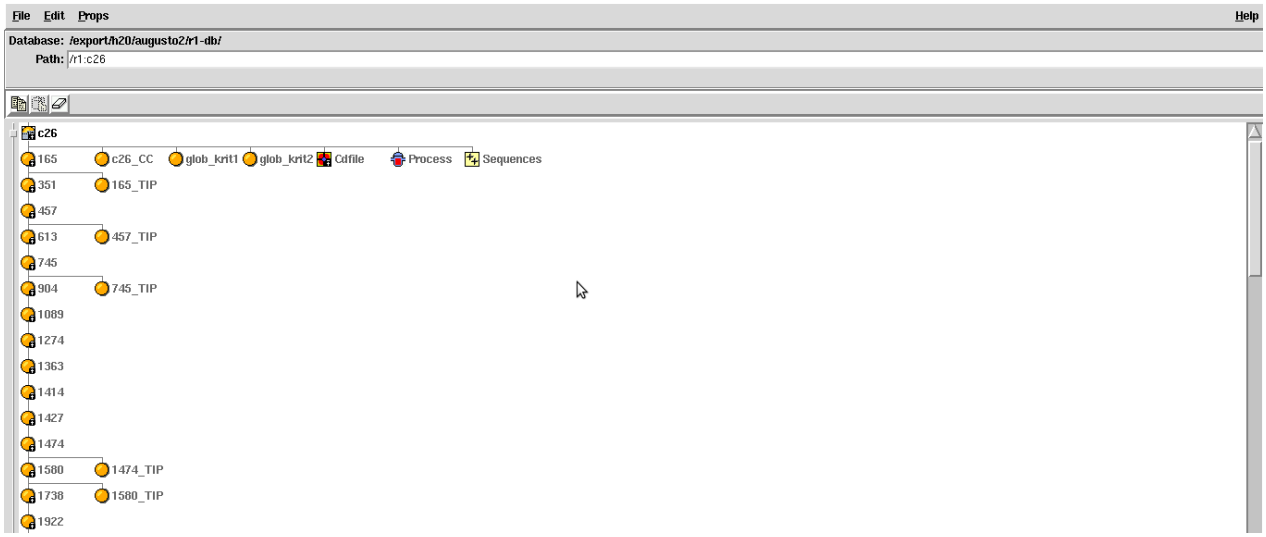

Fig 4.1. Core Master 2 burnup distribution of Ringhals 1, cycle 26

Meanwhile, in figure 4.2, a radial distribution of the core relative power is shown at a point of 904 EFPH. As highlighted in figure 4.2, each colored square represents an active fuel assembly, where the total X-Y mesh is 30 by 30. The core is composed by 648 fuel assemblies, and each assembly has been discretized in 25 axial nodes. As an example of the aforementioned methodology, the 3D nodal distribution of the mean and standard deviation of the thermal absorption macroscopic cross-section based on the depletion calculation of cycle 26 is shown in figure 4.3.

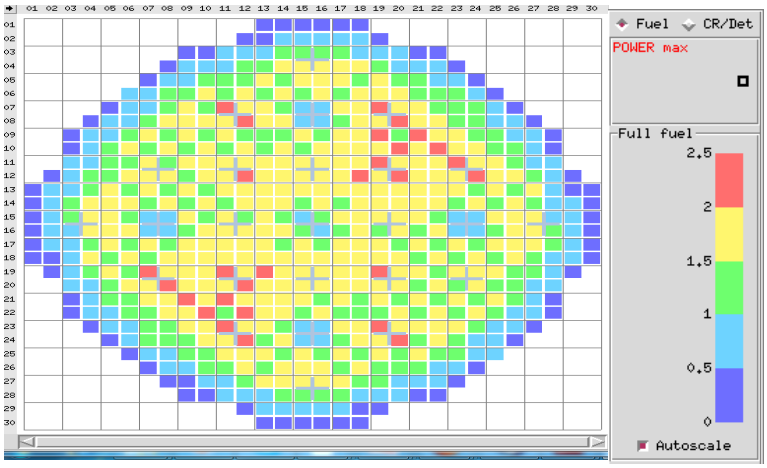

Fig 4.2. Axially-averaged power distribution of R1 (Cycle 26, 904 EFPH) calculated with POLCA7 and displayed by CM2

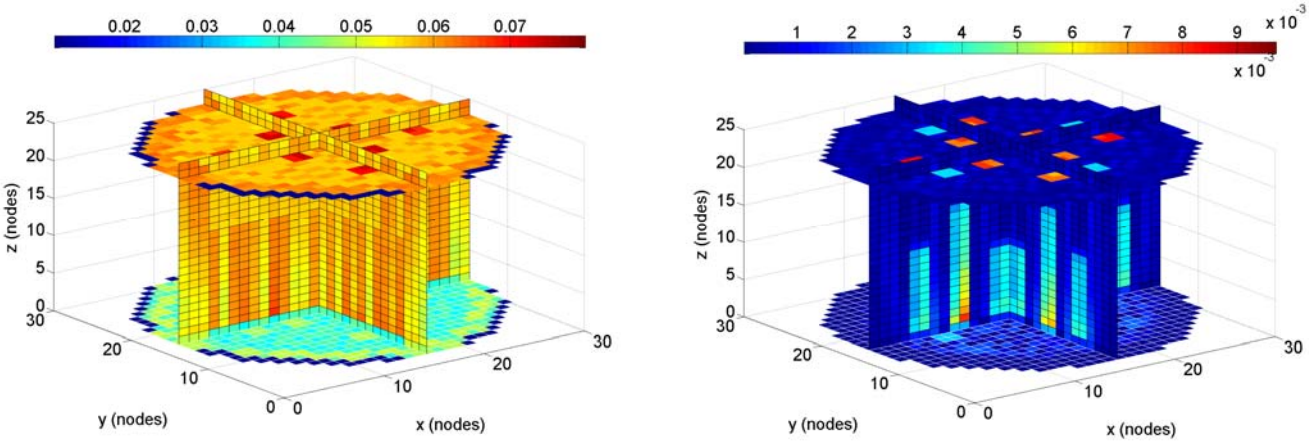

a) *b)*

Fig. 4.3. a) Mean value of the thermal absorption cross-section (1/cm) per node, and b) Standard deviation of the thermal absorption cross-section (1/cm) per node based on data from cycle 26

In this way, the range of variation of the core parameters is assessed without the necessity of a subjective expert opinion, because it is solely based on the depletion information of the cycle.

4.1.2 LHS vs. SRS

Once the corresponding 9 parameters per node are extracted with POLCA7 for each EFPH point, and the input uncertain space has been assessed as previously described, this is sampled either by LHS or SRS. All the sampled nodal parameters from the different 16,200 active nodes are matched assuming independence among each other. In principle, a correlation matrix can be constructed, but it would be extremely computationally expensive to use it in the sampling procedure because a square matrix of size 16,200*9 is required. The fact that a correlation is not taken into account during the sampling procedure may create some samples where the match among the different variables is unphysical. Nevertheless, this is a constraint that can be overtaken with a large sample size.

Once the input uncertain sample is created, this is propagated through an in-house neutronic core simulator known as CORE SIM [42,43]. The calculations performed by this tool rely on the two-group diffusion approximation, while the spatial discretization is based on finite differences. The coding was implemented in *MatLab*, which makes the pre- and post-processing of data easy, as well as the code highly portable between different operative systems and computer platforms. For this particular study, the so called homogeneous or eigenvalue equations are solved. For this purpose, the explicitly-restarted Arnoldi method is used so that the calculation of different eigenmodes is possible. In case of convergence problem, the user has also the possibility of choosing the power iteration method, which was implemented using Wielandt's shift technique. The initial guess of the eigenvalues required for the application of Wielandt's shift technique is provided by an Arnoldi run without restart. Although the accuracy of this tool cannot be compared to commercial core simulators, the tool offers several advantages such as: its ease of use, the robustness of the algorithms, and the fact that nonconventional systems can be easily investigated. Another main strength of the tool is that no input deck writing is required since only few data are required.

In this section, results of the sampling variability studies made on cross-sectional average quantities of the nodal thermal flux are shown below in figure 4.4. Ten replicates of the mean of the core axial profile of the thermal flux were computed for different sample sizes. As highlighted in figure 4.4, the variability of the replicated mean for the LHS case is less than the SRS case, especially at the lower part of the core where the averaged flux tends to peak the most. This is a clear indication that for a full core analysis of the thermal flux, the input uncertain space is being covered in a more efficient way when LHS is employed.

As an example of the computed uncertainties on cross-sectional average quantities of the nodal thermal flux, uncertainty limits obtained with LHS and SRS are shown in figure 4.5 when the sample size corresponds to 100 cases. Uncertainty limits correspond to the cross-sectional average of the maximum values obtained for the nodal flux. As expected, the uncertainty limits obtained when LHS is employed are larger than the ones obtained by SRS at the lower part of the core. This is due to the fact that the flux is much more sensitive to the different changes of the macroscopic cross-sections at the lower part than at the upper part of the core.

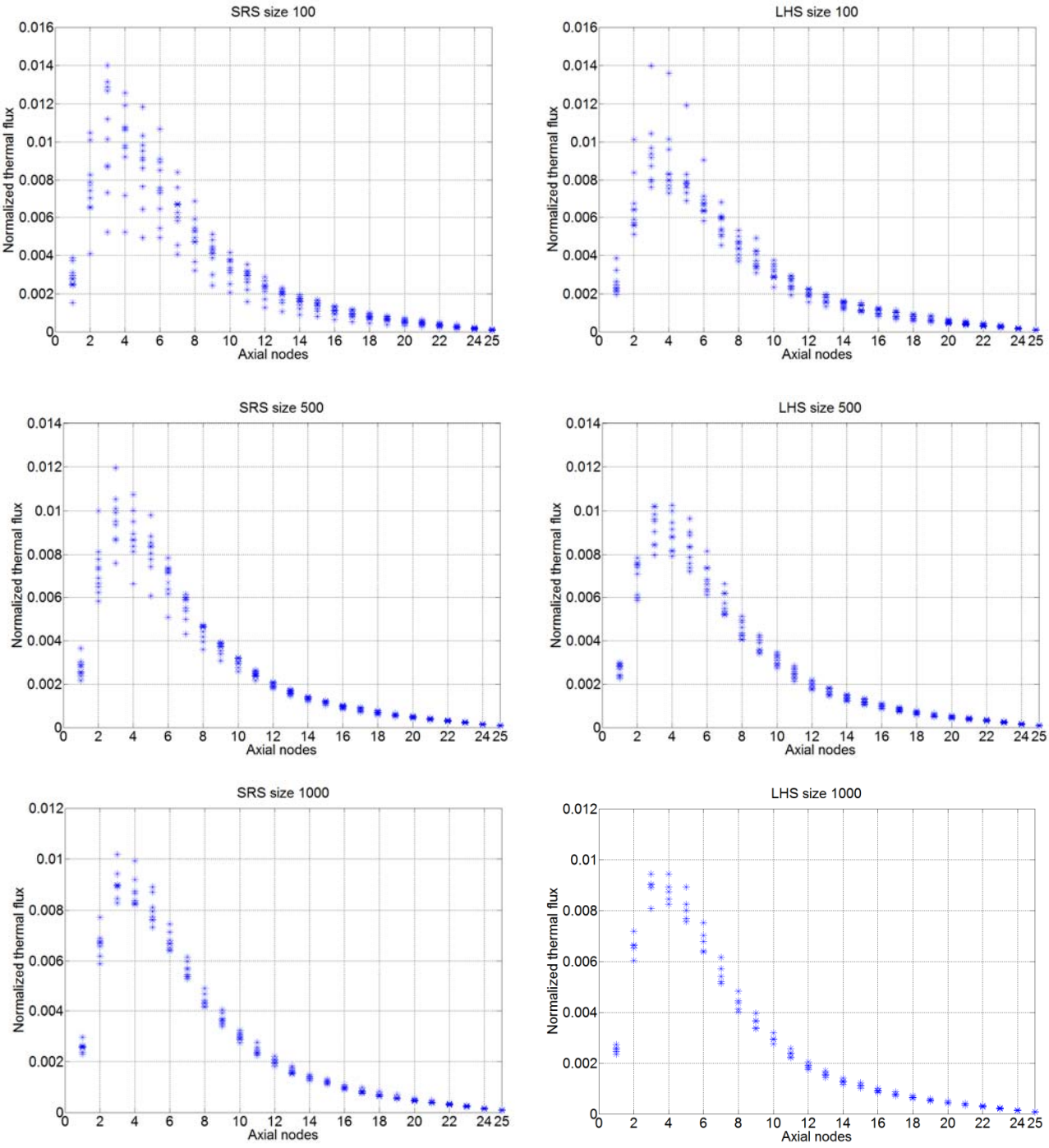

Fig.4.4. Sampling variability study of the mean of the core thermal flux axial profile between LHS and SRS for 10 replicated samples

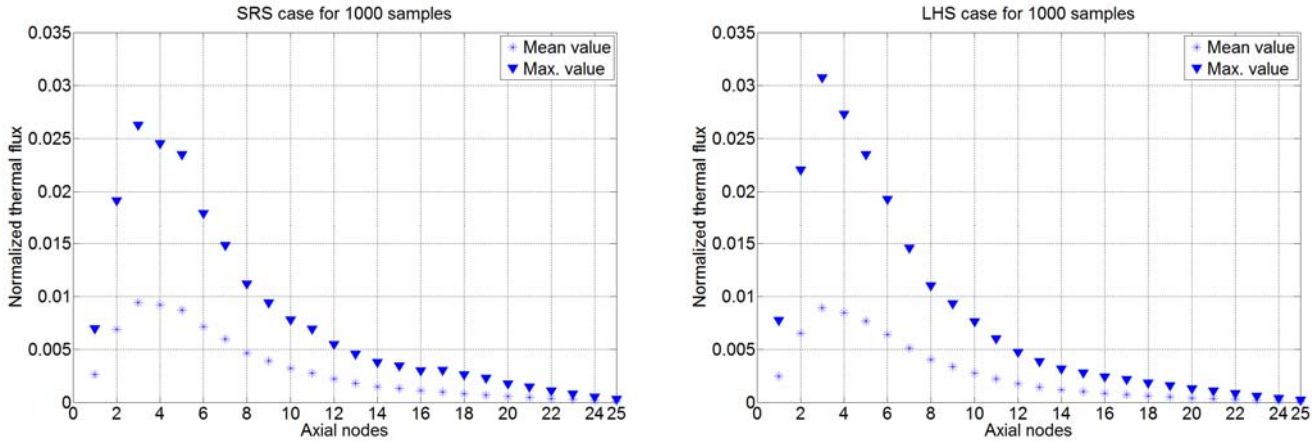

Fig. 4.5. Uncertainty analysis of the core averaged thermal flux axial profile for a sample size of 1000 cases both for SRS and LHS

In the uncertainty analysis applied to safety calculations of nuclear reactors, it is of particular interest to monitor the maximum value of the power throughout the core. Since the thermal power is proportional to the neutron flux, it can be a good idea to compute the possible maximum value of the thermal flux than can be achieved during an uncertainty analysis that is based on information from the whole cycle. Since a total of 16,000 core calculations were performed both with LHS and SRS, a convergence study was performed in order to analyze how many code runs are necessary so that the maximum value of the nodal flux within the core converges to a certain quantity. Such a study is shown in figure 4.6.

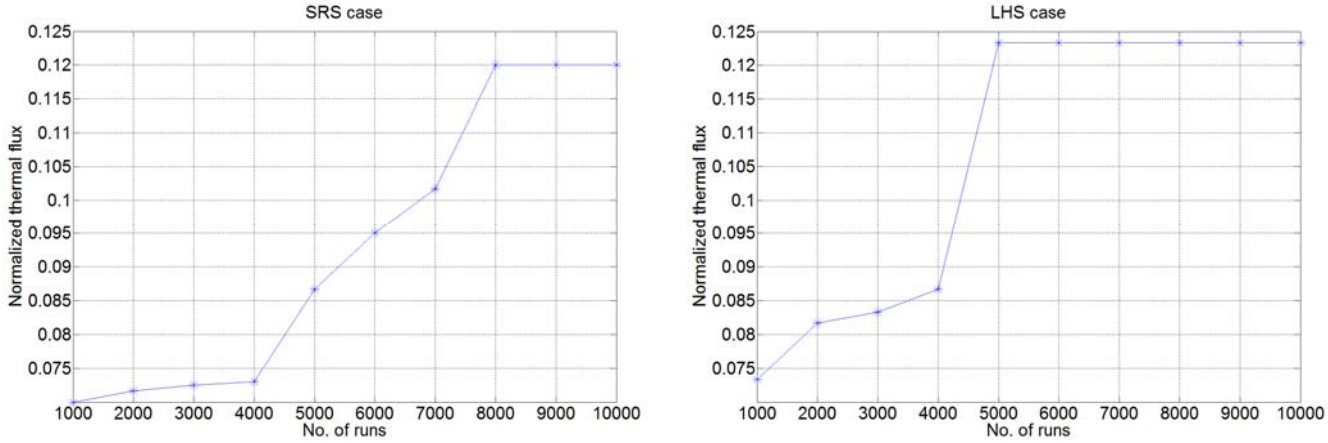

Fig. 4.6. Convergence analysis of the required number of runs for the convergence of the maximum value of the core nodal flux both for LHS and SRS

A much faster convergence towards the maximum value of the nodal thermal flux it can be seen for the LHS case, than for the SRS case. For instance, the maximum nodal thermal flux within the core has converged with LHS after 5,000 calculations, whereas for the SRS case it converges only after 8,000 calculations. This means that if we increase the sample size in order to cover as much as possible the probable input combinations, LHS will converge much faster than SRS to saturate all the probable permutations of the input variables and therefore, the output variables will not change their value anylonger. Also, the maximum value achieved with LHS for the normalized thermal flux corresponds to a value of 0.1233, while the maximum value achieved with SRS corresponds to a value of 0.120. This is a clear indication that the limits of the uncertainty assessment are more realistic when LHS is employed.

4.2 Bayesian uncertainty assessment of BWR core parameters based on flux measurements

In this section, discrepancies between spatial measured and calculated fluxes in R1 are used to perform an inverse uncertainty analysis on the spatial dependence of core nodal parameters. This analysis is carried out using Bayesian statistics, where, for a certain cycle, the a priori distributions of the nodal macroscopic cross-sections and diffusion coefficients at every assembly node are updated based on the error distribution of the spatial thermal flux. The first study of this kind was performed based on information from cycle 13 of R1, and published in paper No. 3 included in this thesis. In this section, results of the Bayesian uncertainty analysis based on information from R1-cycle 26 are presented. As previously explained, the cycle No. 26 database of R1 consists of POLCA7 predictions performed at 62 different EFPH conditions, and for 14 of these EFPH points, TIP measurements are available. In reality, TIP detectors measure the reaction rate of the thermal flux. Since only 36 TIP detectors are radially located along the core, an unfolding methodology of the flux is required to estimate the spatial dependence of the measured flux. This methodology is included in the POLCA7 core simulator, and the final result of the unfolding algorithm [44] gives the nodal dependence of the measured thermal flux.

Bayes theorem [45] states that the frequency of occurrence of random variables can be modified if some evidence that depends on such variable is available. Applying this concept to our particular case, a thermal flux error or evidence distribution that depends both on the measurements and calculations can be computed for each node and defined as $P(e = error|\theta)$ (where θ represents the nodal parameters). Such a distribution is used to update the simulator input parameters distributions (defined as $P(\theta)$) through the following equation:

$$P(\theta|e) = \frac{P(\theta)P(e|\theta)}{\int P(\theta)P(e|\theta)d\theta} \tag{4.1}$$

Where $P(\theta|e)$ is the so called updated (or posterior) distribution of the nodal parameters. Assessment of the parameters and evidence distributions is described below.

4.2.1 Evidence distribution

Since measurements were only performed at 14 different conditions along the cycle, nodal evidence distributions can only be assessed with 14 samples. It is common to assume that the distribution of the errors follows a normal distribution [46,47] mostly because in general, a normal distribution can approximate errors of various sources very well due to the central limit theorem [48]. Therefore, nodal samples of the error between measured and calculated thermal flux will be considered to be taken from a normal distribution. For instance, normality tests can be applied to any nodal sample of the error to confirm such a hypothesis. As an example, the flux error histogram for the top axial node of a fuel assembly located at the center of the core is shown in figure 4.7. A Lilliefors test was applied to such a sample in order to make a normality test. The *p*-value of the test was 0.0023, so it can be significant not to reject the null hypothesis that the sample follows a normal distribution.

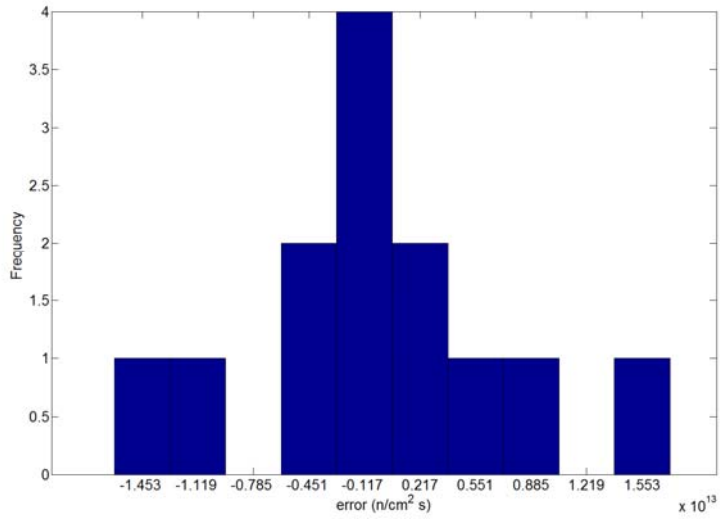

Fig. 4.7. Histogram of the discrepancies between predicted and measured thermal flux at the top node of a central fuel assembly along cycle 26

4.2.2 Computation of the denominator of eq. 4.1

To update the parameter distributions, an integral over the whole domain of the parameters range per node should be computed. Due to the fact that this is a multidimensional function, an estimation of the integral of the product between all the inputs distributions and the evidence distribution is made through Marko Chain Monte Carlo (MCMC) integration. Using random walks and the Metropolis-Hastings (M-H) algorithm [49], numerical integration is possible.

To generate a Markov chain in the parameter space, the M-H algorithm is run by repeating a proposing step and a moving step. In each proposing step, the algorithm generates a new point c_{new} on the basis of the previously accepted point c_{k-1} with a proposal distribution $q(c_{new}/c_{k-1})$. In each moving step, the point c_{new} is tested against the Metropolis criterion to examine if it should be accepted or rejected. If the $L(\theta)$ is the targeted stationary distribution of $P(\theta|e)$, a *Matlab* implementation of the M-H algorithm can be done as follows:

1) Choose an arbitrary initial point $c_{(0)}$ in the parameter space.
2) (Proposing step). Propose a candidate point c_{new} according to a proposal distribution $q(c_{new}/c_{k-1})$.
3) (Moving step). Calculate:
$$P(c_{k-1}, c_{new}) = min\{1, \big(L(c_{new})q(c_{k-1}/c_{new})\big)/\big(L(c_{k-1})q(c_{new}/c_{k-1})\big)\}$$
and compare the value with a random number from the uniform distribution *U* [0,1]. Set $c_k = c_{new}$ if $U \leq P(c_{k-1}, c_{new})$; otherwise set $c_k = c_{k-1}$. This is the Metropolis criterion.
4) Repeat steps 2 and 3 until enough samples are obtained.

The proposal distribution $q(c_{new}/c_{k-1})$ can strongly affect the efficiency of the M-H algorithm. To find an effective proposal distribution, it was required to make a first test run of the algorithm with 20,000 simulations using a uniform proposal distribution centered at the currently accepted point, such as:

$$c_{new} = c_{k-1} + \left[r_d\left(L_m^u - L_m^l\right) + L_m^l\right] \tag{4.2}$$

Where r_d is a random number uniformly distributed between 0 and 1, and L_m^u and L_m^l are the upper and lower values controlling the proposing step size. Based on the test run, a normal distribution $N(0, cov_0(\theta))$ was constructed. Therefore, the following proposal distribution was adopted to execute the MCMC simulations:

$$c_{new} = c_{k-1} + N[0, cov_0(\theta)] \tag{4.3}$$

In each proposing step of the M-H algorithm a new point c_{new} is generated from its predecessor c_{k-1} from a normal distribution with mean c_{k-1}, constant variances estimated from the previous run, and zero parameter covariance. The acceptance rates for the newly generated samples were about 30-40% for a posterior 50,000 runs.

4.2.3 A-posteriori nodal distributions of core parameters

Posterior distributions of macroscopic-cross sections and diffusion coefficiens per node are of interest. Based on a prior multivariate normal distribution, the ranges of the posterior PDFs are based on experimental data, and therefore, their associated uncertainties are computed based on information from a particular BWR cycle. In figure 4.8, a comparison between the prior and posterior distributions for some parameters are shown for the top node of the central fuel assembly.

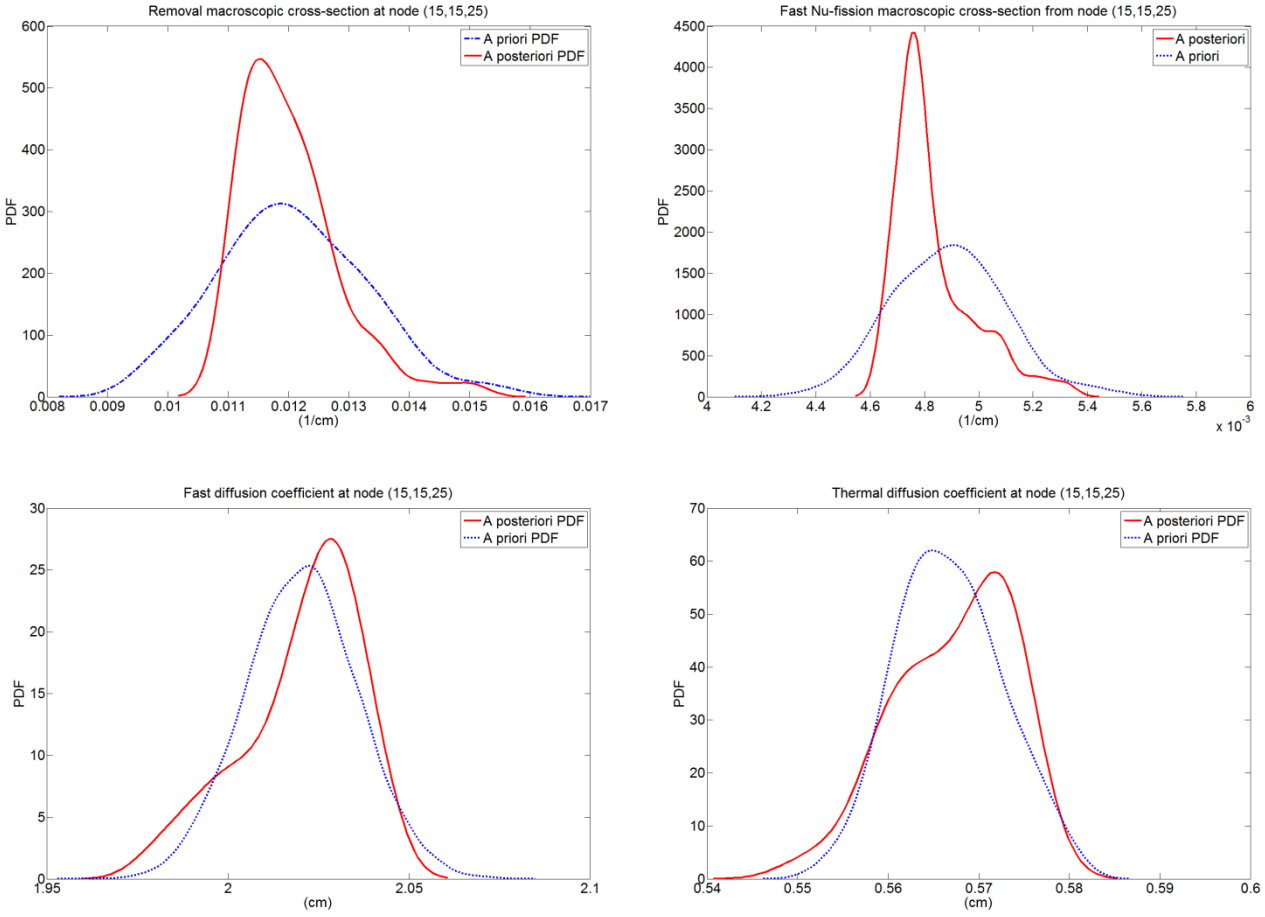

Fig. 4.8. Comparison between prior and posterior PDFs of various nodal parameters based on data from R1, cycle 26

It can be seen from the previous figure that posterior distributions are far away from being normal. This technique is a good way of performing a realistic uncertainty analysis, since the probability

density functions of the input parameters of a core simulator are assessed without the need of expert opinion.

4.3 Uncertainty analysis of a nodal cross-section regression model by means of a non-parametric bootstrap method

Nodal macroscopic cross-sections and diffusion coefficients depend on instantaneous and past (history effects) conditions described by state variables such as burnup, thermal power, moderator temperature and density, etc. Core simulators require nodal parameters as a function of many states in order to calculate neutronic and thermal-hydraulic variables in one or many cycles. One approach to functionalize these dependences is through multivariate functions. Some of the existing models are commonly built as a linear combination of suitable multivariate polynomials, where usually, a unique set of regression coefficients are computed for various fuel depletion points and the reconstructed nodal data are interpolated between the sampled fuel depletions. In general, each fuel segment type uses the same polynomials to functionalize the different cross-sections.

The fuel pattern analysis of R1-cycle 26 was based on a depletion calculation performed at 62 different burnup points along the cycle. Since nodal state variables can be retrieved from POLCA7, their respective cycle frequency distributions are based on samples of 62 elements. In this section, the bootstrap method is employed to estimate a multivariate linear regression model of the space formed between nodal macroscopic cross-sections and core reactor state variables. This work is presented in paper No. 4. Nodal cross-sections are sampled from posterior probability density functions (PDFs) that were previously obtained from a Bayesian uncertainty analysis. The idea is to sample, from various nodes that are related to the same fuel segment, both the frequency distributions of the nodal state variables and any posterior cross-section PDFs in order to create the following input-output mapping:

$$\left(\bar{y}_{nj}, \bar{\bar{x}}_{nm}\right) \tag{4.4}$$

Where $\bar{y}_{nj} = (y_{1j}, \dots, y_{nj})$ is the *i-th* sample of the *j-th* cross-section, and $\bar{\bar{x}}_{nm}$ is the matrix formed by the different *i-th* samples of the different $k = (1,2, \dots, m)$ state varaibles, i.e.:

$$\bar{\bar{x}}_{nm} = \begin{pmatrix} x_{11} & \cdots & x_{n1} \\ \vdots & \ddots & \vdots \\ x_{1m} & \cdots & x_{nm} \end{pmatrix} \tag{4.5}$$

Therefore, a relationship between any nodal macroscopic cross-section and a few nodal state variables from a specific fuel segment is analyzed through a multivariate regression analysis of the form:

$$\hat{y}_j = b_0 + \bar{x}\bar{b} \tag{4.6}$$

The $\bar{b} = (b_1, \dots, b_m)$ regression coefficients, which are bounded not only by the cycle information of the state variables but also by the ranges of the posterior distributions of the macroscopic cross-sections, are derived with the bootstrap method. This is important due to the fact that such posterior PDFs ranges are based on experimental data, and not anymore on expert opinion. The aim of this work is to assess a degree of uncertainty to the regression coefficients by computing their respective confidence intervals. Due to tremendous advances in modern computing capabilities, the non-parametric bootstrap method has been widely used in the statistical assessment of regression parameters and their associated degree of variability [50]. In general, uncertainty analysis in reactor calculations are performed to lattice and core simulators in a separate manner [51,52]. Although the cross-section models derived in this work are rather simple, the main goal is to point out the

importance of assessing uncertainty at all stages in the modeling of nuclear reactors, including regression parameters that are used to functionalize macroscopic cross-sections as a function of the core state variables.

4.3.1 Creation of the input-output space

Cross-section models are used to arrange the different nodal core parameters in space as a function of the state variables for the same type of fuel. Therefore, a specific model is assessed for a specific fuel segment. In this work, a cross-section model and its associated uncertainties are derived for a fuel segment that is comprised between the 2nd and the 24th axial node of an ABB 10x10 SVEA96 assembly, located in the periphery of the core. Since 23 nodes comprise the fuel segment of interest, the final sample of each state variable is composed by 1,426 elements. Therefore, the macroscopic cross-section being studied should be randomly sampled the same amount of times in order to perform the linear multivariate regression analysis. In figure 4.9, the points defined by 1,426 samples from the different removal cross-section, burnup, fuel temperature, moderator density and moderator density history PDFs are presented. These are the actual spaces that are going to be bootstrapped in order to estimate the regression coefficients and their uncertainties.

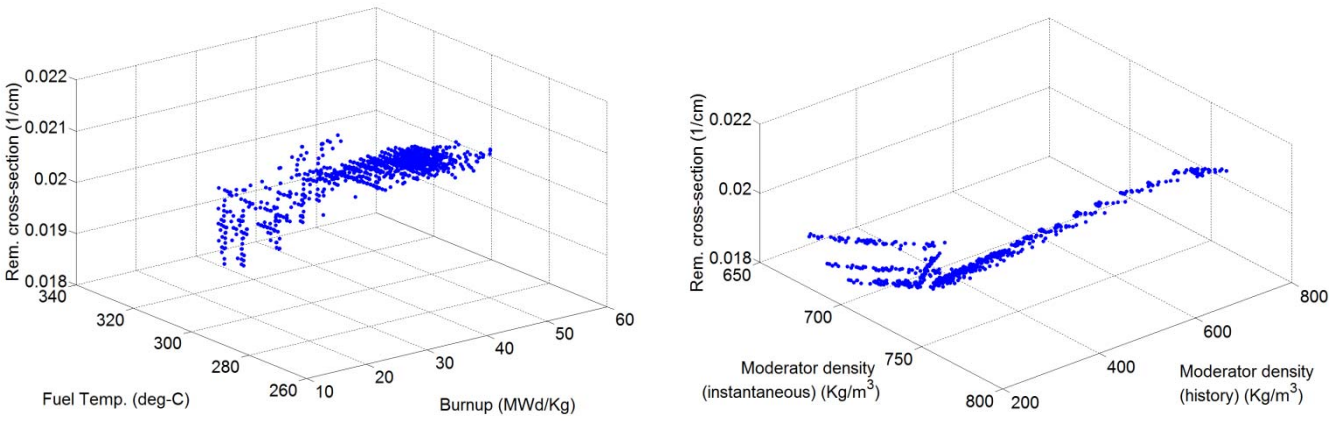

a) *b)*

Fig. 4.9. Space defined by the samples obtained from the a) removal cross-section, fuel temperature and burnup and b) removal cross-section, moderator density (instantaneous) and moderator density (history)

4.3.2 Main features of the multivariate linear regression analysis

Regression analysis is a statistical technique that characterizes the relationship between two or more variables for prediction and estimation by a mathematical model. Finding the variance of the estimated $\widehat{\boldsymbol{\beta}}$ coefficients, as well as constructing confidence intervals for $\boldsymbol{\beta}$ is of main interest. In the usual construction of a linear regression model for a certain y_j that was obtained from the $i = (1, \dots, n)$ samples such as:

$$y_i = b_0 + \sum_{k=1}^{m} b_k x_{ik} + \varepsilon_i \tag{4.7}$$

it is assumed that the residuals $\varepsilon_i = y_i - \hat{y}_i$ are uncorrelated and normally distributed with zero mean, i.e. $\varepsilon_i \sim N(0, \sigma)$. Furthermore, σ is assumed to be the same for all values of $\bar{x}$. It is the distributional assumption involving ε that allows the construction of statistical tests and parametric

confidence intervals for the $\bar{b}$ coefficients [8]. For instance, if such assumptions are true and $\bar{y}_r$ and $\bar{\bar{x}}_r$ are defined such as:

$$\bar{y}_r = \begin{bmatrix} y_1 \\ \vdots \\ y_n \end{bmatrix}, \quad \bar{\bar{x}}_r = \begin{bmatrix} 1 & x_{11} & \cdots & x_{n1} \\ \vdots & \vdots & \ddots & \vdots \\ 1 & x_{1m} & \cdots & x_{nm} \end{bmatrix} \tag{4.8}$$

The least square estimator given by:

$$\bar{b} = \left(\bar{\bar{x}}_r{}^T \bar{\bar{x}}_r\right)^{-1} \bar{\bar{x}}_r^T \bar{y}_r \tag{4.9}$$

has an associated variance-covariance matrix $Var(\bar{\bar{b}}) = \sigma\left(\bar{\bar{x}}_r{}^T \bar{\bar{x}}_r\right)^{-1}$ and the following $100(1-\alpha)\%$ confidence intervals [53]:

$$b_k \pm t_{n-m,\alpha/2} \cdot S_e(b_k) \tag{4.10}$$

Where $t_{n-m,\alpha/2}$ is the *t*-distribution with *(n-m)* degrees of freedom, and $S_e(b_k)$ is the standard deviation of the b_k coefficient.

Common statistical tests that are used to prove the significance of the regression coefficients strongly rely on the aforementioned assumptions. If $\bar{y}$ is the mean of the y_i observations, an approximation to σ^2 can be derived as [8]:

$$\hat{s}^2 = \frac{\sum_{i=1}^{n}(y_i - \hat{y}_i)^2}{(n-m-1)} \tag{4.11}$$

The well-known *F*-test statistic given by:

$$F = \frac{\sum_{i=1}^{n}(\hat{y}_i - \bar{y})^2}{ms^2} \tag{4.12}$$

Can be regarded as a randomly sampled value from an *F*-distribution with *(m,n-m-1)* degrees of freedom. This statistic can be used to test the accuracy of the constructed linear model, or, in other words, to test that $\bar{b} = (b_1, \ldots, b_m) = \bar{0}$.

Nevertheless, if the residuals distribution is unknown or difficult to derive, one cannot entirely rely on the parametric approach to build linear regression models. For instance, if the residuals do not follow a normal distribution, the *F*-statistic does not follow an *F* distribution.

4.3.3 *Bootstrap method*

Bootstrapping is a non-parametric and specific resampling technique that substitutes the traditional distributional assumptions with computational effort. It offers a significant number of advantages [54]:

- Because it does not require any distributional assumption (such as normally distributed errors), the bootstrap approach can provide more accurate inferences when the data are not well behaved or when the sample size is small.
- It is possible to apply the bootstrap to statistics with sampling distributions that are difficult to derive, even asymptotically.
- It is a general technique and relatively easy to implement with modern computational resources.

One of the bootstrap methods that can be used in a linear regression analysis, and that is based on the resampling of observations is described hereafter. This approach is applied when the coefficients and the response of the regression model are considered random variables. The bootstrap procedure based on the resampling of observation is as follows:

1) Draw n' independent bootstrap samples with replacement of the form $w_i^{\beta} = \left(\bar{y}_{ij}, \bar{\bar{x}}_{im}\right)$ from the estimated input-output space defined by $\left(\bar{y}_{nj}, \bar{\bar{x}}_{nm}\right)$. Thus, $\left(w_1^{\beta}, w_2^{\beta}, \dots, w_{n'}^{\beta}\right)$ are created.

2) Calculate the ordinary least square (OLS) coefficients from the bootstrap sample as follows:

$$\bar{b}^{(\beta 1)} = \left(\bar{\bar{x}}_r^{(\beta)T} \bar{\bar{x}}_r^{(\beta)}\right)^{-1} \bar{\bar{x}}_r^{(\beta)T} \bar{y}_r^{(\beta)} \tag{4.13}$$

3) Repeat steps 1 and 2 for *r=1,…,B,* where *B* is the number of repetitions.
4) Obtain the distribution $F\left(b^{(\beta)}\right)$ from the bootstrap estimates $b^{(\beta 1)}$, $b^{(\beta 2)}$,…, $b^{(\beta B)}$, and use $F\left(b^{(\beta)}\right)$ to estimate regression coefficients, variances, etc. Therefore, the bootstrap estimate of the regression coefficient is the mean of the distribution $F\left(b^{(\beta)}\right)$ [55]:

$$\bar{b} = \frac{\sum_{r=1}^{B} \bar{b}^{(\beta r)}}{B} \tag{4.14}$$

Non-parametric confidence intervals are easy to derive from the quantiles of the bootstrap sampling distribution $F\left(b^{(\beta)}\right)$. By ranking the bootstrap $b^{(\beta 1)}$, $b^{(\beta 2)}$,…, $b^{(\beta B)}$ estimations, the $(\alpha/2)\%$ and $(1-\alpha/2)\%$ confidence interval for a certain coefficient is given by:

$$b_{(\alpha/2)B}^{(\beta)} < b < b_{(1-\alpha/2)B}^{(\beta)} \tag{4.15}$$

For example, if *B*=1000 replicates are taken and a 95% (i.e. $\alpha = 0.05$) confidence interval of the *b* parameter is desired, once the bootstrap samples have been ordered, the 25th sample and the 975th sample will give the corresponding upper and lower limits of the interval.

In addition to providing standard errors and confidence intervals, the bootstrap can also be used to test statistical hypothesis. If we want to test if the computed coefficients $\bar{b} = (b_1, \dots, b_m) = \bar{0}$, a bootstrap analysis can be performed in order to estimate the distribution of the test statistic. By denoting *F* as the original *F*-statistic of the input-output space defined by $\left(\bar{y}_{nj}, \bar{\bar{x}}_{nm}\right)$, the estimated $\bar{b}$ coefficients can be used to bootstrap the residuals and obtain, for each sample, an F^*-statistic as follows [55]:

1) Fit the regression model and obtain the residuals $e_i = y_i - (b_0 + b_1 x_{1i} + b_2 x_{2i} + \cdots + b_k x_{ki})$ from the original space.
2) For a single bootstrap iteration, obtain a bootstrap sample of the residuals e_i and form a fix $\left(w_1^{\beta}, w_2^{\beta}, \dots, w_{n'}^{\beta}\right)$ bootstrap sample as previously explained. Compute the $F^{(\beta 1)*}$ statistic from Eq. 10.
3) Repeat step 2 many times for *r=1,…,B.*

Therefore, the bootstrap *P*-value for the test of interest is the fraction of $F^{(\beta r)*}$ values that are greater than or equal to the originally observed *F*-value.

4.3.4 Results

Two cases will be studied, one corresponding to the mapping between the removal cross-section, burnup and fuel temperature and the other one corresponding to the mapping between the removal cross-section, moderator density and moderator density history, respectively. *P*-values of the hypothesis test $H0\colon \bar{b} = (b_1, \dots, b_m) = \bar{0}$, 95% confidence limits of the regression coefficients as well as other statistical parameters of interest are presented. Each bootstrap sample consisted of 1,426 elements, a total of 10,000 replicates were performed in order to perform the different regression analyses.

Case 1: Linear regression analysis on the input-output space formed by the removal cross-section, burnup and fuel temperature

In table 4.1, a summary of the regression coefficients and their corresponding confidence intervals are presented, while the corresponding ANOVA (Analysis of Variance) test of the regression analysis is illustrated in table 4.2.

Table 4.1. Summary statistics of regression coefficients for case 1

Variables	*Related Coefficient* (b_k)	*Skewness of the distribution*	*95% Confidence Interval*
Constant	0.0295	-0.0234	(0.0292,0.0297)
Burnup	1.530e-05	-0.0013	(1.420,1.641)e-05
Fuel Temp.	-3.310e-05	0.0176	(-3.392,-3.226)e-05

Table 4.2. ANOVA results for case 1

Source	*DofF*	*SS*	*MS*	*F*	*P-value*
Regression	*2*	*2.936e-04*	*-*	*3088.3*	*0.000*
Residual	*1423*	*7.354e-05*	*4.754e-08*		
R-square=0.799					

In figure 4.10, the estimated planes formed by the regression analyses $y = (0.0292,0.0297) + (1.420,1.641)e-05 \cdot x_1 + (-3.392,-3.226)\text{e}-05 \cdot x_2$ are shown, as well as all the observations defined in the input-output space of case 1.

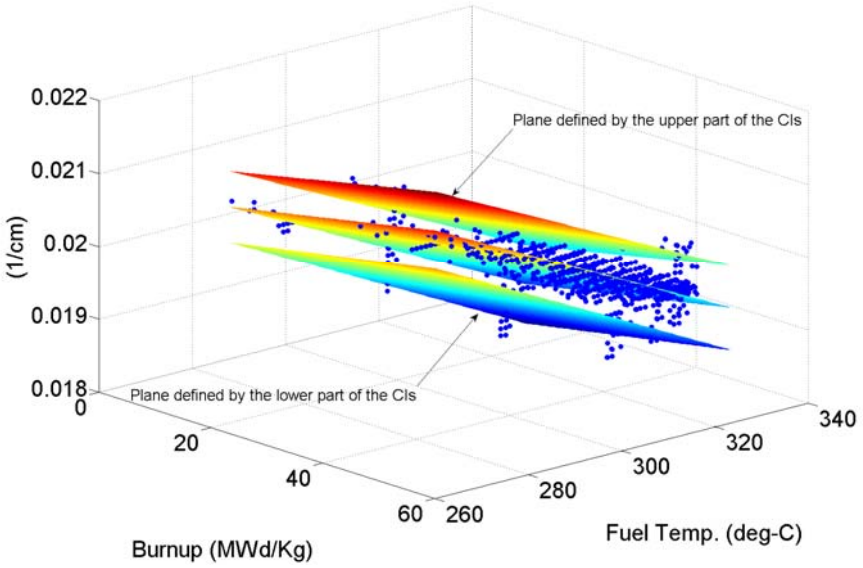

Fig. 4.10. Uncertainty assessment of the regression analysis of case 1

Case 2: Linear regression analysis on the input-output space formed by the removal cross-section, moderator density and moderator density history

In table 4.3, a summary of the regression coefficients and their corresponding confidence intervals are presented, while the corresponding ANOVA (Analysis of Variance) test of the regression analysis of this case is illustrated in table 4.4.

Table 4.3. Summary statistics of regression coefficients for case 2

Variables	*Related Coefficient* (b_k)	*Skewness of the distribution*	*95% Confidence Interval*
Constant	0.0086	0.1219	(0.0079,0.0094)
Moderator Density	1.421e-05	-0.1211	(1.322,1.521)e-05
Moderator Density Hist.	0.166e-05	0.0454	(0.157,0.175)e-05

Table 4.4. ANOVA results for case 2

Source	*DofF*	*SS*	*MS*	*F*	*P-value*
Regression	2	2.818e-04	-	2554	0.000
Residual	1423	8.535e-05	5.517e-0888		
R-square=0.767					

In figure 4.11, the estimated planes formed by the regression analyses $y = (0.0079,0.0094) + (1.322,1.521)\mathrm{e}-05 \cdot x_1 + (0.157,0.175)\mathrm{e}-05 \cdot x_2$ are shown, as well as all the observations defined in the input-output space of case 2.

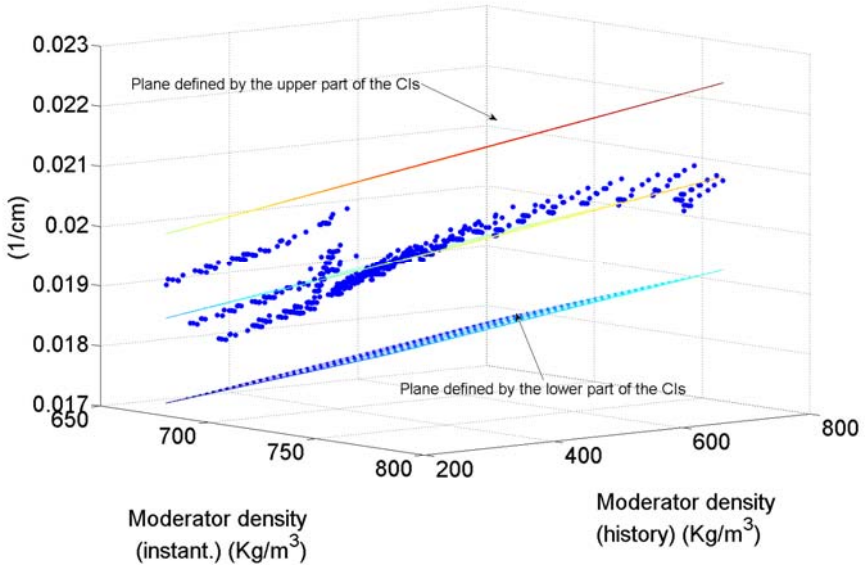

Fig. 4.11. Uncertainty assessment of the regression analysis of case 2

As early appreciated in figure 4.9, the space defined among the removal cross-section, moderator density and moderator density history for the fuel segment of interest, is more scattered and farther away to be represented by a plane than the space defined by the removal cross-section, burnup and fuel temperature. Indeed, the ANOVA test for case 1 reflects a lower sum of the squares in the residuals and a better *R-square* ratio than case 2, which indicates that the space of case 1 fits better a linear model than the space from case 2. Due to this fact, the computed confidence intervals for the coefficients of the first case are relatively lower, than the computed confidence intervals for the coefficients of the second case. Therefore, higher uncertainties are expected for regression models that try to adjust a linear relationship among the different points of the sampled space.

The objective of this methodology presented is to estimate the uncertainty on the regression coefficients used in cross-section models. Although a very simple case was proposed in this chapter where the coefficients are considered constant, the aim is to emphasize the importance of performing uncertainty analysis at all the different stages in the modeling of nuclear reactors. For instance, cross-sections models are very important because they are the link between thermal-hydraulic calculations and core simulators.

CHAPTER 5

UNCERTAINTY AND SENSITIVITY ANALYSES APPLIED TO THERMAL-HYDRAULIC CALCULATIONS

"If nuclear power plants are safe, let the commercial insurance industry insure them. Until these most expert judges of risk are willing to gamble with their money, I'm not willing to gamble with the health and safety of my family".

Donna Reed

While the licensing regulations were being codified, an international effort was initiated in parallel to:

a) Develop BE codes with the capability to calculate accurate values of the key phenomena that restrict plant operational limits;
b) Obtain data to enable validation and verification of the system analysis codes;
c) Perform code validation and verification to ensure that the capabilities of the code are known and acceptable.

Such a need to validate and refine BE codes that are used in the predictions of relevant reactor safety parameters, led to the organization of international benchmarks based on high quality experimental data. The OECD/NRC BWR Full-Size Fine-Mesh Bundle Test (BFBT) benchmark was established in 2002 based on available data from the Nuclear Power Engineering Corporation (NUPEC) in Japan, and offers a good opportunity to assess the accuracy of thermal-hydraulic codes in predicting, among other parameters, single and two phase bundle pressure drops, cross-sectional averaged void fraction distributions and critical powers under a wide range of system conditions. With respect to the void distribution inside a fuel assembly, which has been regarded as an important factor in the determination of boiling transition in boiling water reactors (BWRs), NUPEC performed from 1987 to 1990 a series of radial void measurements at four axial locations in a full-size mock-up test facility able to simulate the high pressure, high temperature fluid conditions found in BWRs through electrically-heated rod bundles. Therefore, since other important parameters such as system pressure, inlet sub-cooling and power input conditions were also supplied, these test series form a substantial database for the assessment of the accuracy of thermal hydraulic codes in predicting radial and axial assembly void distributions, under both steady-state and transient conditions.

Nevertheless, due to uncertainties coming from, e.g. approximations in the physical models, variation and imprecise knowledge of initial and boundary conditions, scatter of measured experimental data, etc., it has been recognized in the last years that uncertainty analysis would not only be necessary if useful conclusions are to be obtained from BE calculations, but would also complete the validation process of BE codes [56].

The work presented in this chapter has two main objectives. The first one is to enhance the validation process of the thermal-hydraulic features of the Westinghouse code POLCA-T. This is achieved by computing a quantitative validation limit based on statistical uncertainty analysis. This validation theory is applied to some of the benchmark cases of the following macroscopic BFBT exercises, based on a one dimensional model of the NUPEC ITF:

1. Exercise 0, Phase II. Steady-state single and two phase pressure drops

2. Exercise 2, Phase I. Steady-state cross-sectional averaged void fraction
3. Exercise 3, Phase I. Transient cross-sectional averaged void fraction
4. Exercise 1, Phase II. Steady-state critical power benchmark

Sensitivity analysis is also performed to identify the most important uncertain parameters for each exercise.

The second objective consists in showing the clear advantages of using the quasi-random Latin Hypercube Sampling (LHS) strategy over simple random sampling (SRS). For cross-sectional averaged void fraction predictions under both steady-state and transient conditions, a comparison between statistical uncertainty analyses by means of LHS and SRS is presented. The aim is to show that the replicated void fraction mean (either in steady-state or transient conditions) has less variability when using LHS than SRS for the same number of calculations (i.e. same input space sample size) even if the resulting void fraction axial profiles are non-monotonic.

5.1 Description of the NUPEC test facility

The facility is able to simulate the high pressure, high temperature fluid conditions found in nuclear reactors. An electrically-heated rod bundle has been used to simulate a full scale BWR fuel assembly. In the test section, the simulated full scale BWR fuel assembly was installed within a pressure vessel. Two bundle types, a “current 8x8 type” and a “high burn-up 8x8 type” were simulated. Three types of axial power profiles were used: uniform, cosinusoidal and inlet peak. Also, different radial power distributions were achieved through different pin power factors.

Two types of void measurement systems were employed as shown in figure 5.1: an X-ray computed tomography (CT) scanner and an X-ray densitometer. Under steady-state conditions, fine mesh radial void distributions were measured using the X-ray CT scanner located 50 mm above the heated length. The attained spatial resolution was as small as 0.3 mm X 0.3 mm. However, the X-ray densitometer measurements of void distributions around each rod were performed at three different axial elevations from the bottom (i.e. 682 mm, 1706 mm and 2730 mm) under both steady-state and transient conditions. For the each of the four different axial locations, the cross-sectional averaged void fraction was also measured.

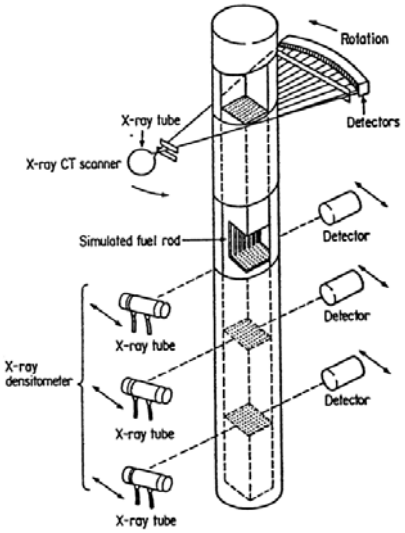

Fig. 5.1. Void fraction measurement system

Absolute and differential pressures were measured using diaphragm transducers. The inlet flow rate was measured using a turbine flow meter, and the inlet sub-cooling was measured using double thermistors. Table 5.1 shows the estimated measurement accuracy of these process parameters.

Table 5.1. Accuracy (%) of the main processes that were recorded

Quantity	Accuracy
Pressure	1 %
Flow	1 %
Power	1.5 %
Inlet fluid temperature	$\pm$ 1.5 ℃
Cross-sectional averaged void fraction	2%

The BFBT offers the possibility to benchmark averaged cell void fraction predictions under two types of simulated transient scenarios: a half re-circulation pump trip, and a half turbine trip without bypass. The "half" scenario means that after some time from the occurrence of the corresponding transient, nominal operating conditions were fed again into the fuel assembly in order to avoid rod cladding damages. In a pump trip scenario, the core mass flow rate is suddenly decreased, exposing the coolant left in the core to a sudden increase of temperature and therefore, to a sudden increase in the void fraction. Regarding the turbine trip case, a sudden increase on the outlet pressure will collapse the coolant void. In a real BWR, this will increase the neutron moderation leading to a power increase and ergo, leading to a sudden increase on the void fraction. For these purposes, the code used time dependent boundary and power input conditions artificially created and released by NUPEC, which are shown in figure 5.2.

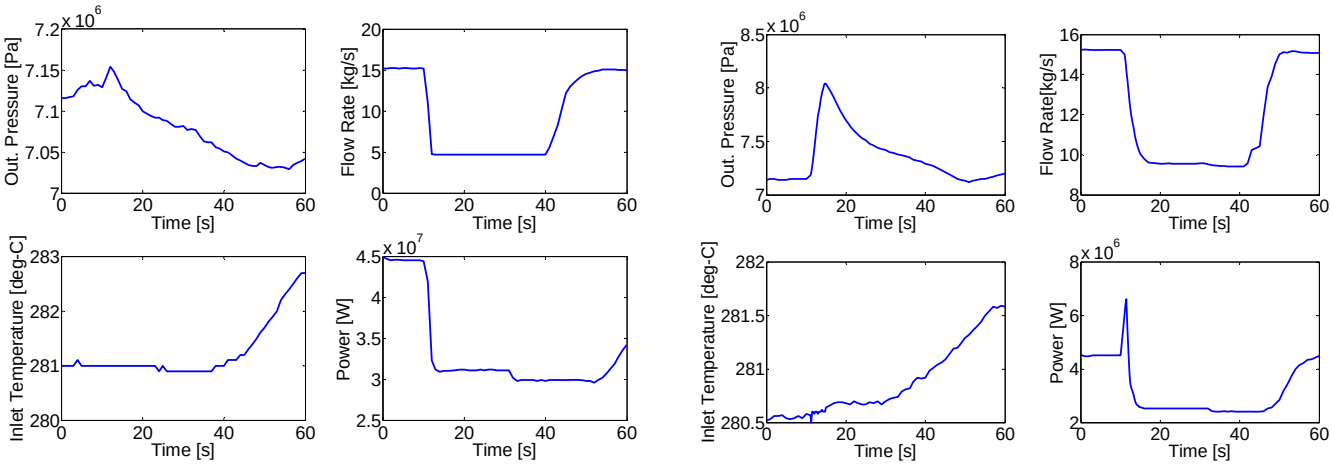

a) *b)*

Fig. 5.2. Boundary and input power conditions representing the a) half recirculation pump trip, and b) half recirculation turbine trip

In contrast to the CT scanner, the X-ray densitometers were not rotating but fixed during a measurement. Thereby, a pencil type beam was shot through a certain alley of sub-channels between two neighboring rod rows. As discussed in [57], because of this principle only parts of the sub-channel cross-sections have been scanned in between the rod rows. Therefore, sub-channel

center effects are overestimated while near wall effects are neglected. Depending on the prevailing flow regime two opposite phenomena led to systematic measurement errors.

In case of *high* void fractions the vapor concentration in the sub-channel center is higher than near the walls (slug and churn flow regime). Therefore, a higher average void fraction than in reality was measured. Because of the systematic deviations of the densitometer measurements, Aydogan et. al [58] developed correlations in order to correct the experimental values. Since the two types of fuel assemblies used for the measurements have different flow areas, two different correlations were derived. Such correlations should correct X-ray densitometers void fraction measurements that lie between 20% and 90%. These are illustrated in Eqs. 5.1 and 5.2.

- For the current 8x8 assembly:

$$\alpha_{corrected} = \frac{\alpha_{measured,DEN}}{-0.001\alpha_{measured,DEN} + 1.231} \tag{5.1}$$

- For the high burn-up 8x8 assembly:

$$\alpha_{corrected} = \frac{\alpha_{measured,DEN}}{-0.001\alpha_{measured,DEN} + 1.167} \tag{5.2}$$

For both transient scenarios, the fuel assembly simulating high burn-up conditions was employed with a uniform axial power profile. The three different axial positions of the X-ray densitometers correspond to the calculations given by nodes 19th, 12th and 5th, respectively, of the POLCA-T output deck. For both transient scenarios, Eq. (5.2) was applied in order to have the correct void fraction measurements.

5.2 Description of the POLCA-T system code

The Westinghouse transient code POLCA-T is a three-dimensional coupled simulator solving for the thermal-hydraulic and neutronic fields. The code is used mainly for transient analysis of BWRs. The thermal-hydraulic part of the code [59] corresponds to a 5-equation model based on the conservation equations of mass and energy for gas and liquid phases, and on the conservation equation of momentum for the mixture. For each defined control volume cell, values of pressure, phase enthalpies and phase masses are determined by the solution of the conservation equations. The most important constitutive relations are friction and local pressure drop correlations, critical flow correlations and a drift-flux model employed to solve the velocities of the two phases for all flow regimes. For the BFBT benchmark, the drift-flux Holmes correlation was chosen. The thermal model calculates the heat conduction and heat transfer from the heat structures to the coolant. Equations are resolved in Eulerian coordinates, where a fully implicit numerical method is employed to solve the hydraulic model and the simultaneous heat transfer and thermal conduction equations.

Since the main process parameters measured in the integral test facility (ITF) are available in the database, the test fuel assembly was modeled in POLCA-T (version 1.6.0/T5-1.9.0) as a one-dimensional BWR channel considering as boundary conditions the inlet fluid temperature, the mass flow rate and the assembly outlet pressure. The seven spacers were modeled with constant *K*-loss coefficients to take into account local pressure drops. In order to model the axial power profile, a heat structure was used to combine the effects of all heated rods. Thus, radial pin power factors were not taken into account. The channel nodalization was set to 24 equidistant axial volumes of 0.154 m in length, assigning the nodes numbering from bottom to top from 1 to 24, respectively, as shown in figure 5.3.

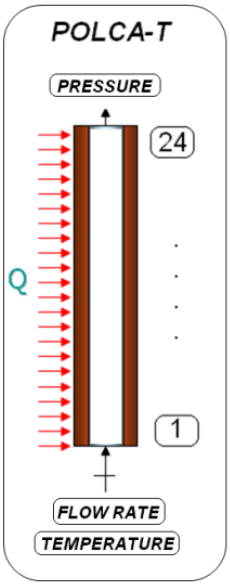

Fig. 5.3. BFBT equivalent model in POLCA-T

5.3 Statistical uncertainty analyses of void fraction predictions using LHS and SRS

This section focuses on the results of sampling variability studies and uncertainty analyses performed with LHS and SRS on predicted cross-sectional averaged void fractions. The estimations are for both a steady-state condition and a simulated re-circulation pump trip scenario. These results constitute a summary of paper No. 5.

The most important sources of uncertainty that are present in the BFBT benchmark were identified by the different organizers and participants, and can be found in [60]. By the use of "expert opinion", a PDF and standard deviation was assigned to each parameter. The uncertain input space for this section is based on 8 parameters that are directly available in the POLCA-T input deck. Four of them correspond to the boundary and power input conditions released by NUPEC, and their probabilistic assessment was based on their experimental accuracy. Two parameters correspond to important geometrical parameters such as the hydraulic diameter and the total flow area, whereas the last parameters correspond to the rod cladding surface roughness and spacer *K* loss coefficient, respectively. The *K* loss factor was set to a value of 0.94, and the rod roughness was considered to be 2.5 μm, according to some changes in the BFBT specification and stated in [61]. Table 5.2 describes the assessment of the uncertain input space for further uncertainty analyses.

Table 5.2. Input space uncertain parameters

Parameter	PDF	Mean	Stand. Dev.
Pressure	Normal	Nominal	1%
Flow rate	Normal	Nominal	1%
Inlet temperature	Uniform	Nominal	± 1.5 ℃
Power	Normal	Nominal	1.5%
Hydraulic diameter	Normal	1.295 cm	1%
Flow area	Normal	97.81 cm^2	1%
Roughness	Normal	2.5 μm	5%
Spacer *K* loss coefficient	Normal	0.94	5%

5.3.1 Steady-state case

The nominal values of the boundary conditions corresponding to the BFBT 0021-18 steady-state test case are shown in table 5.3.

Table 5.3. Nominal conditions for the steady-state test case

Parameter	Nominal value
Pressure	7.17 MPa
Flow rate	15.37 kg/s
Inlet temperature	279 ℃
Total power	3.5 MW

For the sampling variability study between LHS and SRS, ten replicates of the axial void fraction profile mean were computed for different sample sizes. Figure 5.4 shows the results of such a study, where it can be noticed that in all four cases LHS performs much better than SRS. It should be noted that the axial void fraction profile forms a monotonic function.

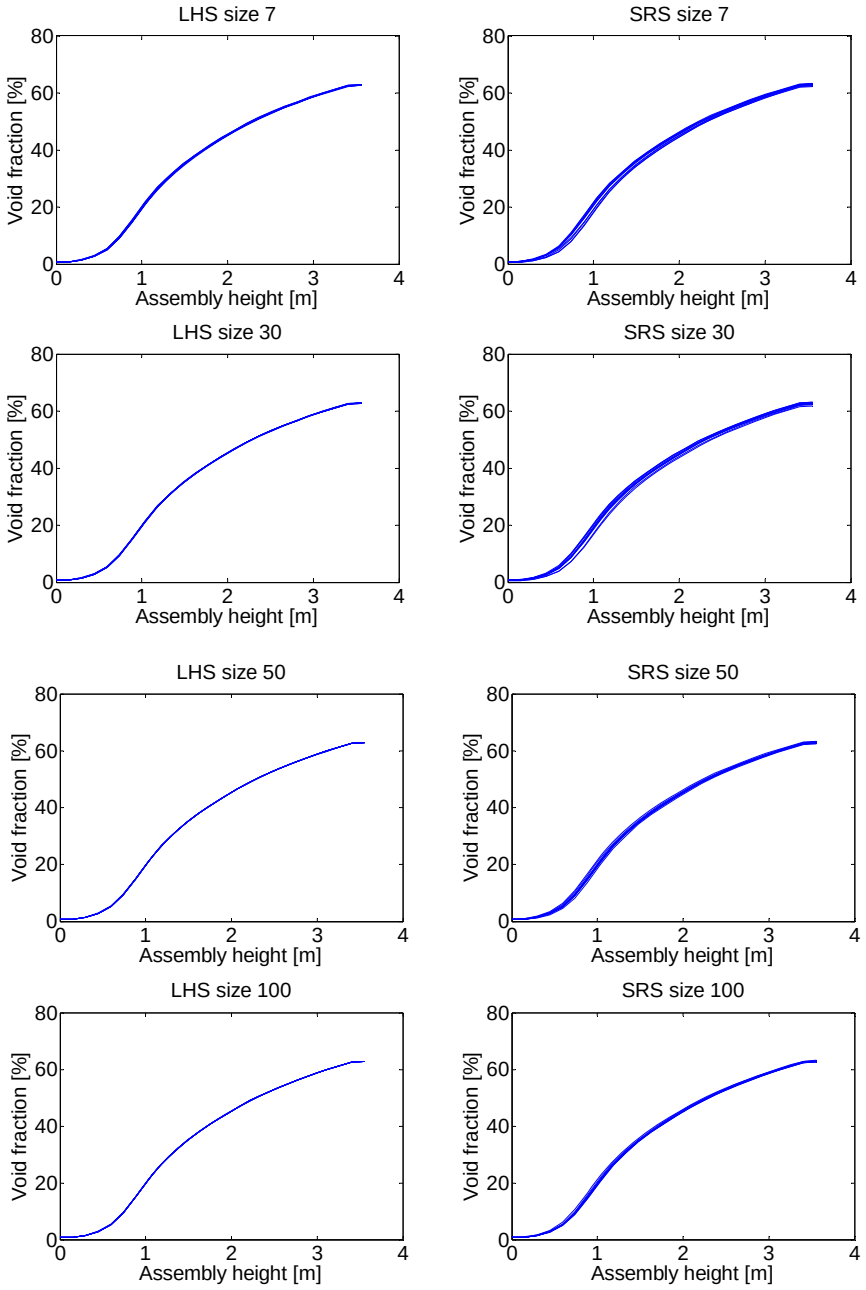

Fig. 5.4. Sampling variability study between LHS and SRS for 10 mean replicates (Steady-state)

5.3.2 Transient case

Uncertainty analysis is presented on the transient case corresponding to the half re-circulation pump trip scenario. Since for this case the boundary and input power conditions are time dependent, a protocol to sample the input space should be followed. POLCA-T is designed to handle transient cases in an easy way; for instance, a file containing a look-up table of any parameter as a function of time can be defined. Thereby, at every specific time defined in the table, the nominal value of the parameter is considered to be the mean value and from its characteristic PDF, the required sample is taken. Boundary and input conditions are defined in the input deck of the code every second and thus, at every second there exists a particular sample from the input space.

As for the steady-state case, a sampling variability study is presented in figure 5.5 for the predicted time-dependent cross-sectional averaged void fraction at the axial location of 687 mm (same location as the lowest densitometer). Ten replicates of void fraction mean were computed for different

sample sizes. It can be seen that, even if the void fraction is not monotonic in time, LHS performs much better than SRS.

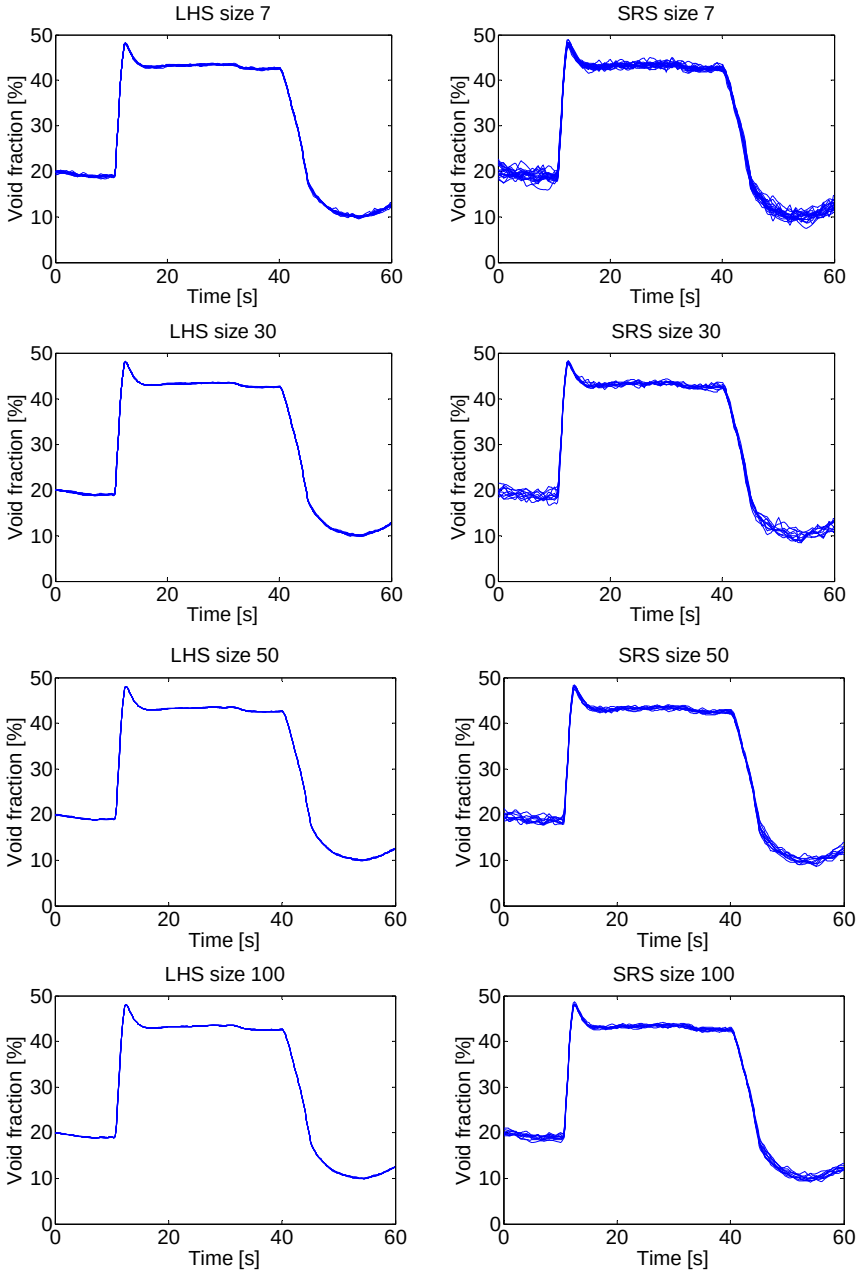

Fig. 5.5. Sampling variability study between LHS and SRS for 10 mean replicates (transient)

5.4 Uncertainty and sensitivity analysis as a validation tool

In this section, statistical uncertainty and sensitivity analyses are used to validate the thermal-hydraulic features of the POLCA-T code, based on a one dimensional model of some test cases of the BFBT macroscopic exercises. A methodology to set validation limits is derived from both measurement and code uncertainty. The results shown below are a summary of the paper No. 6.

5.4.1 Overall validation methodology

The error (δ) is the difference between a simulated or an experimental value and the truth. Since accuracy indicates the closeness of agreement between a simulated/experimental value of a quantity and its true value, accuracy increases as error approaches zero. However, the true values of simulated/experimental values are rarely known and thus, errors must be estimated.

For our particular case, since validation is the process of assessing simulation uncertainty by using benchmark experimental data, it would be necessary first to estimate the errors involved in the measurement systems of the different parameters included in table 3.1. It is natural to consider that measurement errors follow a normal distribution and thus, they can be estimated with a certain degree of confidence. It was agreed in the benchmark specifications for uncertainty analysis [61], that a generic measurement standard deviation can be obtained by multiplying the nominal measurement by its accuracy, i.e.:

$$\sigma_D = Measurement \cdot (Accuracy\ (\%)) \tag{5.3}$$

Therefore, following a normal distribution, a generic uncertainty U_D would estimate an error with a 95% of confidence if it is calculated as:

$$U_D = Measurement \pm 2\sigma_D \tag{5.4}$$

Once both the experimental (U_D) and the simulation or code (U_S) uncertainty have been computed, a validation uncertainty U_v can be defined as the combination of all uncertainties that can be estimated as:

$$U_v^2 = U_D^2 + U_S^2 \tag{5.5}$$

If the absolute value of the error between the prediction S and the experiment D defined as:

$$|E| = |D - S| \tag{5.6}$$

is less than the validation uncertainty U_v, it can be said that validation has been achieved at the U_v level. Then, U_v is the key metric in the validation process and it is imposed by the uncertainties inherent in the experiments, the numerical solution and the model input space [62].

5.4.2 Results of the uncertainty and sensitivity analyses

In this section, the results of the uncertainty and sensitivity analysis on the different BFBT exercises are presented. For each specific exercise, the parameters considered to be the most important sources of uncertainty and that are directly available in the input deck are indentified, defining a particular uncertain input space. To each of these parameters, a PDF is assigned using expert opinion.

For the simulation uncertainty analysis of each test case, the size of the uncertain input space sample is 100. The upper and lower predicted uncertainty limits correspond to the 99th and 1st percentiles of the output sample, respectively. These limits represent a 95-95% confidence interval of the possible values of the code output population. Measurement uncertainty is also present at each case and it is computed from Eqs. (5.3) and (5.4). On the other hand, sensitivity analysis is only performed in a selected test. In this case, 100 samples are taken from each source of uncertainty in order to evaluate which parameter has the greatest effect on the code output.

- *Ex. 0, Phase II. Steady-state single phase pressure drop exercise*

For this exercise, a PDF was assigned to 5 important uncertain parameters. Table 5.4 describes the assessment of this particular uncertain input space, where the mean of each parameter PDF corresponds to the values used in the nominal calculation.

Table5.4. Sources of uncertainty considered for the single phase pressure drops exercise

Parameter	PDF	Mean	Stand. Dev.
Flow rate	Normal	Nominal	1%
Hydraulic diameter	Normal	1.295 cm	1%
Flow area	Normal	97.81 cm^2	1%
Roughness	Normal	2.5 μm	5%
Spacer *K* loss coefficient	Normal	0.94	5%

Six different tests were selected for the study, where the boundary conditions for each case are shown in table 5.5. For the pressure transducer experimental uncertainty, a standard deviation of 1% of the nominal measurement was considered. The benchmark with uncertainty analysis for each test can be appreciated in figure 5.6, where the horizontal blue bar corresponds to the measurement uncertainty, while the vertical blue bar corresponds to the code uncertainty. It can be seen that all nominal predictions lie within the [-10%,+10%] band, and that the code has the tendency to under-predict the bundle pressure drop tests. Regarding the validation process for each test case, a comparison between the absolute error and the validation uncertainty can be found in table 5.5. In all cases, the absolute prediction error was less than the validation uncertainty. Thus, the code predicts bundle single phase pressure drops accurately for a wide range of mass flow rates.

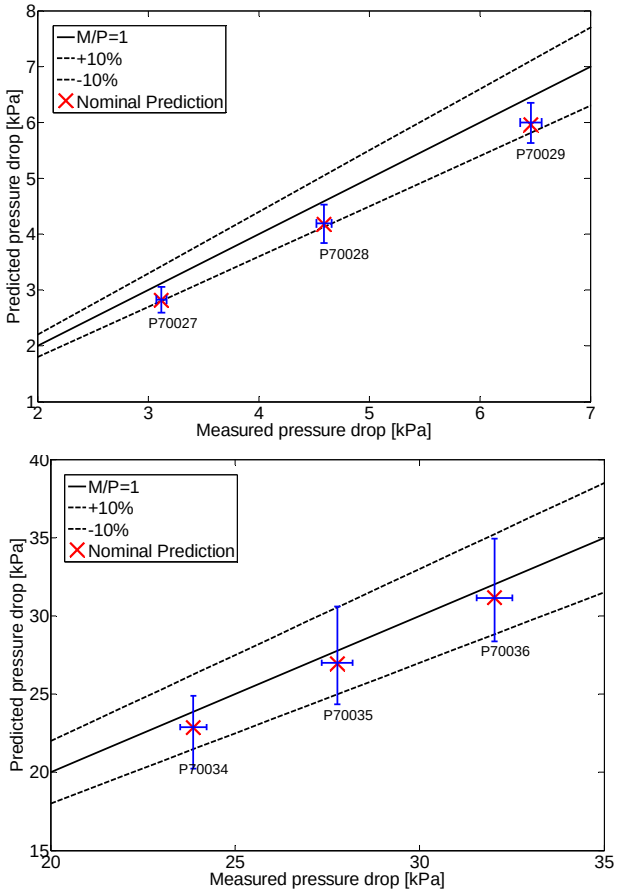

Fig. 5.6. Single phase pressure drops benchmark uncertainty analysis

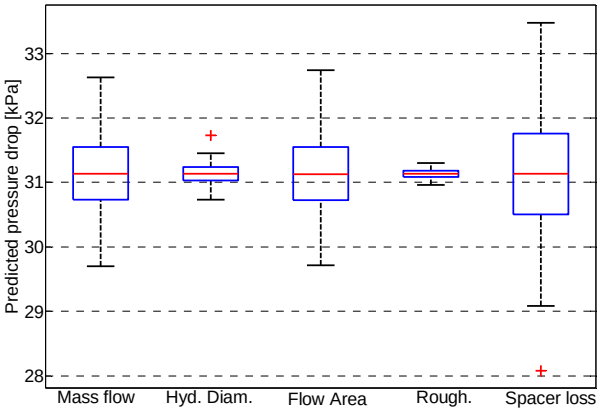

Fig. 5.7. Sensitivity analysis of single phase pressure drops (P70036 test)

Table 5.5. Nominal conditions and validation limits of the single phase pressure drops tests

Test. No.	Outlet Pressure (MPa)	Inlet Temp. (°C)	Mass flow rate (kg/s)	Reynolds number ($x10^4$)	$\|E\|$ (MPa)	U_v (MPa)
P70027	7.15	284.9	5.64	8.07	0.291	0.346
P70028	7.16	285.1	6.92	9.91	0.397	0.506
P70029	7.16	285.1	8.28	11.86	0.460	0.683
P70034	7.15	284.8	16.59	23.74	0.980	1.445
P70035	7.16	284.6	18.00	25.76	0.770	2.041
P70036	7.15	284.8	19.42	27.79	0.878	2.001

Sensitivity analysis was performed on test P70036. In figure 5.7, a group of boxplots show how the pressure drop changes to each parameter defined in the uncertain input space. The box accounts for 50% of the predicted output sample, whereas the limits of the dashed lines correspond to the 2nd and 98st sample percentiles. These represent approximately 90% of the output pressure drop population with 100 calculations. Finally, if the maximum and/or minimum values of the sample do not fit between the limits of the dashed lines, they are considered outliers and are exposed as stars.

As expected, the spacer *K* loss coefficient is shown to have a great effect on the pressure drop since it dominates local losses predictions. Other two important geometric parameters are the flow area and hydraulic diameter, since these have a great impact on the friction pressure drop. Therefore, it can

be concluded that the wall friction and local pressure loss models are well implemented and accurate enough.

- *Ex. 0, Phase II. Steady-state two phase pressure drop exercise*

Accurate predictions of two phase pressure drop are fundamental for a proper determination of the momentum continuity equations and therefore, are fundamental for accurate predictions of averaged void fractions in BWR calculations.

For this exercise, a PDF was assigned to 7 important uncertain parameters as described in table 5.6.

Table 5.6. Sources of uncertainty considered for the two phase pressure drops exercise

Parameter	PDF	Mean	Stand. Dev.
Flow rate	Normal	Nominal	1%
Inlet temperature	Uniform	Nominal	± 1.5 ℃
Power	Normal	Nominal	1.5%
Hydraulic diameter	Normal	1.295 cm	1%
Flow area	Normal	97.81 cm^2	1%
Roughness	Normal	2.5 μm	5%
Spacer *K* loss coefficient	Normal	0.94	5%

Six different tests with a cosinusoidal axial power profile were selected for the study, where the boundary conditions for each case are shown in table 5.7. The selected power range is between 0.863 MW and 6.478 MW. The first three tests correspond to a low mass flow rate condition, while the last three correspond to a nominal BWR bundle flow rate condition. The benchmark with uncertainty analysis for each test can be appreciated in figure 5.8.

It can be seen that all nominal predictions lie within the [-10%,+10%] band. The code under predicts the two phase pressure drops of the low flow rate cases; however, for nominal BWR flow rates, it predicts the bundle two phase pressure drop reasonably well (difference smaller than 1.5%). A comparison between the absolute error and the validation uncertainty can be found in table 5.7. In all cases, the absolute prediction error was less than the validation uncertainty. Thus, the code predicts bundle two phase pressure drops accurately both for a wide range of power and flow rate conditions.

Sensitivity analysis was performed on test P60011, and it is shown in figure 5.9. It can be seen that the flow area is the parameter having the biggest influence on the pressure drop correlation when a two phase flow condition is present. Also, as seen in the previous exercise, the spacer *K* loss coefficient is also an important factor in the constitutive pressure drop correlation. Regarding the effect of the three perturbed boundary conditions, the three are more or less equally important to the code pressure drop model.

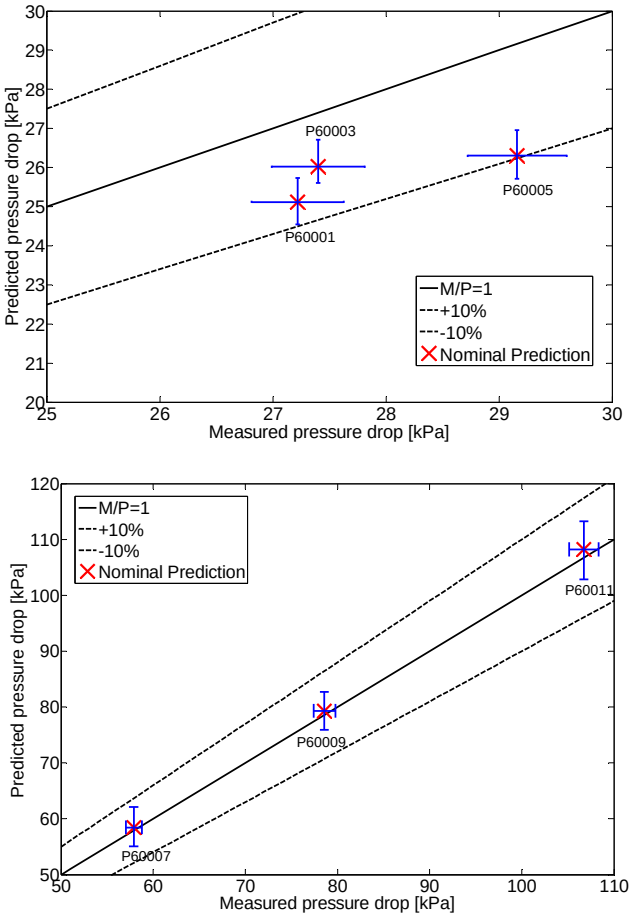

Fig. 5.8. Two-phase pressure drops benchmark uncertainty analysis

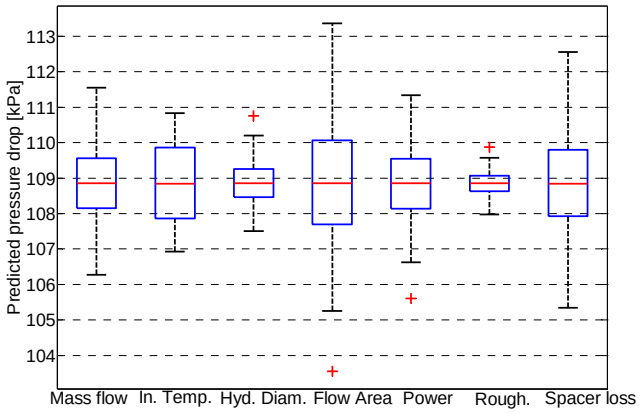

Fig. 5.9. Sensitivity analysis of two-phase pressure drops (P60011 test)

Table 5.7. Nominal conditions and validation limits of the two phase pressure drops tests

Test. No.	Outlet Pressure (MPa)	Inlet Temp. (℃)	Mass flow rate (kg/s)	Input Power (MW)	$\|E\|$ (MPa)	U_v (MPa)
P60001	7.16	277.3	5.62	0.863	1.379	2.761
P60003	7.16	277.8	5.59	1.521	2.100	2.746
P60005	7.16	277.7	5.56	2.357	2.860	2.940
P60007	7.17	277.8	15.28	2.357	0.560	6.158
P60009	7.17	277.8	15.28	4.197	0.730	8.431
P60011	7.17	278.0	15.25	6.478	1.490	11.061

- *Ex. 2, Phase I. Steady-state cross-sectional averaged void fraction*

In this exercise, uncertainty analysis is performed on the predictions of three different cross-sectional averaged void fraction axial profiles. Boundary and input power conditions for such tests are described in table 5.8. All tests were performed using a uniform axial power profile.

Table 5.8. Nominal conditions of the void fraction tests

Test No.	Outlet Pressure (MPa)	Inlet Temp. (°C)	Mass flow rate (kg/s)	Input Power (MW)
0021-16	7.190	277.47	15.24	1.91
0021-18	7.17	279.00	15.37	3.50
0021-20	7.164	277.69	15.23	4.85

For both the steady-state and transient void fraction exercises, the uncertain input space corresponds to the one given in table 5.2. For the cross-sectional averaged void fraction experimental uncertainty, a standard deviation of 2% of the nominal measurement was considered according to the CT scanner accuracy of table 5.1. The uncertainty analysis of the void fraction profiles is shown in figures 5.10, 5.11 and 5.12. Experimental uncertainty is expressed by the vertical blue bar across the measurement point.

It can be seen for all tests that the four measurements are within the uncertainty bands, validating the four calculations. In all three tests, the largest errors between code predictions and measurements are observed at low void fractions (less than 10%). It should be noticed that the code is more sensitive to changes of the uncertain input space when predicting void fractions under bubbly flow, than under slug flow. Nevertheless, it can be concluded that the code predicts with good accuracy cross-sectional averaged void fractions.

At the axial level of 1.773 m from test 0021-16, sensitivity analysis was performed to the cross-sectional averaged void fraction under bubbly flow. The corresponding boxplots are shown in figure 5.13. As expected, it can be seen that void fraction is driven by momentum. Nevertheless, the gas conservation equation is also very sensitive to the inlet sub-cooling state of the flow, a precise determination of its nominal value being very important for an accurate prediction of the averaged cell void fraction.

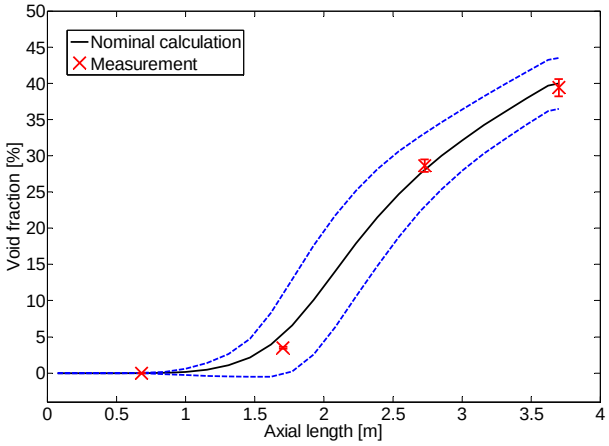

Fig. 5.10. Uncertainty analysis of the void fraction axial profile for test 0021-16

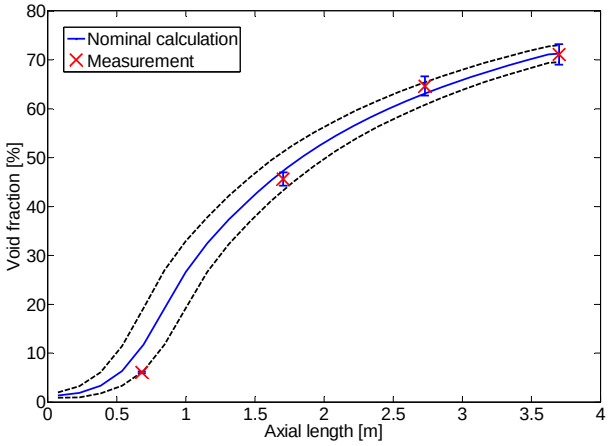

Fig. 5.12. Uncertainty analysis of the void fraction axial profile for test 0021-20

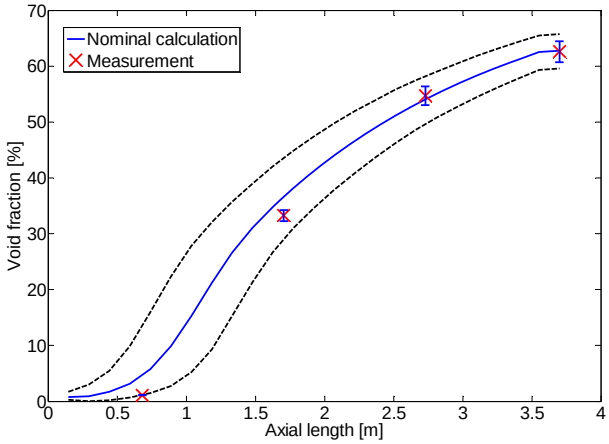

Fig. 5.11. Uncertainty analysis of the void fraction profile for test 0021-18

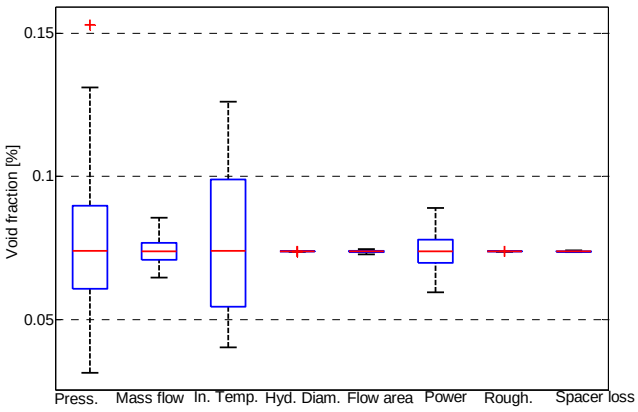

Fig. 5.13. Sensitivity analysis of averaged axial void fraction under bubbly flow (0021-16)

- *Ex. 3. Phase I. Transient cross-sectional averaged void fraction*

In figures 5.14 and 5.15, predicted and experimental uncertainty analyses are shown for the pump trip and the turbine trip scenarios, respectively.

The uncertainty analysis of the re-circulation pump trip shows that all the measurement points from the different densitometers are within the predicted uncertainty limits. This means that the absolute errors are well below the validation uncertainty. It is also worth mentioning that the code captures very well the qualitative behavior of the phenomena during the whole transient.

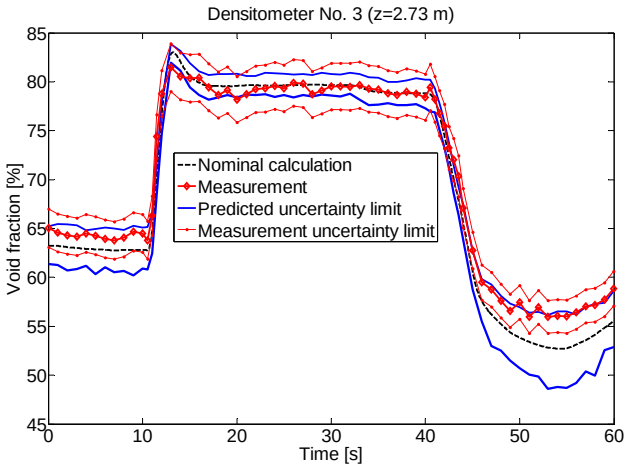

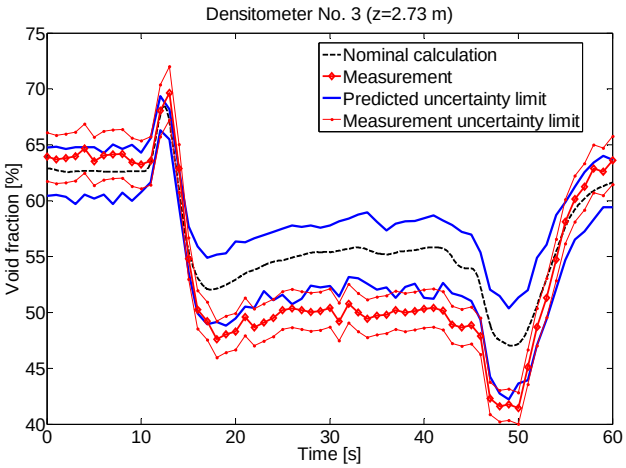

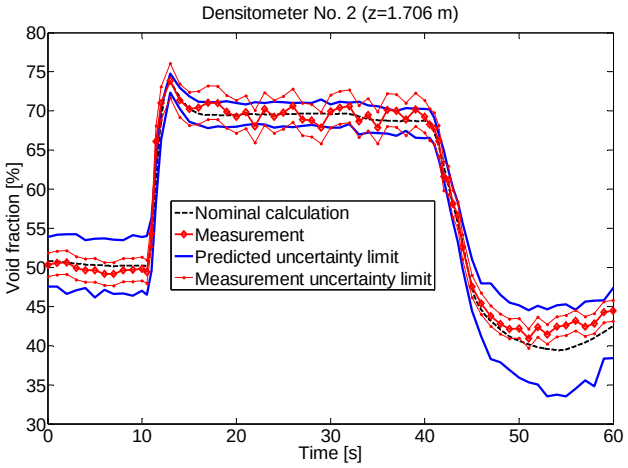

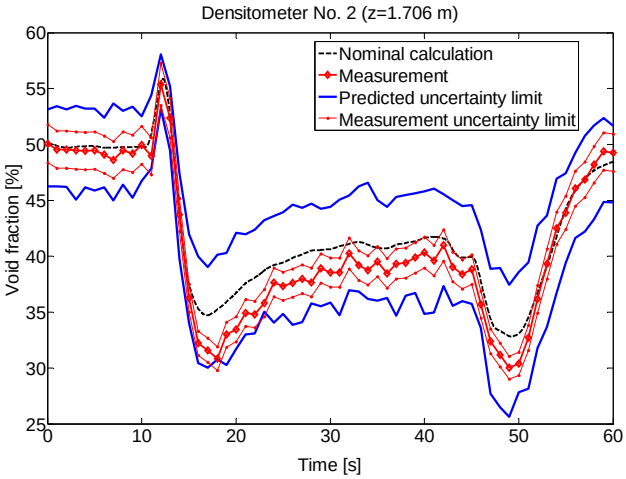

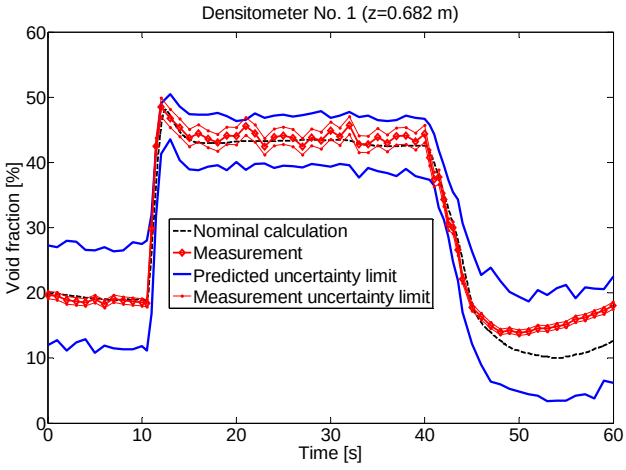

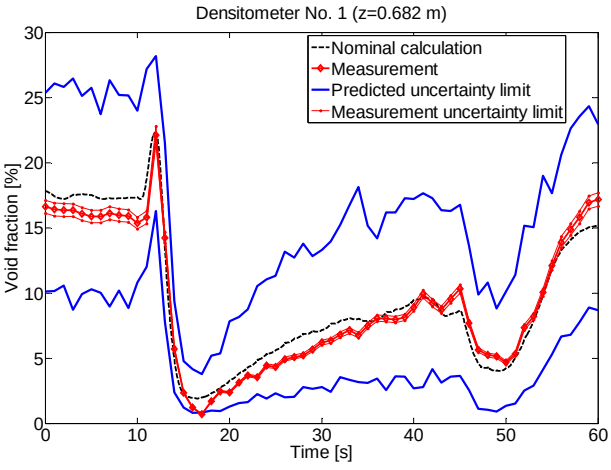

Fig. 5.14. Uncertainty analysis of the pump trip

Fig. 5.15. Uncertainty analysis of the turbine trip

Regarding the analysis of the turbine trip, it is observed that all the measurement points from densitometer No. 1 and 2 are within the predicted 95% tolerance interval with at least a 95% of confidence. However, during the time interval from 18 to 50 seconds, the nominal measurement from densitometer No. 3 falls outside the predicted limits, demonstrating that the code over predicts

the void fraction by up to 12%. The absolute errors of the three points lying outside the validation uncertainty can be found in table 5.9.

Table 5.9. Points lying outside the validation uncertainty from densitometer No. 3 (Turbine trip)

Time (s)	$\|E\|$ (%)	U_v (%)
48	20.968	20.034
49	20.830	20.548
50	21.151	19.126

Finally, just like in the pump trip case, it can be concluded that the code captures the qualitative behavior of the turbine trip very well during the whole transient.

- *Ex. 1, Phase II. Steady-state critical power benchmark*

The uncertain input space for this exercise is defined in table 5.10, where a PDF was assigned to 7 parameters.

Table 5.10. Sources of uncertainty considered for the critical power benchmark (Steady-state)

Parameter	PDF	Mean	Stand. Dev.
Outlet pressure	Normal	Nominal	1%
Flow rate	Normal	Nominal	1%
Inlet temperature	Uniform	Nominal	± 1.5 ℃
Hydraulic diameter	Normal	1.295 cm	1%
Flow area	Normal	97.81 cm^2	1%
Roughness	Normal	2.5 μm	5%
Spacer *K* loss coefficient	Normal	0.94	5%

The four test cases requested by the benchmark organizers for the uncertainty analysis [60] are presented hereafter. Boundary conditions are described in table 5.11, where it can be seen that such conditions are very different for each test case. To all of them, a cosinusoidal axial power profile was applied. For the power experimental uncertainty, a standard deviation of 1.5% of the nominal measurement was considered. The uncertainty analysis is shown in figure 5.16.

It can be appreciated that not all the benchmarked tests lie within the [-10%,+10%] band, the code over predicting the critical power for the majority of the cases. This is due to the fact that the flux-quality correlation is tuned to work properly under BWR nominal conditions, just like test SA603901, whereas other tests are far from nominal BWR conditions. Another conclusion from this study is the fact that the code is not too sensitive to the defined uncertain input space, since for all cases the predicted uncertainty is not larger than 1.6%.

Sensitivity analysis was performed on test SA812800, and the results are shown in figure 5.17. It can be noticed that the most relevant parameter is the inlet sub-cooling boundary condition, which is crucial (as seen before in the void fraction case) to the boiling transition point.

Table 5.11. Nominal conditions and validation limits of the critical power tests

Test. No.	Outlet Pressure (MPa)	Inlet Temp. (°C)	Mass flow rate (kg/s)	Initial Power (MW)	Exp. Critical Power (MW)	$\|E\|$ (MW)	U_v (MW)
SA603901	7.18	282.75	2.78	1.5	3.2	0.050	0.346
SA505900	5.49	264.69	5.59	3.5	5.980	0.948	0.458
SA812800	8.67	275.66	18.13	6.5	8.90	0.483	0.571
SA512800	5.50	242.8	18.20	8.5	11.09	1.395	0.642

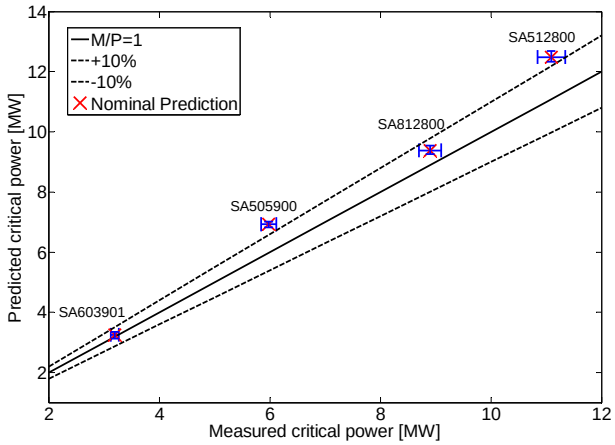

Fig. 5.16. Critical power benchmark uncertainty analysis

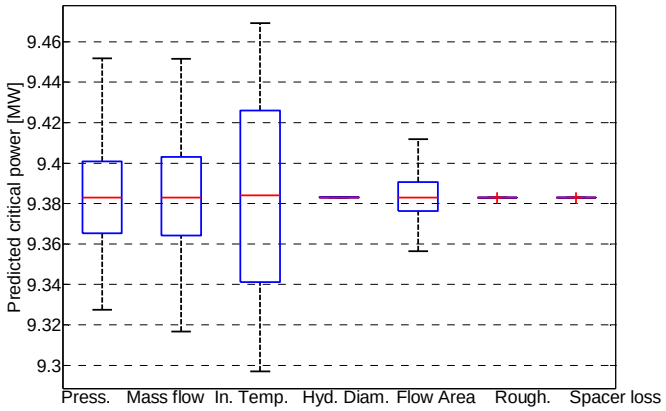

Fig. 5.17. Sensitivity analysis of critical power benchmark (SA812800 test)

CHAPTER 6

CONCLUSIONS AND FUTURE WORK

"If you follow reason far enough it always leads to conclusions that are contrary to reason."

Samuel Butler

In this work, uncertainty analysis is performed at every stage in the modeling of LWRs, in an ongoing effort made by the nuclear community to rely on the simulations performed by neutronic and thermal-hydraulic BE codes. The statistical approach for performing uncertainty analysis based on Latin Hypercube sampling proved to be more efficient in the coverage of input uncertainties than simple random sampling. This is one of the first works that employs LHS to sample the input uncertain space, and then uses the concept of non-parametric tolerance intervals for the code output uncertainty assessment in both neutronic and thermal-hydraulic calculations. It was shown at every stage in the modeling of LWRs that LHS offers the possibility to assess more realistically non-parametric tolerance limits than SRS, because code non-linearities are much better handled when the input space is covered in an efficient way. Therefore, the combination of both LHS and non-parametric statistical coverage of the code output space is valid, because such a theory solely relies on the ranking of the output sample and the size of such a sample. In principle, there should not be concern about using LHS in the code output uncertainty assessment while this one is being based on the theory of non-parametric tolerance intervals.

A summary of the main achievements and general conclusions is given as follows:

- In chapter 3, uncertainty analysis was applied to lattice calculations of the DRAGONv4.05 code. It was found that the computed uncertainties of k_∞, homogeneized and energy-collapsed macroscopic cross-sections and diffusion coefficients based on JENDL-4 data are much larger than for instance, computed uncertainties based on ENDF/B-VII.1 data. This is one of the first attempts to compute and propagate multi-group microscopic cross-section uncertainty from newly released nuclear libraries through lattice codes. Also, it is one of the first attempts to perturb the DRAGLIB library, which is compatible with advance self-shielding models used in deterministic lattice calculations.

- In chapter 4, a statistical uncertainty analysis was performed on nodal thermal flux calculations of a full BWR core. From a simple Monte Carlo-based strategy of input uncertainty propagation, it was shown that LHS converged much faster to compute the maximum possible value of the nodal thermal flux along the core than SRS. The dimension of the input uncertain space was based on the cycle 26 depletion calculation of the Ringhals 1 BWR. On the other hand, a Bayesian approach was used to infer posterior distributions of the different nodal parameters based on actual flux measurements performed along cycle 26 of R1. Even though the ranges of such posterior PDFs could only be based on evidence distributions obtained for a full cycle, such a theory opens the possibility to infer parameter uncertainty based on real experiments and not anymore on expert opinion. Emphasis was made on performing uncertainty analysis at all possible modeling stages, including the coefficients of a nodal cross-section model. Although a very simple model was derived, the

aim is to propose an uncertainty assessment based on replicated sampling techniques such as the general bootstrap method.

- The ongoing efforts to validate BE thermal-hydraulic codes widely used in the nuclear industry were enhanced with the uncertainty and sensitivity analysis presented in chapter 5. Based on the different exercises of the BFBT benchmark, it can be said that the POLCA-T code is very accurate in predicting steady-state pressure drops and cross-sectional averaged void fractions under a wide range of conditions, where the absolute error of all test cases was below the validation uncertainty. Regarding the transient analyses, the qualitative behavior of the code tracked very well the measured void fraction, and only three comparison errors were found to be slightly higher than the validation limit on the turbine trip scenario. Finally, regarding the critical power exercise, four different tests with very different nominal conditions were analyzed. This fact has a big impact on the code accuracy since the critical power ratio (CPR) model is designed to work with nominal BWR pressure conditions. This explains why the absolute errors of the two low pressure test cases were higher than the validation uncertainty.

The present study performs a realistic analysis of nuclear reactors, particularly in the uncertainty prediction of important neutronic and thermal-hydraulic LWR parameters at different stages of the calculations. Nevertheless, the nature of the different parameter uncertainties were not coupled in this work. State-of-the art calculations require the use of coupled codes in order to fully apply the BE concept of multi-physics modeling. The key aspect for handling uncertainties in coupled calculations is to first compute the uncertainties in the cross-sections models, because they are the link between neutronic and thermal-hydraulic predictions. In this thesis, it was shown that the uncertainties of these models are accounted in their respective coefficients. Even though statistical uncertainty analysis relies on first principles, some research still needs to be done on how to implement it at all modeling stages for coupled calculations.

REFERENCES

[1]. OECD, International Atomic Energy Agency (IAEA). *"Uranium 2011: Resources, Production and Demand"*, ISBN: 9789264178038, pp. 408, (2012).

[2]. International Atomic Energy Agency (IAEA). *"Best Estimate Safety Analysis for Nuclear Power Plants: Uncertainty Evaluation",* Safety Reports Series No. 52, (2008).

[3]. Nuclear Regulatory Comission (NRC). Domestic Licensing of Production and Utilization Facilities, Code of Federal Regulations 10, Part 50 NRC, Washington D.C., (1995).

[4]. International Atomic Energy Agency (IAEA). *"Safety Assessment and Verification for Nuclear Power Plants"*, IAEA Safety Standards Series No. NS-G-1.2, Vienna, (2001).

[5]. Helton J. C., Davis F. J. *"Latin hypercube sampling and the propagation of uncertainty in analyses of complex systems",* Realiability Eng. & System Safety, Vol. **81**, pp. 23-69, (2003).

[6]. International Atomic Energy Agency (IAEA). *"Safety of Nuclear Power Plants: Design*", IAEA Safety Standards Series No. NS-R-1, Vienna, (2000).

[7]. International Atomic Energy Agency (IAEA). *"Safety of Nuclear Power Plants: Operation"*, IAEA Safety Standards Series No. NS-R-2, Vienna, (2000).

[8]. Helton J., Davis F.J. *"Sampling-Based Methods for Uncertainty and Sensitivity Analysis*", SANDIA REPORT SAND99-2240, pp. 1-101, (2000).

[9]. Hernández-Solís A. *"Uncertainty and sensitivity analysis applied to the validation of BWR bundle thermal-hydraulic calculations"*, Chalmers University of Technology, Licentiate Thesis, CTH-NT-231, pp. 49, (2010).

[10]. Glaeser H. *"GRS Method for Uncertainty and Sensitivity Evaluation of Code Results and Applications"*, Science and Technology of Nuclear Installations, Vol. **2008**, pp. 1-6, (2008).

[11]. Harper F.T., Breeding R.J., Brown T.D. *"Evaluation of severe accident risks: Quantification of major input parameters. Expert opinion elicitation on In-Vessel Issues",* NUREG/CR-4551, SAND86-1309 Vol. **2**., (1990).

[12]. Electric Power Research Institute (EPRI). *"Probabilistic seismic hazard evaluations at Nuclear power plant sites in the central and eastern United States",* NP-6395D, (1989).

[13]. Booker J.M., Anderson M.C., Meyer M. *"The role of expert knowledge in uncertainty quantification (Are we adding more uncertainty or more understanding?)"*. Los Alamos Nat. Lab. Report, (To be published).

[14]. Petruzzi A. *"Development and Application of Methodologies for Sensitivity Analysis and Uncertainty Evaluation of the Results of the Best Estimate System Codes Applied in Nuclear Technology"*, PhD thesis, University of Pisa, etd-11082008-094257, (2008).

[15]. McKay MD, Beckman RJ, Conover WJ. *"A comparison of three methods for selecting values of input variables in the analysis of output from a computer code",* Technometrics, Vol. **21** (2), (1979).

[16]. Iman R. L., Conover W. J. *"A distribution-free approach to inducing rank correlation among input variables"*, Commun. Stat.- Simula. Computa., **B11** (3), pp. 311-334, (1982).

[17]. Glaeser H., Hofer E., Kloos M., Skorek T. *"Uncertainty and sensitivity analysis of a post-experiment calculation in thermal hydraulics"*, Reliability Eng. & System Safety, Vol. **45** (1-2), pp. 19-33, (1994).

[18]. Wilks S. S. *"Determination of sample sizes for setting tolerance limits"*, Annals of Mathematical Statistics, Vol. **12** (1), pp. 91-96, (1941).

[19]. Wilks S. S. *"Statistical prediction with special reference to the problem of tolerance limits"*, Annals of Mathematical Statistics, Vol. **13** (4), pp. 400-409, (1942).

[20]. Wilks S. S. *"Mathematical Statistics"*, Wiley Ed., New York, (1962).

[21]. Wald A. *"An extension of Wilks' method for setting tolerance limits"*, Annals of Mathematical Statistics, Vol. **14**, pp. 44-55, (1943).

[22]. Wald A., Wolfowitz J. *"Tolerance limits for a normal distribution"*, Annals of Mathematical Statistics, Vol. **17**, pp. 208-215, (1946).

[23]. Guba A., Makai M., Pal L. *"Statistical aspects of best estimate method-I"*, Reliability Eng. & System Safety, Vol. **80** (3), pp. 217-232, (2003).

[24]. Noether G.E. *"Elements of Nonparametric Statistics"*, Wiley Ed., New York, (1967).

[25]. Scheffe H., Tukey J.W. *"A formula for sample sizes for population tolerance limits"*, Annals of Mathematical Statistics, Vol. **15** (2), pp. 217, (1944).

[26]. Ackermann H, Abt K. *"Designing the sample size for non-parametric, multivariate tolerance regions"*. Biometrical Journal, Vol. **26** (7), pp. 723-734, (1984).

[27]. McKay, M.D. *"Uncertainty Analysis, Chapter 4"*, Yigal Ronen, CRC Press, 1st. Ed., pp. 296, (1988).

[28]. Matala A. *"Sample Size Requirement for Monte Carlo – Simulations using Latin Hypercube Sampling"*, 60968 Internal Report, Dep. of Eng. Phys. and Math., Helsinki University of Technology, pp. 1-24, (2008).

[29]. Macfarlane R. E., Kahler A. C. *"Methods for Processing ENDF/B-VII with NJOY"*, Nuclear Data Sheets, Vol. **111**, pp. 2739-2890, (2010).

[30]. Hébert A. *"A nuclear data library production system for advanced lattice codes",* International Conference on Nuclear Data for Science and Technology, pp. 701-704, (2007).

[31]. Chiba G. *"ERRORJ – A Code to Process Neutron-nuclide Reaction Cross Section Covariance, Version 2.3*", JAEA-Data/Code 2007-007, (2007).

[32]. Kosako K. et. al. *"Preparation of a Covariance Processing System for the Evaluated Nuclear Data File, JENDL (III)"*, JNC TJ9440 99-003, (1999).

[33]. Chiba G., Ishikawa M. *"Revision and Application of the Covariance Data Processing Code, ERRORJ"*, International Conference on Nuclear Data for Science and Technology, pp. 468-471, (2005).

[34]. Stacey W. M. *"Nuclear Reactor Physics"*, Wiley – VCH, Germany, (2004).

[35]. OECD/NEA Databank. *"ERRORJ, Multigroup covariance matrices generation from ENDF-6 format"*, Package No. NEA-1676/07, (2010).

[36]. Marleau G., Hébert A. *"A User Guide for DRAGON 3.06",* École Polytechnique de Montréal, IGE–174 Rev. 7 Report, (2008).

[37]. Khan A. A., Lye L., Husain T. *"Latin hypercube sampling for uncertainty analysis in multiphase modeling"*, Journal of Environmental Eng. & Science, Vol. **7** (6), pp. 617-626, (2008).

[38]. Ball M. *"Uncertainty Analysis in Lattice Reactor Physics Calculations",* McMaster University, PhD Thesis No. 6565, (2012).

[39]. Pusa M. *"Incorporating sensitivity and uncertainty analysis to a lattice physics code with application to CASMO-4"*, Annals of Nuclear Energy, Vol. **40**, pp. 153-162, (2012).

[40]. Ivanov K. et. al. *"Benchmark for Uncertainty Analysis in Modeling (UAM) for Design, Operation and Safety Analysis of LWRs vol. I: Specification and Support Data for the Neutronic Cases (Phase I)"*, NEA/NSC/DOC(2011), Version 2, (2011).

[41]. Muller E. *"CoreLink Methodology",* Westinghouse Electric Sweden AB report, BCM 98-040 rev 9, pp. 69, (2007).

[42]. Demazière C. *"Description of the models and algorithms used in the CORE SIM neutronic tool"*, Chalmers University of Technology CTH-NT-241 report, pp. 33, (2011).

[43]. Demazière C. *"User's manual of the CORE SIM neutronic tool"*, Chalmers University of Technology CTH-NT-243 report, pp. 24, (2011).

[44]. Lindahl S. *"POLCA7-Detector Adapted Power Distribution and Thermal Margins (UPDAT*)", Westinghouse Electric Sweden AB report, BCM 97-211 rev 3, pp. 14, (2008).

[45]. Lee P. "Bayesian statistics: An introduction" Wiley, 3rd. Ed., ISBN 978-0-470-68920-2, (2009).

[46]. Braswell B.H., Sacks W.J., Linder E., Schimel D.S. *"Estimating diurnal to annual ecosystem parameters by synthesis of a carbon flux model with eddy covariance net ecosystem exchange observations"*, Global Change Biol., Vol. **11**, pp. 335–355, (2005).

[47]. Raupach M.R., Rayner P.J., Barrett D.J., Defries R.S., Heimann M., Ojima D.S., Quegan S., Schmullius C.C. *"Model data synthesis in terrestrial carbon observation: methods, data requirements and data uncertainty specifications"*, Global Change Biol., Vol. **11**, pp. 378–397, (2005).

[48]. Von Mises R., *"Mathematical Theory of Probability and Statistics"*, Elsevier, New York, (1964).

[49]. Gelfand A.E., Smith A.F.M. *"Sampling-based approaches to calculating marginal densities*", Journal of the American Statistical Assoc., Vol. **85**, pp. 398–409, (1990).

[50]. Effron B. *"More Efficient Bootstrap Computations"*, Journal of the American Statistical Assoc., Vol. **86**, pp. 79-89, (1990).

[51]. Macian R., Zimmermann M., Chawla R. *"Statistical Uncertainty Analysis Applied to Fuel Depletion Calculations"*, Nuclear Science and Technology, Vol. **44** (6), pp. 875-885, (2007).

[52]. Anchel F. et. al. *"Uncertainty and sensitivity analysis in the neutronic parameters generation for BWR and PWR coupled thermal-hydraulic simulations*", Nuclear Engineering & Design, Vol. **246**, pp. 98-106, (2012).

[53]. Sahinler S., Topuz D. *"Bootstrap and Jackknife Resampling Algorithms for Estimation of Regression Parameters"*, Journal of Applied Quantitative Methods, Vol. **2** (2), pp. 188-199, (2007).

[54]. Efron B., Tibshirani R.J. *"An Introduction to the Bootstrap",* Chapman & Hall, New York, (1993).

[55]. Fox J. "Applied Regression Analysis, Linear Models and Related Methods", Sage, (1997).

[56]. Mehta U.B. *"Credible Computational Fluid Dynamics Simulations",* AIAA Journal. Vol. **36**, (1998).

[57]. Gluck, M. *"Validation of the sub-channel code F-COBRA-TF: Part I. Recalculation of single-phase and two-phase pressure loss measurements",* Nuclear Engineering and Design, Vol. **238** (9), (2008).

[58]. Aydogan, F., Hochreiter, L.E., Ivanov, K. *"Correlation for the bundle averaged void fraction measured with X-ray densitometers in the OECD/NRC BFBT benchmark database"*. Technical note within the scope of the OECD/NRC BFBT benchmark, April 29, (2007).

[59]. Bredolt U. *"POLCA-T user guide",* Report SES 02-061, Westinghouse Electric AB Sweden, (2008).

[60]. Gluck, M. "Validation of the sub-channel code F-COBRA-TF: Part II. Recalculation of void measurements", Nuclear Engineering and Design, Vol. **238** (9), (2008).

[61]. Aydogan F, Hochreiter L., Ivanov K. *"NUPEC BWR Full-Size Fine-Mesh Bundle Tests (BFBT) Benchmark. Volume II: Uncertainty and Sensitivity Analyses of Void Distribution and Critical Power"*, NEA/NSC/DOC, (2007).

[62]. Stern F., Wilson R., Coleman H., Patersson E. *"Comprehensive Approach to Verification and Validation of CFD simulations-Part 1: Methodology and Procedures",* Journal of Fluids Eng., Vol. **123**, (2001).

ACKNOWLEDGEMENTS

Hopefully Davide, the part of the thesis that everyone reads…

At the end of the road, I still think that being a shared PhD student between two departments at Chalmers has been one of the most complicated things in my life. Nevertheless, I keep on feeling that I will always be endlessly grateful to the two persons that made this happen: Prof. Christian Ekberg and Prof. Christophe Demazière. You both were very supportive in personal and scientific matters!

Thank you Christian for your endless guidance on statistics and other stuff! It is indeed, as you said, a horrible thing that scientist try to avoid at all cost. Although I took as a compliment that sometimes you considered me as a nerd, I wish I was!!… Thanks for your time and for your open door policy…

Tack så mycket boss!

This work would definitely have gone nowhere without the guidance of whom I considered to be my mentor in reactor physics. Thank you Christophe for all your time, nice humor and patience in answering my dumb questions. As one good old physics dude once said: "I must do the short version"…

Un grand, grand merci a toi!

Dr. Arvid Ödegard-Jensen helped me a lot in statistics and in the revision of the manuscripts. Thank you Arvid for the nice mood at the office. You are really missed at the department.

Prof. Gunnar Skarnemark had always time for my questions and inquietudes. While at Physics, Prof. Imre Pazsit had endless (but very useful) homework's and nice stories, and Dr. Jozsef Banati, my "Catalan friend", had always time for nice discussions in thermal-hydraulics and football matters. To my colleagues and other students, both at Physics and Chemistry, thank you for your friendship and for all your time and help. You guys made the Swedish adventure the best ever!

All my gratitude to Dr. Henryk Nylen for his support and useful comments. Together with Magnus Rappe from the Ringhals power plant, they released the R1 database that was used in this work. SKC, the Swedish Centre for Nuclear Technology, is gratefully acknowledged for financing this project. Special thanks to Ulf Bredolt from Westinghouse for all the provided help related to the POLCA-T code. Thank you Ulf for having the time to answer to all my e-mails!

There is one special person to whom I owe becoming a nuclear engineer. Prof. Jaime Morales from the National University of Mexico have always supported me since I was a bachelor student. Thank you "Doc" for always believing in me! Certainly, I will always admire your work and your passion for teaching.

Monia, "moja sliczna", and the best partner in crime to expend the rest of my life I could ever imagine. Thank you for all your love, patience, weird sense of humor and everything that surrounds you. Where would I end up without you? You are the best part of my every day! Kocham Cie…

I truly hope that this work will make your life a little less uncertain…

During all my life I had the fortune to be close to my super hero. How many people can actually say that? Thanks Vladi for being my best friend during all these years! Being the younger brother definitely has its advantages, like being spoiled by his elder brother at all times. When I grow up, I definitely want to be like you!

The last words have been reserved to endlessly thank my parents, who have always been my greatest example of love and perseverance. I truly think that if love could shape a boy like me, then love can definitely shape everything! It is incredible that I just realized that your only mission in life was to see us happy. Well, guess what? There is nothing else in the world that makes me happier, than knowing that you have been together during all this time…

Mom, Dad, mission accomplished…